Second-Order Phase Transition in Magnetic and non-Magnetic ZnO

by

Prime Niyongabo

Submitted in partial fulfilment of the requirements for the degree

Philosophiae Doctor

in the Faculty of Natural and Agricultural Sciences
University of Pretoria
Pretoria

2014

Declaration

I, Prime Niyongabo declare that the thesis, which I hereby submit for the degree *Philosophiae Doctor* at the University of Pretoria, is my own work and has not previously been submitted by me for a degree at this or any other tertiary institution.

Signature of Author: .....
Prime Niyongabo
Student number: 0440 3878

Certified by: .....
Dr. A.G.J Machatine
Co-supervisor

Certified by: .....
Prof. H.W. Kunert
Emeritus Professor
Promoter

Accepted by: .....
Prof. C. Theron
Head of Physics Department

Acknowledgements

I wish to extend my sincere gratitude to the following people and institutions for their contribution to this thesis:

- My promoter Prof. H.W. Kunert and my Co-promoter Dr A.G.J. Machatine for expert guidance and for being understanding and being a great source of advice and inspiration.
- My parents, especially my Mother, who recently passed away, for their inspiring encouragements, love and assistance through my years of studies.
- My wife Ndayikeze Janviere, my daughters Niyonkeza Gueritha and Nkenguruke Marie-Curie, my sons Niyongabo Brillant and Niyongabo Michael James for encouragement, patience and support.
- My fellow students, especially Louwrens van Schalkwyk at the Department of Physics at the University of Pretoria, for helping with the LaTeX 2_ε document preparation system.

Financial Support

This work is based upon research supported by the National Institute for Theoretical Physics (NITheP)[1] in respect of the costs of the study. The institute's assistance is hereby acknowledged.

[1]Disclaimer: Any opinion, findings and conclusions or recommendations in this material are those of the author(s) and therefore the NITheP do not accept any liability in regard thereto.

Contents

List of Tables

List of Figures

Chapter 1

Introduction

The aim of this thesis is to investigate the second- order phase transitions (S.Or.Ph.Tr.) in magnetic and non magnetic ZnO.

A crystal can undergo several phases from higher to lower, and from lower to higher symmetries when temperature and pressure change.

When ZnO is doped with magnetic elements such as Co, Mg, Mn etc, during synthesis, a layer of the magnetic elements place themselves between two sublattices of ZnO and Co, Mg or Mn (Zn-Co-O, Zn-Mg-O, Zn-Mn-O), and the whole crystal becomes magnetic. Consequently, the symmetry of ZnO (C_{6v}^4; $P6_3mc$; number 186 (CDML)[1]; enumeration of 230 space groups) changes because the symmetry operators (which reverse the magnetic moments of dopants) are added to the symmetry operators of $C_{6v}^4(P6_3mc)$ resulting in magnetic space groups. The irreducible representations of the magnetic groups are called corepresentations (coreps). The states of particles and quasi particles in non magnetic and magnetic crystals are classified according to irreducible representations (irreps) and corepresentations (coreps) respectively.

The important application of coreps theory is the phenomenon of second-order phase transition (S.Or.Ph.Tr) in magnetic crystals.

The theory of S.Or.Ph.Tr for non magnetic crystals has been developed by Landau- Lifshitz [2] and Lyubarskii [3](LLL). The LLL theory of S.Or.Ph.Tr. in non magnetic crystals is well known and has been applied to many compounds like V_3Si and β- Wolfram crystals [4]. Many magnetic crystals experience S.Or.Ph.Tr. due to the change of temperature and pressure.

In terms of coreps we have determined symmetrized and anti-symmetrized squares and cubes of coreps needed for determination of S.Or.Ph.Tr.

To our best knowledge this kind of calculations have been not yet investigated.

In this thesis we have investigated the S.Or.Ph.Tr for non-magnetic and magnetic ZnO by means of group theoretical techniques. We have also studied Raman spectroscopy experimental technique for the appropriate identifications for magnetic crystal symmetry before and after transitions. .

The scope of the thesis is as follows:

In section 1 we have introduced the thesis with an overview of group theory and of S.Or.Ph.Tr. according to LLL theory of magnetic and non magnetic crystals.

In the section 2 we discuss the basic algebra of unitary groups for non magnetic groups.

In section 3 we recall the LLL theory of S.Or.Ph.Tr. for non magnetic space groups in order to extend it to magnetic space groups in section 7.

In section 4 we discuss the basic algebra of antiunitary groups for magnetic groups.

In section 5 we use the theory of Bradley and Davies [5] to build the magnetic space groups originating from the subgroups of $P6_3mc$.

In section 6 we use the Wigner theory of coreps [8] that has been discussed by Bradley and Davies [5] to calculate the coreps of magnetic groups originating from ZnO. In Appendix E we have calculated and tabulated all coreps of magnetic space groups originating from the subgroups of $P6_3mc$.

In section 7 we discuss LLL theory of S.Or.Ph.Tr. in magnetic crystals and we tabulate the coreps that are involved in the S.Or.Ph.Tr.of magnetic crystals originating from ZnO.

In section 8 we tabulate and discuss the experimental Raman spectra of ZnO magnetic

The section 9 concludes the thesis with a brief summary, followed by the reference list and the Appendices.

Chapter 2

The basics of unitary Group Theory related to second-order phase transitions in non magnetic groups

2.1 Unitary Operators

The operator u is called a unitary operator if :

$$(ux, uy) = (x, y) \tag{2.1}$$

for all x,y. This means that the scalar product of the image vector $x' = ux, y' = uy$ is the same as the scalar product of x, y for all vectors x, y.

The matrix of u is a unitary matrix satisfying the following equation.

$$u^{\dagger}u = uu^{\dagger} = 1 \tag{2.2}$$

where $u^{\dagger}$ is the conjugate transpose of u.

- The composition of two unitary transformations u and v is also unitary.

$$(uv)^{\dagger} = u^{\dagger}v^{\dagger} = v^{-1}u^{-1} = (uv)^{-1} \tag{2.3}$$

For unitary group G of a crystal the Hamiltonian: $\hat{\mathbf{H}}\psi_i = E\psi_i$ is invariant with respect to $\hat{u} \in$ G:

$$\hat{u}H = H\hat{u} \tag{2.4}$$

$$\hat{u}^{-1}\hat{\mathbf{H}}\hat{u} = \hat{\mathbf{H}} \tag{2.5}$$

and its eigenfunctions satisfy

$$\hat{u}(\hat{\mathbf{H}}\psi_i) = \hat{u}(E\psi_i) \tag{2.6}$$

$$\hat{\mathbf{H}}(\hat{u}\psi_i) = E(\hat{u}\psi_i) \tag{2.7}$$

where

$$\hat{u}\psi_i = \sum_u \psi_j D_{ji}(u) \tag{2.8}$$

where D_{ji} are unitary matrix elements of unitary irreducible representations D.

The above equations have the following meaning:

1. The Hamiltonian H is invariant with respect to $\hat{u}$

2. New eigenfunctions ψ_i are also the eigenfunctions of H, but expressed as a linear combination of ψ_j.

3. The coefficients $D_{ji}(\mathrm{u})$ are matrix elements of representation D of the space group G to which operators belong: $\hat{u} \in G$

4. The number of ψ_j determines the dimension of representation D and the degeneracy of states of energy.

5. Therefore the energy levels E of states ψ_i are classified according to irreducible representations of D of G.

The generating matrices D and their characters for 230 space groups are tabulated in (CDML)[1].

This thesis is concerned with magnetic ZnO originating from the subgroups $C_6^6, C_{3v}^4, C_{3v}^1, C_3^4$ and C_3^1 of non magnetic ZnO $C_{6v}^4(p6_3mc, 186)$ space group (CDML). The space group of non magnetic ZnO ($C_{6v}^4(p6_3mc, 186)$) consists of symmetry operators:

$C_{6v}^4 : E(1), (C_6^+|00\frac{1}{2})(2.1), C_3^+(3), (C_2|00\frac{1}{2})(4.1), C_3^-(5), (C_6^1|00\frac{1}{2})(6.1),$

$\sigma_{v_1}(19), (\sigma_{d_2}|00\frac{1}{2})(20.1), \sigma_{v_3}(21), (\sigma_{d_1}|00\frac{1}{2})(22.1),$

$\sigma_{v_2}(23), (\sigma_{d_3}|00\frac{1}{2})(24.1)$

where $1 = (00\frac{1}{2})\frac{\pi}{a}$ are non primitive translations associated with rotational parts of operators and a is a lattice constant.

The first six operators form a subgroup $C_6^6(P6_3; 173)$ of C_{6v}^4 space group. The number 173 denotes the number of a group. We have tabulated in Appendix B the Sconflies and international notations of hexagonal and trigonal ordinary space groups (CDML).

The calculated irreps of all high symmetry points: Γ, A, H, K, L and M of space group symmetries: $G^{k_\Gamma}, G^{k_A}, G^{k_H}, G^{k_K}, G^{k_L}$ and G^{k_M} are listed in Appendix D.

The theory of S.Or.Ph.Tr. requires the Kronecker product (KP) of irreps and coreps for non magnetic and magnetic crystals, respectively.

in particular the antisymmetrized squares and symmetrized cubes are of most importance in the determination of active irreps and coreps those may cause transitions.

For ordinary irreps the KPs of two irreps are:

$$D^i \otimes D^j = \sum_k c_{ij,k} D^k \tag{2.9}$$

Where the Clebsch-Gordan coefficients series $c_{ij,k}$ are known:

$$c_{ij,k} = \frac{1}{G} \sum_{u \in G} \chi^i(u) \chi^j(u) \chi^{k^*}(u) \tag{2.10}$$

where χ^i, χ^i and χ^k are the characters of Γ^i, Γ^j and Γ^k; respectively and G is any unitary crystallographic point or space group.

The KP decomposition of ordinary irreps for 32 crystallographic unitary point groups and 230 ordinary unitary space groups are calculated and tabulated in (CDML) tables. Some results of the decomposition of KP at Γ point of the Brillouin zone (BZ) for the subgroups of $P6_3mc$ earlier mentioned are tabulated in the Table 2.1.

Any KP of two irreps can be decomposed into symmetrized and antisymmetrized parts [9].

$$D^i \otimes D^j = \left[D^i \otimes D^j\right] + \left\{D^i \otimes D^j\right\} \tag{2.11}$$

Table 2.1: The Reduction of the Kronecker products of the representations for various space groups at Γ point of the Brillouin zone (CDML).

(a) C_6^6

Γ_1	Γ_2	Γ_3	Γ_4	Γ_5	Γ_6	
Γ_1	Γ_2	Γ_3	Γ_4	Γ_5	Γ_6	Γ_1
	Γ_1	Γ_4	Γ_3	Γ_6	Γ_5	Γ_2
		Γ_5	Γ_6	Γ_1	Γ_2	Γ_3
			Γ_5	Γ_2	Γ_1	Γ_4
				Γ_3	Γ_4	Γ_5
					Γ_3	Γ_6

(b) C_{3v}^4

Γ_1	Γ_2	Γ_3	
Γ_1	Γ_2	Γ_3	Γ_1
	Γ_1	Γ_3	Γ_2
		$\Gamma_1+\Gamma_2+\Gamma_3$	Γ_3

(c) C_{3v}^1

Γ_1	Γ_2	Γ_3	
Γ_1	Γ_2	Γ_3	Γ_1
	Γ_1	Γ_3	Γ_2
		$\Gamma_1+\Gamma_2+\Gamma_3$	Γ_3

(d) C_3^4

Γ_1	Γ_2	Γ_3	
Γ_1	Γ_2	Γ_3	Γ_1
	Γ_3	Γ_1	Γ_2
		Γ_2	Γ_3

(e) C_3^1

Γ_1	Γ_2	Γ_3	
Γ_1	Γ_2	Γ_3	Γ_1
	Γ_3	Γ_1	Γ_2
		Γ_2	Γ_3

Similarly, the triple KP

$$D = D^i \times D^j \times D^k \tag{2.12}$$

can be decomposed into symmetrized and antisymmetrized parts.

The characters of any element u of G in the representations $[D^i]^2$ and $\{D^i\}^2$ are:

$$\chi = \frac{1}{2}\left[(\chi(u))^2 + \chi(u^2)\right] \tag{2.13}$$

and

$$\chi = \frac{1}{2}\left\{(\chi(u))^2 - \chi(u^2)\right\} \tag{2.14}$$

respectively.

The symmetrized and antisymmetrized squares and cubes are calculated and tabulated in (CDML). In Appendix C we have tabulated the symmetrized and antisymmetrized squares for ZnO non magnetic without taking into account time reversal symmetry.

Chapter 3

The second-order phase transitions in non magnetic ZnO

3.1 Landau's Theory of second-order phase transitions

The basic theory of symmetry changes of crystals at continuous phase transition has been formulated by Landau (1937)[2]. A well known exposition of that theory is given in the book on statistical physics by Landau and Lifshitz. The next presentation of that theory is due to Lyubarskii (1960)[3]. It has been followed by the review articles of Birman [4] and the exposition in the book by Cracknell [6].

An extension of Landau's theory to magnetic crystals has been presented by Cracknell [7].

The Second-order phase transitions (S.Or.Ph.Tr) occur when a new state of reduced symmetry develops continuously from the disorder (high temperature) phase. The order phase has the lower symmetry. This means that a crystal structure changes continuously through the Curie temperature (transition point) where infinitesimal displacements of atomic positions can occur. Such a transition is usually reversible, and this can be investigated with X-ray diffraction, neutron diffraction, cold neutron scattering, Raman spectroscopy, as well as with I-V measurement. In our case we use the rigid theoretical method in the framework of Landau-Lifshitz [2] and Lybarskii [3] theory, which strictly resolves the symmetry of a crystal after transitions and predicts correctly the phonon modes involved in transitions. See Table 3.3.

The thermodynamical state of a crystal is characterized by the thermodynamical potential ψ = E - TS + pV, where E is the energy, S is the entropy, p is the pressure and V is the volume. In equilibrium state, the ψ must have a minimum value $\psi'(p, T, \rho)$.

The state of a crystal can be characterized by the density function $\rho_0(x, y, z)$, which describes the probability of finding a particle in a given volume $\psi'(p, T, \rho)dv$ [3].

The density function can be determined from the minimum of the thermodynamic potential $\psi'(p, T, \rho)$ at equilibrium with the change of p and T.

At the equilibrium state (p_0, T_0) the density state ρ_0 (x,y,z) corresponds to highest symmetry group G_0 and at the state (p,T), the density state corresponds to the lower symmetry group G of the crystal. The density state can be written as

$$\rho(x, y, z) = \rho_0(x, y, z) + \delta\rho(x, y, z) \tag{3.1}$$

where $\delta\rho \to 0$ when p,T $\to p_0, T_0$. The $\delta\rho_0$ term denotes a small change of density ρ_0 due to the transition, which is invariant with respect to g $\in G$ of

the crystal. The $\delta\rho_0$ term can be expressed as a linear combination of the basis wave-functions ϕ_i written as $\delta\rho_0 = \sum_i c_i\phi_i$, and so $g\delta\rho_0 \Rightarrow \sum \psi_m D_{mn}$ and transform according to irreps of G after the S.Or.Ph.Tr. takes place. The low symmetry group G must be a subgroup of higher symmetry group G_0.

According to Landau-Lifshitz-Lyubarskii (LLL) theory, the $\psi(p, T, \rho)$ can be expended in a series of polynomials up to the fifth order and can be expressed as

$$\psi = \psi_0 + \psi_2(c_i, p, T) + \psi_4(c_i, p, T) \tag{3.2}$$

The aim is to find all possible symmetries of G after S.Or.Ph.Tr.

3.2 The selection of Active Irreps of ZnO space group with C_{6v}^4 symmetry

According to the LLL theory, only active irreps can cause S.Or.Ph.Tr. The labelling used here for symmetry operators, irreps and Kronecker products follow from CDML tables. There are several criteria that are involved for a given irreps to be active, and these are outlined here.

1. The lower space symmetry group G after transition must necessarily be a space subgroup of higher initial space group G_0 before transition. The inspection of CDML tables yields the space subgroups of C_{6v}^4 listed in the Table 3.1.

2. The irreps of G_0 must be real, and must satisfy the "reality test" mentioned in Table 3.2.

Table 3.1: Subgroups H of C_{6v}^4 and their symmetry operators.

$c_{6v}^4(P6_3mc, 186)$	1	2.1	3	4.1	5	6.1	19	20.1	21	22.1	23	24.1
$C_6^6(P6_3; 173)$	1	2.1	3	4.1	5	6.1						
$C_{3v}^4(P31c; 159)$	1		3		5			20.1		22.1		24.1
$C_{3v}^1(P3m1; 156)$	1		3		5		19		21		23	
$C_3^4(R3; 146)$	1		3		5							
$C_3^1(P3; 143)$	1		3		5							

Table 3.2: Criteria for real and complex irreps [12]: here σ represents the number of cosets of G_0, g is the order of the group, k_1 is the first wave-vector of G_0, and χ is the character of irreps.

$$(\sigma/|g|)\Sigma_{g\in k_1}\chi(g|\tau_g)^2 = \begin{cases} 1, \text{ case (a)D is real} \\ 0, \text{case (b)D is complex} \\ -1, \text{ case (c) D is complex} \end{cases}$$

3. The anti-symmetrized square $\{D^l\}_2$ of an irreducible representation must not contain any component of the polar vector (x,y,z). The $\{D^l\}_2$ can be determined by using CDML tables.

4. The symmetrized cube $\left[D^l\right]_3$ must not contain the identity irrep (usually denoted by Γ_1, Γ_{1+} or A_{1g}). The $\left[D^l\right]_3$ can be determined by using CDML

5. D^l must be compatible with the induced full representations (IFRs) of the small groups of G_0. Some IFRs are tabulated in Appendix D.

The above criteria are concerned with unitary space group and their unitary irreps. Regarding magnetic compounds of magnetic space groups, the previous criteria must be adjusted to antiunitary space group and their coreps. The space subgroups of C_{6v}^4 are given in Table 3.1. The hexagonal Brillouin zone (BZ) of C_{6v}^4 is illustrated in Figure 3.1 to show the coordinates of Γ, A, H, M and K high symmetry points.

Applying the reality test on irreps of G^{k_Γ}, G^{k_A}, G^{k_H}, G^{k_K}, G^{k_L} and G^{k_M} according to criterion 2, it was found that all the irreps are real (CDML).

The vector representation (VR) of C_{6v}^4 was found to be $\Gamma_1(z) + \Gamma_6(x, y)$ [13], and so $\{D^l\}_2$ must not contain one or both of these irreps. We have tabulated in Appendix A all vector representations of hexagonal and trigonal point groups. The decompositions of the KPs of $\{D^l\}_2$ and of the KPs of $\left[D^l\right]_3$ according to criterion 3 and 4; respectively have been calculated and tabulated.

From Table D.10 of Appendix D, it follows that the irreps $\Gamma_3, \Gamma_4, \Gamma_5$, and Γ_6 are complex. The LLL theory for S.Or.Ph.Tr. requires real and active irreps. The real irreps of Γ can be constructed in the following way:

$\Gamma_3 \oplus \Gamma_3^* = \Gamma_3 \oplus \Gamma_5 = \Gamma_{3,5}$.

$\Gamma_4 \oplus \Gamma_4^* = \Gamma_4 \oplus \Gamma_6 = \Gamma_{4,6}$.

It means that $\Gamma_{3,5}$ and $\Gamma_{4,6}$ become two dimensions. From this irreps we have constructed the coreps of the magnetic space group $C_{6v}^4(C_6^6)$. See the Table E.1 of Appendix E.

The active irreps responsible for the S.Or.Ph.Trs. to the space subgroups of C_{6v}^4 are summarized in Table 3.3, where the irreps of points Γ, A, H, K, M, and L are obtained from Appendix D.

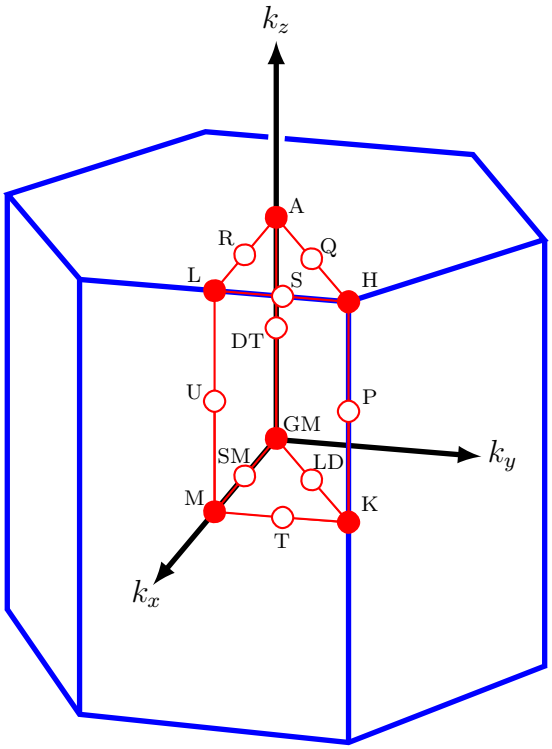

Figure 3.1: Brillouin zone of the hexagonal w-ZnO and their relative positions of high symmetry points. The coordinates of high symmetry points are: $k_\Gamma(0,0,0), k_A(0,0,\frac{1}{2}), k_H(\frac{1}{3},\frac{1}{3},\frac{1}{2}), k_K(\frac{1}{3},\frac{1}{3},0), k_L(\frac{1}{2},0,\frac{1}{2})$ and $k_M(\frac{1}{2},0,0)$

Decompositions of $\{D^l\}_2$ for the selection of active irreps of $P6_3mc$

$\Gamma_1 \otimes \Gamma_1 = \Gamma_2 \otimes \Gamma_2 = \Gamma_3 \otimes \Gamma_3 = \Gamma_4 \otimes \Gamma_4 \Rightarrow \{\}_2 + [\Gamma_1]_2$

$\Gamma_5 \otimes \Gamma_5 = \Gamma_6 \otimes \Gamma_6 \Rightarrow \{\Gamma_2\}_2 + [\Gamma_1, \Gamma_5]_2$

$(A_1 \oplus A_4) \otimes (A_1 \oplus A_4) = (A_2 \oplus A_3) \otimes (A_2 \oplus A_3) \Rightarrow \{\}_2 + [2\Gamma_4]_2 \oplus 2\Gamma_1$

$(A_5 \oplus A_6) \otimes (A_5 \oplus A_5) \Rightarrow \{2\Gamma_3\}_2 + [\Gamma_4, 2\Gamma_6]_2 + 2\Gamma_1 + 2\Gamma_2 + 2\Gamma_5$

$K_1 \otimes K_1 = K_2 \otimes K_2 \Rightarrow \{\Gamma_3\}_2 + [\Gamma_1]_2$

$K_3 \otimes K_3 \Rightarrow \{\Gamma_2, \Gamma_3, \Gamma_6\}_2 + [\Gamma_1, \Gamma_4, \Gamma_5]_2$

$(H_1 \oplus H_2) \otimes (H_1 \oplus H_2) \Rightarrow [2\Gamma_4]_2 + \{2\Gamma_2\}_2 + 2\Gamma_3$

$(L_1 \oplus L_4) \otimes (L_1 \oplus L_4) = (L_2 \oplus L_3) \otimes (L_2 \oplus L_3) \Rightarrow [2\Gamma_4, 2\Gamma_6] + \{\} + 2\Gamma_1 + 2\Gamma_5$

$M_1 \otimes M_1 = M_2 \otimes M_2 = M_3 \otimes M_3 = M_4 \otimes M_4 \Rightarrow \{\}_2 + [\Gamma_1, \Gamma_5]_2$

We see that the antisymmetrized squares of $\Gamma_{1,2,3,4,5,6}$, K_1, $A_{1,4}$, $A_{2,3}$, $A_{5,6}$, $H_{1,2}$, $L_{1,4}$ and $M_{1,2,3,4}$ do not contain any component of the polar vector.

Decompositions of $\left[D^l\right]_3$ for the selection of active irreps of $P6_3mc$

$\Gamma_1 \otimes \Gamma_1 \otimes \Gamma_1 \Rightarrow [\Gamma_1]_3 + \{\}_3$

$\Gamma_2 \otimes \Gamma_2 \otimes \Gamma_2 \Rightarrow [\Gamma_2]_3 + \{\}_3$

$\Gamma_3 \otimes \Gamma_3 \otimes \Gamma_3 \Rightarrow [\Gamma_3]_3 + \{\}_3$

$\Gamma_4 \otimes \Gamma_4 \otimes \Gamma_4 \Rightarrow [\Gamma_4]_3 + \{\}_3$

$\Gamma_5 \otimes \Gamma_5 \otimes \Gamma_5 \Rightarrow [\Gamma_1, \Gamma_2, \Gamma_5]_3 + \{\}_3$

$K_1 \otimes K_1 \otimes K_1 \Rightarrow [\Gamma_1, \Gamma_3]_3 + \{\}_3$

$K_2 \otimes K_2 \otimes K_2 \Rightarrow [\Gamma_2, \Gamma_4]_3 + \{\}_3$

$K_3 \otimes K_3 \otimes K_3 \Rightarrow [\Gamma_1, \Gamma_2, \Gamma_3, \Gamma_4, \Gamma_5, \Gamma_6]_3 + \{\}_3$

$[A_{1,4} \otimes A_{1,4} \otimes A_{1,4}]_3$ does not contain the identity irrep.

$[A_{2,3} \otimes A_{2,3} \otimes A_{2,3}]_3$ does not contain the identity irrep.

$[A_{5,6} \otimes A_{5,6} \otimes A_{5,6}]_3$ does not contain the identity irrep.

$M_1 \otimes M_1 \otimes M_1 \Rightarrow [\Gamma_1]_3 + \{\Gamma_2\}_3$

$M_2 \otimes M_2 \otimes M_2 \Rightarrow [\Gamma_2]_3 + \{\Gamma_1\}_3$

$M_3 \otimes M_3 \otimes M_3 \Rightarrow [\Gamma_3]_3 + \{\Gamma_4\}_3$

$M_4 \otimes M_4 \otimes M_4 \Rightarrow [\Gamma_4]_3 + \{\Gamma_3\}_3$

It follows that the antisymmetrized cubes of $\Gamma_{2,3,4,6}, K_2,$

$A_{1,4}, A_{2,3}, A_{5,6}, H_{1,2}, L_{1,4}$ and $M_{2,3,4}$ do not contain the identity irrep.

From the results of the decompositions of the symmetrized squares and antisymmetrized cubes of irreps, we conclude that $\Gamma_{2,3,4,6}, K_2, A_1 \oplus A_1^*(A_{1,4}), A_2 \oplus A_2^*(A_{2,3}), A_5 \oplus A_5^*(A_{5,6}), H_1 \oplus H_1^*(H_{1,2}),$

$L_1 \oplus L_1^*(L_{1,4})$ and $M_{2,3,4}$ are only active irreps and, consequently, they are involved in the second-order phase transitions. The results are tabulated in the Table 3.3.

Table 3.3: Active Irreducible Representations of initial space group ($G_0 = C_{6v}^4$) that may cause S.Or.Ph.Trs by active modes of Γ, A, K, H, M and L. to lower space group symmetry G[1].

Symmetry operators of the group of high symmetry: G_0	Subgroups of the group of high symmetry: G
$C_{6v}^4(\Gamma: 1, 2.1, 3, 4.1, 5, 6.1, 19, 20.1, 21, 22.1, 23., 24.1)$	$C_{6v}^4 \xrightarrow{\Gamma_2} C_6^6$(1,3,4.1,5,6.1)
	$C_{6v}^4 \xrightarrow{\Gamma_{2,3,4}} C_3^1$ and $C_3^4(1,3,5)$
	$C_{6v}^4 \xrightarrow{\Gamma_3} C_{3V}^4$(1,3,5,20.1,22.1,24.1)
	$C_{6v}^4 \xrightarrow{\Gamma_4} C_{3V}^1$(1,3,5,19,21,23)
$C_{6v}^4(A: 1, 2.1, 3, 4.1, 5, 6.1, 19, 20.1, 21, 22.1, 23., 24.1)$	$C_{6v}^4 \xrightarrow{A_1 \oplus A_1^*} C_{3v}^1$(1,3,5,19,21,23)
	$C_{6v}^4 \xrightarrow{A_2 \oplus A_2^*} C_3^1$ and $C_3^4(1,3,5)$
	$C_{6v}^4 \xrightarrow{A_5 \oplus A_5^*} C_3^1$ and $C_3^4(1,3,5)$
$C_{6v}^4(K: 1, 3, 5, 20.1, 22.1, 24.1)$	$C_{6v}^4 \xrightarrow{K_2} C_3^1$ and $C_3^4(1,3,5)$
$C_{6v}^4(H: 1, 3, 5, 20.1, 22.1, 24.1)$	$C_{6v}^4 \xrightarrow{H_1 \oplus H_1^*} C_3^1$ and $C_3^4(1,3,5)$
$C_{6v}^4(L: 1, 4.1, 20.1, 23)$	$C_{6v}^4 \xrightarrow{L_1 \oplus L_1^*} C_{3v}^1(1,23)$
$C_{6v}^4(M: 1, 4.1, 20.1, 23)$	$C_{6v}^4 \xrightarrow{M_2} C_6^6(1,4.1)$
	$C_{6v}^4 \xrightarrow{M_3} C_{3v}^4(1,20.1)$
	$C_{6v}^4 \xrightarrow{M_4} C_{3v}^1(1,23)$

The phase change in non magnetic crystals can be tested by Raman spectroscopy and I-V measurements. In the following section we will develop the theory of determining the Raman active modes involved in S.Or.Ph.Tr. from the ordinary space group of higher symmetry C_{6v}^4 to C_{3v}^1 of lower symmetry.

[1]From the Table 3.3 it is seen that for example Γ_2 causes S.Or.Ph.Tr and brings ZnO crystal to the subgroup C_6^6

3.3 Raman scattering processes in non magnetic ZnO

3.3.1 Raman tensors

The general mechanism of Raman scattering (RS) is discussed here, followed by analysis of experimentally obtained data of Raman-active modes (RAMs). In the study of elastic and inelastic scattering of light by quasiparticles in solids, it is useful to introduce a scattering tensor which relates the Cartesian components (x,y,z) of the scattered radiation field to that of the incident field. If the unit polarization vector of the incident radiations is $\bar{e}_{i\beta}$ (β = x,y,z), and the unit polarization vector of the scattered radiation is $\bar{e}_{\rho\alpha}$ (α = x,y,z) polarized in the α-direction, then we can relate the intensity of the scattered light by:

$$I = C|e_{\rho\alpha}P_{\alpha\beta}e_{i\beta}|^2 \tag{3.3}$$

where $P_{\alpha\beta}$ is the scattering tensor (ST) and C is a coefficient that modulates the intensity.

Depending upon the physical process under consideration, the ST can be further specified by giving the individual contributions from various subchannels, each of which contributes to the total scattering and can be written as $C'|e_{\rho\alpha}P^{(1)}_{\alpha\beta}e_{i\beta}|^2, C"|e_{\rho\alpha}P^{(2)}_{\alpha\beta}e_{i\beta}|^2$, etc. The $P^{(1)}_{\alpha\beta}$ term represents the first-order (one-excitation) ST, and the term $P^{(2)}_{\alpha\beta}$ term represents the second-order (two-excitations) ST and so on. The incident and scattered electric fields of the photon are given by:

$$\bar{E}_q(r,t) = \bar{E}_{q_0}\bar{e}_q exp(i\bar{k}_q\bar{r} - \omega_q t) \tag{3.4}$$

where q = i,s represents the incident and the scattered wave, respectively, $\bar{e}_q$ is the unit polarization vector which is transverse to $\bar{k}_q$ (the propagation vector), and ω_q is the photon frequency. The total intensity was represented in Eq. (3.3). The operator $P_{\alpha\beta}$ also depends on the ion position $\bar{R} : P_{\alpha\beta}(\bar{R})$. The operator $P_{\alpha\beta}(\bar{R})$ can be expended in a Taylor series in the ion displacements from the equilibrium $\bar{R} = \bar{R}_0 + u$, where $\bar{u}$ is the displacement vector from the equilibrium $\bar{R}_0$. Instead of the individual $\bar{u}$ for each ion, the normal coordinate Q^j_σ can be used, and so Taylor series is [15]:

$$P_{\alpha\beta}(\bar{R}) = P(0)_{\alpha\beta}(\bar{R}^0) + \sum_{j\sigma} P^{(1)}_{\alpha\beta}(\bar{R}^0, j\sigma)Q^j_\sigma \quad + \\ \sum_{jj'}\sum_{\sigma\sigma'} P(2)_{\alpha\beta}(\bar{R}^0, j\sigma, j'\sigma')Q^j_\sigma Q^{j'}_{\sigma'} + ... \tag{3.5}$$

which expresses several orders of STs.

We consider only the first-order ST , $P^{(1)}_{\alpha\beta}$, and its transformation properties which is the most suitable for the study of Raman spectra in this work $C'|e_{\rho\alpha}P^{(1)}_{\alpha\beta}e_{i\beta}|^2$. It consists of two Cartesian vectors $e_{\rho\alpha}$ and $e_{i\beta}$ that transform as ordinary vector $\bar{r}$.

$$\bar{g}\begin{pmatrix} x \\ y \\ z \end{pmatrix} = \begin{pmatrix} VR \\ matrix \end{pmatrix}\begin{pmatrix} x \\ y \\ z \end{pmatrix} = \begin{pmatrix} V_{xx} & V_{xy} & V_{xz} \\ V_{yx} & V_{yy} & V_{yz} \\ V_{zx} & V_{zy} & V_{zz} \end{pmatrix}\begin{pmatrix} x \\ y \\ z \end{pmatrix} \tag{3.6}$$

The vector representations are readily obtainable from CDML tables and are tabulated in Appendix A. Since $e_{\rho\alpha}$ and $e_{i\beta}$ transform according to the VR, their product (Eq.(3.6)), transforms according to the KP of the VR, $VR \times VR$. Microscopic theory indicates that usually for ω_j (frequency of incident laser light) away from resonance, the ST for phonons is symmetric $P_{\alpha\beta} = P_{\beta\alpha}$, which can also be confirmed by Raman spectra. Therefore, $P_{\alpha\beta}$

should be written as :

$$P_{\alpha\beta} = \sum_{\lambda\mu}(V_{\alpha\lambda}V_{\beta\mu} + V_{\alpha\mu}V_{\beta\lambda}) \tag{3.7}$$

Regarding the first-order term of the Taylor series in Eq.(3.5) written as $\sum_{j\sigma} P^{(1)}_{\alpha\beta}(\bar{R}^0, j\sigma)Q^j_\sigma$, we now consider the transformation property of normal coordinates Q^j_σ given by $gQ^j_\sigma = Q^{f'}_\sigma = \sum_\gamma D^{(j)}gQ^j_\gamma$.
The j indicates the irrep of G_0. Consequently, the RAMs are contained in symmetrized square of the VR $([VR]_2$.

3.3.2 Raman-active modes of C^4_{6v} and C^1_{3v}

In order to find the Raman active modes at point Γ we have to decompose the symmetrized square vector representation $[V \oplus V]_2$ onto irreps of C^4_{6V}. Only representations contained in the symmetrized square of the vector representation are Raman actives.
In the case of ZnO, and in terms of CDML labelling, we have $\Gamma_1 \oplus \Gamma_6$ for vector representation with basis (z) for Γ_1 and (x,y) for Γ_6. Our rigid calculations on the decomposition of the $[(\Gamma_1 \oplus \Gamma_6) \otimes (\Gamma_1 \oplus \Gamma_6)]_2$ onto irreps yield RAMs for ZnO with C^4_{6v} symmetry: $2\Gamma_1 \oplus \Gamma_5 \oplus \Gamma_6$.
In the case of C^1_{3v} and in terms of CDML labelling, we have $\Gamma_1 \oplus \Gamma_3$ for vector representation with basis (z) for Γ_1 and (x,y) for Γ_3. Our rigid calculations on the decomposition of the $[(\Gamma_1 \oplus \Gamma_3) \otimes (\Gamma_1 \oplus \Gamma_3)]_2$ onto irreps yields RAMs for crystals with C^1_{3v} symmetry: $2\Gamma_1 \oplus \Gamma_2 \oplus \Gamma_3$.

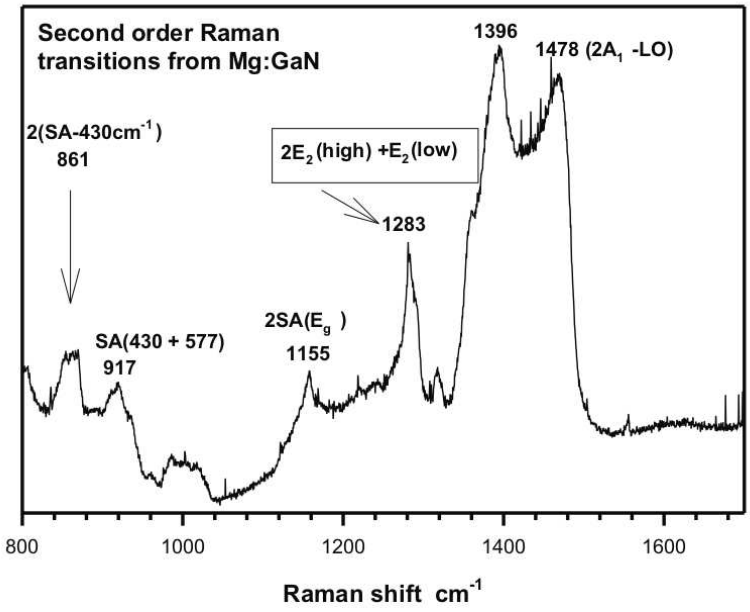

Figure 3.2: Second order Raman transitions from GaN

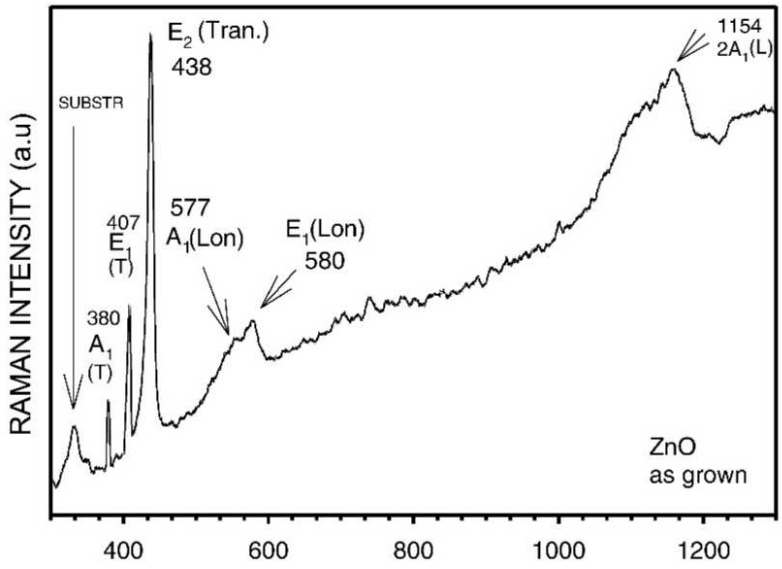

Figure 3.3: First and second order Raman transitions from ZnO

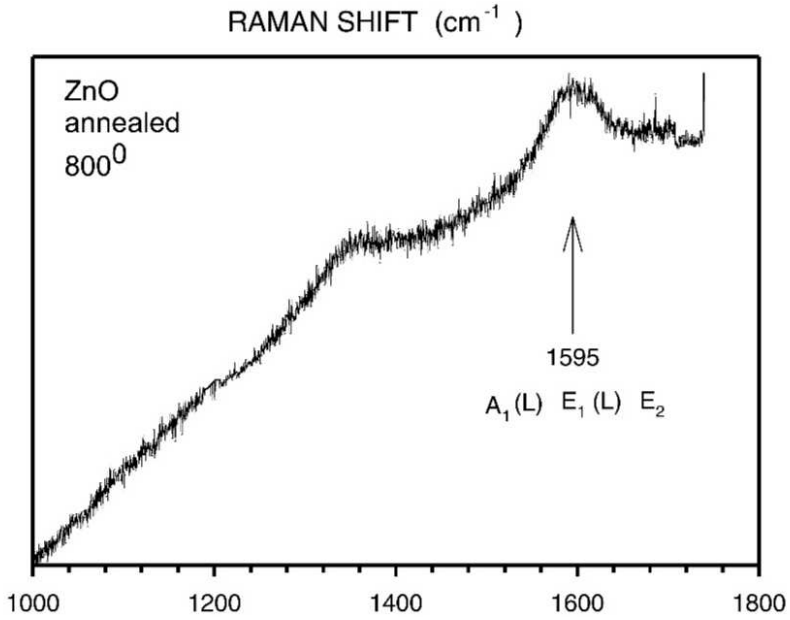

Figure 3.4: Third order Raman transitions from ZnO annealed

3.4 Discussions of the Raman spectra

The first order Raman spectra yield the well known six symmetry that allowed Raman active modes[16].

It follows that only Γ_1, Γ_5, and Γ_6 phonons are Raman active in all compounds with C_{6v}^4 space group and the same number of atoms in the unit cell. For example, in bulk GaN, for Γ_1 we have two modes A_1(TO-533 cm^{-1}) and A_1(LO-735 cm^{-1}), for Γ_5: E_1(TO-561 cm^{-1}), E_1(LO-742 cm^{-1}), and for Γ_6: E_2(low-144 cm^{-1}), E_2(high-570 cm^{-1}). According to the group theoretical results, the Raman spectroscopy reveals all the six Raman active modes as well as their symmetry allowed overtones and combinations.

The Figure 3.2 displays the second-Raman spectrum from GaN/Saphire . Several symmetries allowed overtons and combinations of the first order modes are observed [17, 18]. For example, the mode at 1478 cm^{-1} is overton of the $A_1(\Gamma_1)$-739 cm^{-1}, and the mode at 1283cm^{-1} may result from three

phonon processes; $2E_2(2\Gamma_6)$-high $2 \times 570cm^{-1}$ and $E_1(\Gamma_5)$-low $144cm^{-1}$. We also observe several second order vibrational modes from Saphire - Al_2O_3 (space group D^6_{3v}). These are overtons and combinations of the first order phonons [19]. The assignment of the phonons on Figure 3.2 follows from the complete reduction of the squares and cubes (KP) of the first order species (irrps-of the GaN) and of Siphire, respectively.

The Figure 3.3 exhibits the first and second order Raman active modes in ZnO for which the Raman selection rules are identical to those for GaN. The Figure 3.4 presents the Raman spectrum in the region 1000 cm^{-1}-1800 cm^{-1} from ZnO annealed at 800 C. This region may correspond to the third order Raman transitions. The modes at 1340 cm^{-1} and 1595 cm^{-1} may result from three phonon processes (2× 380 + 577) cm^{-1} and (438 + 577 + 580) cm^{-1}, respectively. For these possible three phonon processes, the selection rules and third order Raman scattering tensors are to be established.

The Raman spectroscopy is able to identify to which subgroup ZnO non magnetic goes after transitions by analysing the Raman active modes of the Raman spectra of the subgroups. Here we mean that the Raman phonon modes of ZnO Raman spectra responsible for S.Or.Ph.Tr must be found in the Raman spectra of the subgroup.

In the forth-coming sections we discuss the properties of the magnetic crystals regarding to the coreps and S.Or.Ph.Tr. after a briefly view on the basic of antiunitary group theory.

Chapter 4

The basic of antiunitary group theory related to second-order phase transitions in magnetic groups

4.1 Antiunitary operators

In this section we briefly recall the antiunitary operator definitions and their properties.

The antiunitary operator A is an antilinear operator satisfying [29]

$$\langle A\phi, A\psi\rangle = \langle\phi|\psi\rangle^* = \langle\psi|\phi\rangle \tag{4.1}$$

where ϕ and ψ are describing a possible state of a physical system and the quantity $|(\phi,\psi)|^2$ is interpreted as a transition probability from the state ψ

to the state ϕ.

- The antiunitary operator A obeys [30]

$$A(\phi\alpha + \psi\beta) = (A\phi)\alpha^* + (A\psi)\beta^* \tag{4.2}$$

- The product of two antiunitary operators is a unitary operator

- The product of antiunitary and unitary operators is an antiunitary operator.

The special antiunitary operator is the time reversal symmetry θ.

The stationary state of a particle in a crystal, is described by equation :

$$H\psi = (-\frac{\hbar^2}{2m}\nabla^2 + V(r))\psi = E\psi \tag{4.3}$$

When the spin-orbit coupling is neglected and no magnetic field is present, The H is real and the Schrodinger equation:

$$H\psi = i\hbar\frac{\partial\psi}{\partial t} \tag{4.4}$$

is invariant under time reversal symmetry.

Taking $t \to -t$ and taking complex conjugates we have :

$$H\psi^* = i\hbar\frac{\partial\psi^*}{\partial t} \tag{4.5}$$

The above equations show that the operation of time reversal symmetry, θ, takes the function ψ into a new function:

$$\theta\psi(\mathbf{r}, t) = \psi^*(\mathbf{r}, -t) \tag{4.6}$$

$$\theta\psi(t) = \theta\sum_k a_k(t)\psi_k = \sum_k a^*(-t)\theta\psi_k \tag{4.7}$$

This shows that $\psi^*(\mathbf{r}, -t)$ satisfies the same equation as $\psi(\mathbf{r}, t)$ when the Hamiltonian is real and consequently is also a solution of the Schroedinger equation if $\psi(\mathbf{r}, t)$ is. It means that ψ is a basis for D and ψ^* is basis for D^*. When an irrep is complex then D and D^* must be joint; $D \oplus D^* \Rightarrow D^{Phy.irrep}$ yielding to so-called physically irreducible representations ($D^{Phy.irrep}$). The dimensions of irreps built up on (ψ, ψ^*) becomes doubled. Consequently, an extra degeneracy of the states can arise [28]. The inclusion of the time reversal symmetry does not change the existing optical selection rules but increases the new states of same symmetries. In [20, 21, 22, 23, 24, 25], they have investigated the optical properties by means of optical selection rules for Si, Ge, wurtzite and rocksalt ZnO non magnetic in the absence and presence of time reversal symmetry.

Chapter 5

The structure of magnetic groups

In this section, we discuss the theory of magnetic groups before building their coreps. The magnetic group M consists of half of unitary and half of antiunitary operators. The group M can be expressed as:

$$M = H + AH \tag{5.1}$$

Where H is any unitary subgroup of an unitary space group G^k from which M originates [5]. The AH is a coset of M consisting only antiunitary operators $a \in AH$, and $A = \theta u_0$. Where u_0 is one of the unitary elements of the G. There are five magnetic space groups originating from C_{6v}^4:
$M(P6_3m'c') \Rightarrow C_{6v}^4(C_6^6)$; $M(P6_{3'}m'c) \Rightarrow C_{6v}^4(C_{3v}^4)$; $M(P6_{3'}mc') \Rightarrow C_{6v}^4(C_{3v}^1)$; $C_{6v}^4(C_3^4)$; $C_{6v}^4(C_3^1)$ where $C_6^6, C_{3v}^4, C_{3v}^1, C_3^4$ and C_3^1 are subgroups of C_{6v}^4.
Here we have considered the magnetic groups M originating from H = $C_6^6, C_{3v}^4, C_{3v}^1, C_3^4$ and C_3^1, space subgroups of C_{6v}^4 see Table 3.1.

As an example of generating the magnetic space groups let us focus on M originating from H = C_6^6 and C_{3v}^4

Regarding the antiunitary operator A in Eq.(5.1), we choose $A = \theta\sigma_{v_1} = \theta 19$. The numbers in brackets follow CDML labelling of operators. We have tabulated the irreducible representations of C_{6v}^4 in appendix D for high symmetry points of the hexagonal Brillouin zone. The meaning of θ (time reversal operator) is explained in the section 4.

Therefore AH : $\theta 19(1, 2.1, 4.1, 5, 6.1) \Rightarrow$

$\Rightarrow \theta 19, (\theta 19)2.1, (\theta 19)3, (\theta 19)4.1, (\theta 19)5, (\theta 19)6.1 \Rightarrow \theta 19, \theta 24.1,$

$\Rightarrow \theta 23, \theta 22.1, \theta 21, \theta 20.1$

The last six antiunitary operators belong to $\theta 19(C_6^6)$.

Therefore the magnetic space group $M(P6_3m'c')$ with subgroup $H = C_6^6$ is:

$M = \{E(1), C_6|1(2.1), C_6^2(3), C_6^3|1(4.1), C_6^4(5), C_6^5|1(6.1),$

$\theta\sigma_{v_1}(19), \theta\sigma_{d_3}|1(20.1), \theta\sigma_{v_2}(21), \theta\sigma_{d_1}|1(22.1), \theta\sigma_{v_3}(23), \theta\sigma_{d_2}|1(24.1)\}$.

For the magnetic space group M = $C_{6v}^4(C_{3v}^4)$:

H = (C_{3v}^4) = 1,3,5, 20.1, 22.1, 24.1

AG = $\theta 19(1, 3, 5, 20.1, 22.1, 24.1) = \theta 19, \theta 23, \theta 21, \theta 6.1, \theta 4.1, \theta 2.1.$

M = $\{1, 3, 5, 20.1, 22.1, 24.1, \theta 19, \theta 23, \theta 21, \theta 6.1, \theta 4.1, \theta 2.1\}$ where $A = \theta 19$.

The first six operators belong to subgroup H of which the irreps are known. The other six are antiunitary belonging to AH.

Before constructing coreps, we have to determine their type. We have calculated all the coreps originating from all subgroups of C_{6v}^4 and these are tabulated in Appendix E.

Chapter 6

Corepresentations

In this section we focus on the theory of the coreps of the magnetic space groups M originating from C_{6v}^4 and their three types.

6.1 Basis functions of corepresentations

As we have shown previously our magnetic group M consists of twelve symmetry operators .

For the unitary operator u, the unitary basis functions of D(u) are:

$$\langle\psi_1, \psi_2, ..., \psi_n| \equiv \langle\psi| \tag{6.1}$$

And $u\psi = \sum \psi_j D_{ij}(u)$ where $D_{ij}(u)$ are unitary matrix elements of irreps D(u) and are tabulated in Appendix D.

In general we write :

$$u\langle\psi| = \langle\psi|D \tag{6.2}$$

To create the basis for antiunitary operators we act antiunitary operators A on unitary basis:

$$A\langle\psi_1, \psi_2, ...\psi_n| = A\langle\psi_i| \equiv \langle\phi_j| \tag{6.3}$$

Therefore the total set of wave functions of M is:

$$\langle f| = \langle\psi_1, \psi_2, ...\psi_n, \phi_1, \phi_2, ...\phi_n| = \langle\psi\phi| \tag{6.4}$$

We also need the effect of u operator on $\langle\phi|$ and we obtain :

$$\begin{aligned} u\langle\phi| &= uA\langle\psi| && (6.5)\\ &= A(A^{-1}uA)\langle\psi| \\ &= A\langle\psi|D(A^{-1}uA) \\ &= \langle\phi|D^*(A^{-1}uA) && (6.6)\\ & && (6.7) \end{aligned}$$

The general notation of the above equation is:

$$u\phi_p = \sum \phi_q C D^*(A^{-1}uA)_{qp} \tag{6.8}$$

The complex conjugate (denoted by an asterisk) appears because A is antilinear.

The coreps are defined by u and θu_0. Therefore we have $u(A\langle\psi|) = A(A^{-1}uA)\langle\psi| = A\langle\psi|D^*(A^{-1}uA)$.
Since A is antiunitary operator the $D(A^{-1}uA)$ must be complex conjugate. And

$a\langle\phi| = a(A\langle\psi|) = \langle\psi|D(aA)$,

$a\langle\psi| = aA^{-1}\langle\phi| = \langle\phi|D^*(A^{-1}a)$.

Again, since A is antiunitary, the $D(A^{-1}a)$ must be complex. These derivation can be summarized as:

$$CD(u) = \begin{pmatrix} u & 0 \\ 0 & u \end{pmatrix} \begin{pmatrix} \langle\psi| & 0 \\ 0 & \langle\phi| \end{pmatrix} = \begin{pmatrix} D(u) & 0 \\ 0 & D^*(A^{-1}uA) \end{pmatrix} \tag{6.9}$$

$$CD(a) = \begin{pmatrix} 0 & a \\ a & 0 \end{pmatrix} \begin{pmatrix} \langle\psi| & 0 \\ 0 & \langle\phi| \end{pmatrix} = \begin{pmatrix} 0 & D(aA) \\ D^*(A^{-1}a) & 0 \end{pmatrix} \tag{6.10}$$

Cleary, the coreps CD(u) and CD(a) defined in Eqs.(6.9) and (6.10) are built up from ordinary irreps because $A^{-1}uA$, aA and $A^{-1}a$ are unitary operators. The group M is antiunitary because it consists of unitary and antiunitary operators u_i and $Au_i = a_i$, respectively.

The above coreps might be reducible . From the theory of irreps and coreps the irreducibility yields three cases (a, b and c). Koster et al. [26] have tabulated all irreps and coreps unitary and antiunitary point groups.

The set of matrices that we have constructed from the matrix representatives of irreps of unitary operators form what is called coreps of M. From what has been said so far their properties may depend on the choice of A.

When a group consists of unitary and antiunitary operators the following relations must be satisfied.

$$
\begin{aligned}
D(u)D(u') &= D(uu') \\
D(u)D(a) &= D(ua) \\
D(a)D^*(u) &= D(au) \qquad (6.11) \\
D(a)D^*(a') &= D(aa')
\end{aligned}
$$

(6.12)

where u and u' are in G and a and a' are in AG. Such coreps may be either reducible or irreducible. The complex conjugate that appears in above equations in general prevent D from being a homomorphism of M.

6.2 The three types of irreducible corepresentations.

The three cases of coreps can be summarised as follows (Wigner) [8](**Nobel prize in 1963**):

- **Case(a) or type I**

$$
\begin{aligned}
D(u) &= PD^*(A^{-1}uA)P^{-1}, \qquad (6.13) \\
PP^* &= D(A^2), \\
CD(u) &= D(u), \\
CD(a) &= \pm D(aA^{-1})P
\end{aligned}
$$

where P is unitary matrix.

The corep with the plus sign is equivalent to the corep with the minus sign.

- **Case(b) or type II**

  $D(u) = PD^*(A^{-1}uA)P^{-1}$

  $PP^* = -D(A^2)$

$$CD(u) = \begin{pmatrix} D(u) & 0 \\ 0 & D(u) \end{pmatrix} \tag{6.14}$$

and

$$CD(a) = \begin{pmatrix} 0 & -D(aA^{-1})P \\ D(aA^{-1})P & 0 \end{pmatrix} \tag{6.15}$$

- **Case(c) or type III**

  $D(u)$ is not equivalent to $D^*(u) = D^*(A^{-1}uA)$

$$CD(u) = \begin{pmatrix} D(u) & 0 \\ 0 & D^*(u) \end{pmatrix} \tag{6.16}$$

and

$$CD(a) = \begin{pmatrix} 0 & D(aA) \\ D^*(aA^{-1}) & 0 \end{pmatrix} \tag{6.17}$$

As we can see, it is very important to recognize the appropriate case of irreps of H in order to build the coreps. For example, taking the case of the Table D.10 of Appendix D, from the relation $(\frac{1}{|H|})\sum_u \chi(u)^2$ for Γ_{1-6} of C_6^6 we obtain $\Gamma_{1,2}$(a), $\Gamma_{3,4,5,6}$(c) and for physically irreps we have $\Gamma_{1,2}$(a), $\Gamma_{3,5}$ (c) and $\Gamma_{4,6}$(c).

Correspondingly, we use Eqs.(6.13) for coreps originating from $\Gamma_{1,2}$ and Eqs.(6.16, 6.17) for $\Gamma_{3,5}$ and $\Gamma_{4,6}$. The irreps and coreps of M = $C_{6v}^4(C_6^6)$ are listed in Appendix E. The set of matrices are of 4×4 dimensions for $C\Gamma_{3,5}$ and $C\Gamma_{4,6}$

The coreps listed in Appendix E are used for the classification of states and selection rules (SRs) for ZnO magnetic.

Regarding the coreps, their KPs are:

$$CD^i \otimes CD^j = \sum_k d_{ij,k} CD^k \tag{6.18}$$

where $d_{ij,k}$ indicates the number of times of CD^k contained in the KP.

The problem which rises here is to reduce the above KP and to see if there is a simple relationship between the Clebsch-Gordan coefficient series $d_{ij,k}$ and the Clebsch-Gordan coefficient series $c_{ij,k}$. According to Karavaev [27] $d_{ij,k}$ are of the form:

$$d_{ij,k} = \frac{1}{G} \sum_{u \in G} \chi^i(u)\chi^j(u)\chi^{k^*} / \frac{1}{g} \sum_{u \in G} \chi^k(u)\chi^{k^*}(u) \tag{6.19}$$

In Table 6.1 the $d_{ij,k}$ coefficients are defined in terms of $c_{ij,k}$ for all possible KPs of different kind of coreps (a, b, c).

It should be noted that the $d_{ij,k}$ are symmetrical with respect to the interchange of i and j.

$$d_{ij,k} = d_{ji,k} \tag{6.20}$$

However, the decomposition of KPs for magnetic space groups has not yet been tabulated. In Table 6.2, we calculated and tabulated the reduction of KPs of the coreps of the magnetic space group M = $P6_3m'c'$ at the Γ point of the Brillouin zone. The results tabulated in Table 6.2 will be used in the

Table 6.1: Clesch-Gordan coefficinet series for Kronecker products of irreducible corepresentations.

CD^i	CD^j	CD^k	$d_{ij,k}$
a	a	a	$c_{ij,k}$
a	a	b	$\frac{1}{2}c_{ij,k}$
a	a	c	$c_{ij,k}$
a	b	a	$2c_{ij,k}$
a	b	b	$c_{ij,k}$
a	b	c	$2c_{ij,k}$
a	c	a	$c_{ij,k} + c_{ij',k}$
a	c	b	$\frac{1}{2}c_{ij,k} + \frac{1}{2}c_{ij',k}$
a	c	c	$c_{ij,k} + c_{ij',k}$
b	b	a	$4c_{ij,k}$
b	b	b	$2c_{ji,k}$
b	b	c	$4c_{ji,k}$
b	c	a	$2c_{ij,k} + 2c_{ij',k}$
b	c	b	$c_{ij,k} + c_{ij',k}$
b	c	c	$2c_{ij,k} + 2c_{ij',k}$
c	c	a	$c_{ij,k} + c_{ij',k} + c_{i'j,k} + c_{i'j',k}$
c	c	b	$\frac{1}{2}c_{ij,k} + \frac{1}{2}c_{ij',k} + \frac{1}{2}c_{i'j,k} + \frac{1}{2}c_{i'j',k}$
c	c	c	$c_{ij,k} + c_{ij',k} + c_{i'j,k} + c_{i'j',k}$

Table 6.2: The reduction of KPs of the coreps of magnetic space group M = $P6_3m'c'$ at the Γ point of the Brilouin Zone

$\mathbf{C\Gamma_1}$	$\mathbf{C\Gamma_2}$	$\mathbf{C\Gamma_{3,5}}$	$\mathbf{C\Gamma_{4,6}}$	
$C\Gamma_1$	$C\Gamma_2$	$C\Gamma_{3,5}$	$C\Gamma_{4,6}$	$\mathbf{C\Gamma_1}$
	$C\Gamma_1$	$C\Gamma_{4,6}$	$C\Gamma_{3,5}$	$\mathbf{C\Gamma_2}$
		$2C\Gamma_1 + C\Gamma_{3,5}$	$2C\Gamma_2 + C\Gamma_{4,6}$	$\mathbf{C\Gamma_{3,5}}$
			$2C\Gamma_1 + C\Gamma_{3,5}$	$\mathbf{C\Gamma_{4,6}}$

analysis of S.Or.Ph.Tr. in magnetic ZnO.

6.3 Symmetrized and antisymmetrized power of corepresentations of the magnetic groups

In the section 2, we have showed that any KP of ordinary irreps $D^i \otimes D^i$ can be decomposed into two parts:

$$D^i \otimes D^i = \left[D^i \otimes D^i\right] \oplus \left\{D^i \otimes D^i\right\} \tag{6.21}$$

where the $[D^i \otimes D^i]$, or $[D^i]^2$ are symmetrized squares (SQ) and $\{D^i \otimes D^i\}$ or $\{D^i\}^2$ are antisymmetrized squares (ASQ).
Similarly, for KPs of coreps:

$$CD^i \otimes CD^i = \sum_k d_{ii,k} CD^k \tag{6.22}$$

where the Clebsch-Gordan coefficients series for the KPs of coreps $d_{ii,k}$ are given in [6] see Table 6.1.

If we separate the KP $D^i \otimes D^i$ into $[D^i]^2$ and $\{D^i\}^2$, for symmetrized and antisymmetrized products we have:

$$\left[D^i\right]^2 = \sum_k c^s_{2i,k} D^k \tag{6.23}$$

similarly for the antisymmetrized product:

$$\left\{D^i\right\}^2 = \sum_k c^a_{2i,k} D^k \tag{6.24}$$

The next question is to determine the coefficients $d^s_{2i,k}$ and $d^a_{2i,k}$ in terms of $c^s_{2i,k}$ and $c^a_{2i,k}$, respectively in the following reductions:

$$\left[CD^i\right]^2 = \sum_k d^s_{2i,k} CD^k \tag{6.25}$$

and

$$\left\{CD^i\right\}^2 = \sum_k d^a_{2i,k} CD^k \tag{6.26}$$

If the irrep D^k accurs only in $\{D^i\}^2$ or only in $[D^i]^2$ then the $c^a_{2i,k}$ and $c^s_{2i,k}$ are immediately available (CDML). Therefore $d^a_{2i,k}$ and d^s_{2ik} are obtained directly by using the Table 6.1. However, if the irrep D^k occurs both in $[D^i]^2$ and $\{D^i\}^2$ the procedure for determining $d^a_{2i,k}$ and $d^s_{2i,k}$ is different [6].

Now let us suppose that $(CD^i) \downarrow H$ denotes the representation of H, the unitary subgroup of M, obtained by taking the matrices of CD^i for the elements of H.

We can identify the irreps of the unitary subgroup H which lead to those coreps of M that are present $\{CD^i\}^2$ by reducing $\{(CD^i) \downarrow H\}^2$.

Let us now let for example $a_{2i,k}$ be the number of times that D^k occurs in $\{(CD^i) \downarrow H\}^2$

$$\left\{(CD^i) \downarrow H\right\}^2 = \sum_k a_{2i,k} D^k \tag{6.27}$$

- If CD^i belongs to case (a)[6]

$$\left\{(CD^i) \downarrow H\right\}^2 = \{D^i\}^2 \tag{6.28}$$

- while if CD^i belongs to case (b) or (c)[6]

$$\left\{(CD^i) \downarrow H\right\}^2 = \{D^i\}^2 \oplus \{\bar{D}^i\}^2 \oplus D^i \otimes \bar{D}^i \tag{6.29}$$

If CD^i belongs to case (b) Eq.(6.29) can be simplified because $\bar{D}^i \equiv D^i$ so that

$$\left\{(CD^i) \downarrow H\right\}^2 = 2\{D^i\}^2 \oplus D^i \otimes D^i \tag{6.30}$$

Therefore, if CD^i belongs to case (a), the coefficient $a_{2i,k}$ is identical to $c_{2i,k}$ of Eq.(6.28) while if CD^i belongs to case (b) or (c), the coefficients $a_{2i,k}$ can be determined by inspection using Eqs. (6.30) or (6.29), respectively.
Having found the coefficients $a_{2i,k}$, the coefficients $d^a_{2i,k}$ can be obtained by using the rules given in the last column of Table 6.3. The coefficients $d^s_{2i,k}$ in

Table 6.3: The reduction of the antisymmetrized square $\{CD^i\}^2$ at the Γ point

$C\Gamma^i$	$\sum_k a_{2i,k}\Gamma^k$	$d^a_{2i,k}$
Case (a)	$\{\Gamma_i\}^2$	$a_{2i,k}$
Case (b)	$2\{\Gamma_i\}^2 \oplus \Gamma_i \otimes \Gamma_i$	$\frac{1}{2}a_{2i,k}$
Case (c)	$\{\Gamma_i\}^2 \oplus \{\bar{\Gamma}_i\}^2 \oplus \Gamma_i \otimes \bar{\Gamma}_i$	$a_{2i,k}$

the reduction of the symmetrized square can be determined when $d^a_{2i,k}$ has

been already determined.

$$d^s_{2i,k} + d^a_{2i,k} = d_{ii,k} \tag{6.31}$$

The problem of the reduction of the symmetrized cube $[CD^i_i]^3$ and the antisymmetrized cube $\{CD^i\}^3$ can be approached in very similar way to the reduction of the square [6]. Thus for case (a), case (b) and case (c) we obtain:

$$\left[(CD^i)\downarrow H\right]^3 = \left[D^i\right]^3 \tag{6.32}$$

for case (a)

$$\left[(CD^i)\downarrow H\right]^3 = 2\left[D^i\right]^3 \oplus 2\left[D^i\right]^2 \otimes D^i \tag{6.33}$$

for case (b)

$$\left[(CD^i)\downarrow H\right]^3 = \left[D^i\right]^3 \oplus \left[\bar{D}^i\right]^3 \oplus \left[D^i\right]^2 \otimes \bar{D}^i \oplus \left[\bar{D}^i\right]^2 \otimes D^i \tag{6.34}$$

for case (c).

The summary of the above prescriptions are found in Table 6.4 for the reduction of $[CD^i]^3$ where :

$$\left[(CD^i)\downarrow H\right]^3 = \sum_k s_{3i,k} D^k \tag{6.35}$$

$$\left[CD^i\right]^3 = \sum_k d^s_{3i,k} CD^k \tag{6.36}$$

In the following section, we will use the theory of antiunitary groups discussed in section 4 to investigate the S.Or.Ph.Tr. in magnetic compounds. The theory of LLL of S.Or.Ph.Tr. in magnetic crystals involves coreps.

Table 6.4: The reduction of the symmetrized cube of $[C\Gamma_i]^3$ at the point Γ

$C\Gamma_i$	$\sum_k s_{3i,k}\Gamma_k$	$d_{3i,k}$
Case (a)	$[\Gamma_i]^3$	$s_{3i,k}$
Case (b)	$2\,[\Gamma_i]^3 \oplus 2\,[\Gamma_i]^2 \otimes \Gamma_i$	$\frac{1}{2}s_{3i,k}$
Case (c)	$[\Gamma_i]^3 \oplus \left[\bar{\Gamma}_i\right]^3 \oplus [\Gamma_i]^2 \otimes \bar{\Gamma}_i \oplus \left[\bar{\Gamma}_i\right]^2 \otimes \Gamma_i$	$s_{3i,k}$

Chapter 7

The second-Order phase transitions in magnetic ZnO

In this section we turn to the question of the adaptation of Landau's theory to the particular case of magnetic phase transitions.

For a magnetic transition we use **M(r)**, the magnetization, as the order parameter. The sign of **M(r)** is changed by θ, the operation of time-reversal symmetry, whereas G(p,T,η), the Gibbs function, is unaffected by the operation of time- reversal.

It was argued by Landau that in the expansion of G(p,T,η) in power of **M(r)** all terms with odd powers of **M(r)** should be identically zero and therefore all transitions between paramagnetic phase and magnetically ordered phase with the same crystallographic structure have the possibility of being continuous transitions.

The thermodynamical results which were summarized in group theoretical terms in case of non-magnetic crystal and which have been used to predict whether or not a given phase transition can be continuous, can be adapted

to the case of transitions between two different magnetically ordered phases [6].

To emphasize that we are now concerned with non unitary magnetic groups, Let us replace G_0 and G_1 by symbols M_0 and M_1 and D^l by CD^l, the irreducible corepresentations of M_0 to which the order parameter η belongs. It is then possible to rewrite conditions for second-order phase transitions in a form appropriate to magnetic phase transitions [2]

1. M_1 must be a subgroup of M_0.

2. $\left[CD^l\right]_3$ must not contain CD^l_1 of M_0.

3. $\left\{CD^l\right\}_2$ must not contain the corepresentation to which a polar vector belongs.

These conditions involve the reduction of the antisymmetrized square $\left\{CD^l\right\}_2$ and the symmetrized cube $\left[CD^l\right]_3$ of an irreducible corepresentation CD^l_i developed in section 6 (see Tables 6.3 and 6.4). The Table 7.1 summarizes the coreps that are involved in the S.Or.Ph.Tr to the lower magnetic space group symmetries.

[2]From the Table 7.1 it is seen that for example corep $C\Gamma_2$ causes S.O.Ph.Tr and bring ZnO magnetic crystal with $C^4_{6v}(C^6_6)(P6_3m'c')$ symmetry to the magnetic subgroup $C^1_{3v}(C^1_3)(P3m'1)$. It means that soft modes of symmetry $C\Gamma_2$ with very low momentum $\hbar\bar{k} \cong 0$ with the change of applied temperature, change their equilibrium position from $C\bar{k}_\Gamma$ of $P6_3m'c'$ to $C\bar{k}_\Gamma$ of $P3m'1$.

Table 7.1: Active irreducible corepresentations of initial magnetic space groups: $M_0 \equiv C_{6v}^4(C_6^6)(P6_3m'c')$, $C_{6v}^4(C_{3v}^4)(P6_3'm'c)$, $C_{6v}^4(C_{3v}^1)(P6_3'mc')$ that may cause S.Or.Ph.Trs by active modes of $C\Gamma$, CA, to lower magnetic space group symmetry M^2.

Symmetry operators of the magnetic group of high symmetry: M_0	Subgroups of the magnetic group of high symmetry: M_1
$C_{6v}^4(C_6^6)$:$P6_3m'c'$ (1, 2.1, 3, 4.1, 5, 6.1, θ19, θ20.1, θ21, θ22.1, θ23, θ24.1)	$P6_3m'c' \xrightarrow{C\Gamma_2,CA_2} C_{3v}^1(C_3^1)$:$P3m'1$(1, 3, 5, θ19, θ21, θ23)
$C_{6v}^4(C_{3v}^4)$:$P6_3'm'c$(1, 3, 5, 20.1, 22.1, 24.1, θ2.1, θ4.1, θ6.1, θ19, θ21, θ23)	$P6_3'm'c \xrightarrow{C\Gamma_2,CA_2} C_6^6(C_3^1)$:$P63'$(1, 3, 5, θ2.1, θ4.1, θ6.1)
$C_{6v}^4(C_{3v}^4)$:$P6_3'mc'$(1, 3, 5, 19, 21, 23,θ2.1, θ4.1, θ6.1, θ20.1, θ22.1, θ24.1)	$P6_3'mc' \xrightarrow{C\Gamma_2,CA_2} C_6^6(C_3^1)$:$P63'$(1, 3, 5, θ2.1, θ4.1, θ6.1)

7.1 The theory of Raman scattering in magnetic materials

In the section, we develop the theory of Raman scattering adapted to magnetic crystals and use it to interpret different intensities of the picks of the Raman spectra of ZnO magnetic (see Table 7.2).

Let I_i and I_s be the intensity of the incident and the scattered radiation respectively, and $\hat{e}_i$ and $\hat{e}_s$ be the electric field unit vectors of the incident and scattered radiation respectively and $\tilde{X}$ be the Raman tensor of the excitation under consideration. Then the scattered intensity I_s is given by

$$I_s = C_0 I_i |\hat{e}_s \tilde{X} \hat{e}_i|^2 \tag{7.1}$$

where C_0 is a constant related to the frequencies of the incident and scattered radiations and the power spectrum of the excitation involved. A magnetic

materials usually has strong absorption it is desirable to study the Raman spectra in a back-scattering arrangement. The incident and scattered radiations travel along the $\pm Z$ axis and the material occupy $Z \sup 0$ space. Then the incident intensity at a position Z is given by

$$I_i(Z) = I_i(0)e^{-\alpha Z} \tag{7.2}$$

where $I_i(0)$ is the intensity of the incident radiation at the material surface and α is the material absorption coefficient. In the presence of the magnetic field Faraday rotation takes place and the polarization of the incident radiation at the position Z is given by

$$\hat{e}_i(Z) = \tilde{T}_F \hat{e}_i(0) \tag{7.3}$$

where $\hat{e}_i(Z)$ and $\hat{e}_i(0)$ are electric field unit vectors at a position Z and the material surface, and $\tilde{T}_F$ is the transformation tensor which rotates the electric field vector to a direction θ given by

$$\theta = \theta_F Z \tag{7.4}$$

where θ_F is the specific Faraday rotation defined as the angle of rotation of the material of unit length. The total intensity of the back-scattered radiation is given by

$$I_s = \int_0^\infty C_0 I_i\left(0\right) |\hat{e}_s\left(0\right) \tilde{T}_F \tilde{X} \tilde{T}_F \hat{e}_i\left(0\right)|^2 e^{-2\alpha Z} dZ \tag{7.5}$$

The exponential $e^{-2\alpha Z}$ appears due to the fact that the radiation travels twice the distance Z in the back-scattering arrangement.

The symbols $\hat{e}_i(0), \hat{e}_s(0), \tilde{T}_F$ and $\tilde{X}$ have the following matrix:

$$\hat{e}_i(0) = \begin{bmatrix} \alpha_1 \\ \alpha_2 \\ 0 \end{bmatrix}, \hat{e}_s = \begin{bmatrix} \beta_1 & \beta_2 & 0 \end{bmatrix}, \tilde{T}_F = \begin{bmatrix} cos\theta & sin\theta & 0 \\ -sin\theta & cos\theta & 0 \\ 0 & 0 & 1 \end{bmatrix}, \tilde{X} = \begin{bmatrix} a & b & e \\ c & d & g \\ f & h & i \end{bmatrix}, \tag{7.6}$$

If we introduce these expressions in Eq.(7.5) and integrating it one obtains the following expressions:

$$\begin{aligned} I_s &= \frac{C_0 I_i(0)}{2\alpha}\left[\frac{A^2+B^2+2C^2}{2} + \frac{B^2-A^2}{2(1+16Q^2)} + \frac{2BC}{(1+4Q^2)} + \right. \\ &+ \left. \frac{4QCA}{(1+4Q^2)} + \frac{4QAB}{(1+16Q^2)}\right] \end{aligned} \tag{7.7}$$

where $Q = \frac{\theta_E}{2\alpha}$ is called figure of merit and is a characteristic property of the material and A, B and C are constant given by:

$$\begin{aligned} A &= \frac{1}{2}[a(\alpha_2\beta_1 - \alpha_1\beta_2) - b(\alpha_1\beta_1 + \alpha_2\beta_2) + c(\alpha_1\beta_1 + \alpha_2\beta_2) \\ &+ d(\alpha_2\beta_1 - \alpha_1\beta_2)] \end{aligned} \tag{7.8}$$

$$\begin{aligned} B &= \frac{1}{2}[a(\alpha_1\beta_1 + \alpha_2\beta_2) + b(\alpha_2\beta_1 - \alpha_1\beta_2) + c(\alpha_1\beta_2 - \alpha_2\beta_1) \\ &+ d(\alpha_2\beta_2 + \alpha_1\beta_1)] \end{aligned} \tag{7.9}$$

$$\begin{aligned} C &= \frac{1}{2}[a(\alpha_1\beta_1 - \alpha_2\beta_2) + b(\alpha_2\beta_1 + \alpha_1\beta_2) + c(\alpha_1\beta_2 + \alpha_2\beta_1) \\ &+ d(\alpha_2\beta_2 - \alpha_1\beta_1)] \end{aligned} \tag{7.10}$$

In the absence of Faraday rotation Q = 0 and Eq.(7.7) becomes:

$$I_s' = \frac{C_0 I_i(0)}{2\alpha}(B + C) \tag{7.11}$$

For non-absorbing crystals, $\alpha = 0$ and therefore, Q is no longer a well-defined property of the material. Under such conditions, the intensity of the scattered radiation is given by,

$$\begin{aligned} I_s &= C_0 I_i(0) \Big[U^2 \int cos^4(\theta_F Z)dZ + V^2 \int sin^4(\theta_F Z)dZ + \\ &+ W^2 \int sin^2(\theta_F Z)cos^2(\theta_F Z)dZ + 2UV \int sin^2(\theta_F Z)cos^2(\theta_F Z)dZ + \\ &+ 2VW \int sin^3(\theta_F Z)dZ + 2UW \int sin(\theta_F Z)cos^3 dZ \Big] \end{aligned} \tag{7.12}$$

where, U = B + C, V = C - B and W = 2A

If we assume that the thickness (L) of the sample is finite along the Z direction the Eq.(7.12) becomes:

$$\begin{aligned} I_s &= \frac{C_0 I_i(0)}{\theta_F} \Big[U^2 \left(\frac{12\theta_F L + 8sin2\theta_F L + sin4\theta_F L}{32}\right) + \\ &+ V^2 \left(\frac{12\theta_F L - 8sin4\theta_F L}{32}\right) + (2UV + W^2)\times \\ &\times \left(\frac{4\theta_F L - sin4\theta_F L}{32}\right) + \frac{2VW sin^4\theta_F L}{4} + \frac{2UW(1 - cos^4\theta_F L)}{4} \end{aligned} \tag{7.13}$$

If $\theta_F L = 2n\pi$ where n is an integer the Eq.(7.13) becomes:

$$I_s = C_0 I_i(0) L \left[C^2 + \frac{1}{2}(A^2 + B^2)\right] \tag{7.14}$$

Further, in the absence of the Faraday rotation, ($\theta_F = 0$) Eq.(7.13) gives the scattered intensity as zero. It is understandable because the only mechanism for back-scattering in this formulation is the Faraday rotation.

Thus, from Eqs (7.7) and (7.12) it is clear that the intensity of the scattered rotation depends on θ_F irrespective of whether the material is absorbing or not. Using the formulas developed in this part we have found the intensities of scattered light for C_{4v}^4 . The adjusting intensities that we have got from the Table 7.2 are in good agreement with our Raman spectra in magnetic ZnO of section 8.

Table 7.2: Calculated intensities
where $I_A = \frac{C_0 I_i(0) a^2}{2\alpha}$, $I_E = \frac{C_0 I_i(0) b^2}{2\alpha}$, $I_r = \frac{C_0 I_i(0) d^2}{2\alpha}$

	$\langle 100\rangle_\perp$		$\langle 100\rangle_\parallel$		$\langle 110\rangle_\perp$		$\langle 110\rangle_\parallel$		$\langle 100\rangle_{45^0}$	
Phonon mode	I'_s	I_s	I'_s	I_s	I'_s	I_s	I'_s	I_s	I'_s	I_s
Γ_1	0	$I_A\frac{8Q^2}{1+16Q^2}$	I_A	$I_A\frac{1+8Q^2}{1+16Q^2}$	0	$I_A\frac{8Q^2}{1+16Q^2}$	I_A	$I_A\frac{1+8Q^2}{1+16Q^2}$	$\frac{I_A}{2}$	$\frac{I_A}{2}(1+\frac{4Q}{1+16Q^2})$
Γ_2	0	0	I_E	I_E	I_E	I_E	0	0	$\frac{I_E}{2}$	$\frac{I_E}{2}$
Γ_3	0	$\frac{I_E}{3}\frac{8Q^2}{1+16Q^2}$	$\frac{I_E}{3}$	$\frac{I_E}{3}\frac{1+8Q^2}{1+16Q^2}$	0	$\frac{I_E}{3}\frac{8Q^2}{1+16Q^2}$	$\frac{I_E}{3}$	$\frac{I_E}{3}\frac{1+8Q^2}{1+16Q^2}$	$\frac{I_E}{6}$	$\frac{I_E}{6}(1+\frac{4Q}{1+16Q^2})$
Γ_4	I_r	I_r	0	0	0	0	I_r	I_r	$\frac{I_r}{2}$	$\frac{I_r}{2}$
Γ_5	0	0	0	0	0	0	0	0	0	0
Γ_6	0	0	0	0	0	0	0	0	0	0

Chapter 8

Raman experimental spectra of magnetic ZnO and discussions

8.1 Discussions

The Raman active modes in magnetic crystals are obtained by the decomposition of the KP of the vector corepresentation.
The corerepresentations in the symmetrized KP are Raman active modes.
We have six Raman active modes at the Zone center of the BZ:
$[(C\Gamma_1 \oplus C\Gamma_{4,6})(C\Gamma_1 \oplus C\Gamma_{4,6})] = 2C\Gamma_1 \oplus C\Gamma_{3,5} \oplus C\Gamma_{4,6}$ because the vector representation of ZnO non magnetic is the same as in ZnO magnetic.
The Figure 8.2 shows the room temperature Raman spectra of pure and Mn-doped ZnO (magnetic) bulk crystal.
Five modes are observed in both the two Raman spectra in the region 100 cm^{-1} - 900 cm^{-1}[31]:

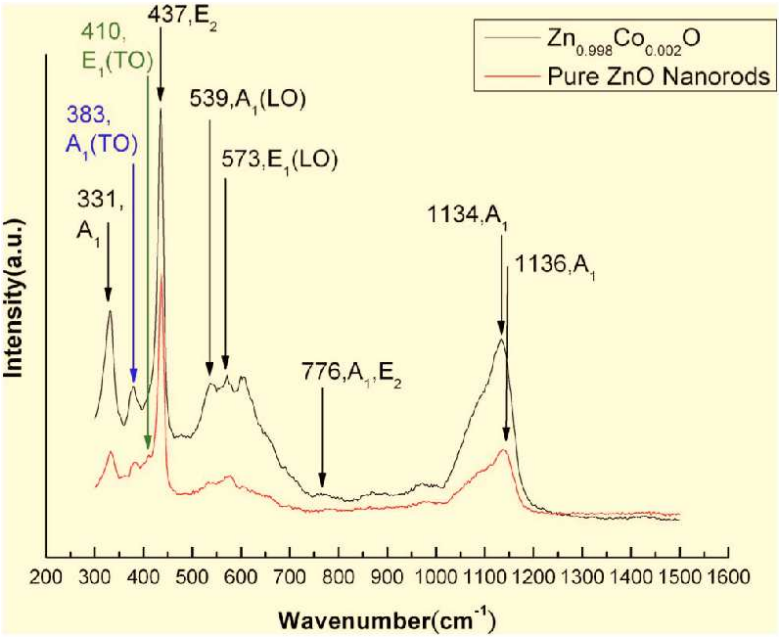

Figure 8.1: Raman spectra of the Co-doped ZnO [33]

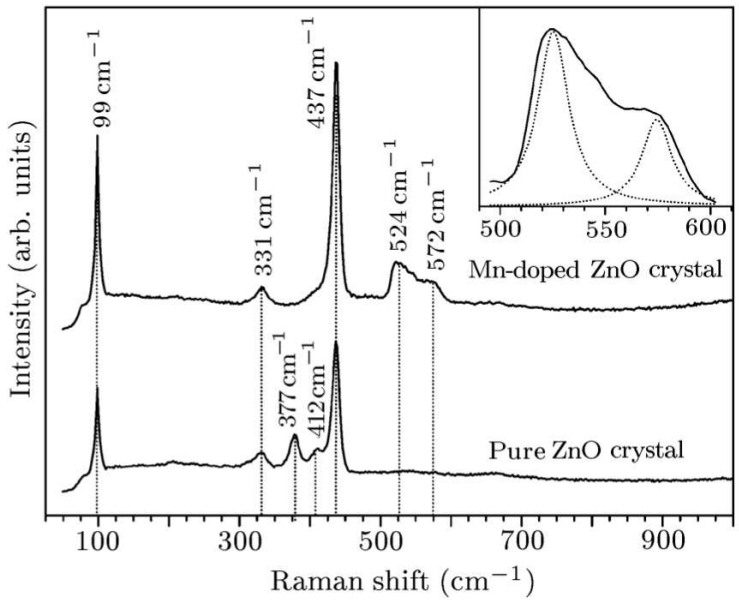

Figure 8.2: Room-temperature Raman spectra of pure and Mn-doped ZnO single crystal [31]

- For pure ZnO: we see several lines at 99, 331, 377, 412, and 437 cm^{-1}. These lines correspond to the symmetry allowed modes: E_2-low, A_1-TO , E_1- TO and E_2-high , respectively.

- For Mn-doped ZnO: we see several lines at 99, 331, 437, 524, and 572 cm^{-1} These lines correspond to the symmetry allowed modes: $E_2(C\Gamma_{4,6})$-low, $E_2(C\Gamma_{4,6})$-high, Mn feature [32], and $A_1(C\Gamma_1)$-LO, respectively.

From the Figure 8.1 in the region 300 cm^{-1}- 1200 cm^{-1}, we see for Co-doped Zno several lines at 383, 410, 438, 540 and 584cm^{-1} [33].

The lines correspond to $A_1(C\Gamma_1)$ (TO), $E_1(C\Gamma_{3,5})$ (TO), $E_2(C\Gamma_{4,6})$, $A_1(C\Gamma_1)$ (LO) and $E_1(C\Gamma_{3,5})$ (LO) Raman modes respectively. The other lines are assigned to be overtones and combinations [33]. The first-order Raman active modes are observed in both ZnO non and magnetic. By Analysing the Raman spectra of both Zno magnetic and non magnetic we observe the change in Raman activity in magnetic ZnO due to the lowering of the crystal symmetry. Such lowering of the crystal symmetry would result in the observation of more Raman frequencies.

Peng-Xiang (1983) has traced the origin of these additional frequencies to the effect of Faraday rotation on the phonon Raman scattering causing intensity anomalies. Using our group theoretical techniques, we explain the additional picks by the number of degeneracy of the phonons due to the increase in dimensions of the corepresentations describing the phonons symmetries. The Raman spectroscopy is able to identify to which subgroup ZnO magnetic goes after transitions by analysing the Raman active modes of the Raman spectra of the subgroups. Here we mean that the Raman phonon modes of ZnO magnetic Raman spectra responsible for S.Or.Ph.Tr must be found in the Raman spectra of the subgroup.

Chapter 9

Conclusion

The calculation of irreps and coreps using theoretical techniques are in general tedious, lengthy and complex.

The ordinary Landau-Lifschitz theory for non-magnetic crystals has been reformulated and expanded to magnetic crystals. In this context, the thesis for the first provides the novel conceptual framework for magnetic structural phase transitions. The group-subgroup relation in magnetic crystals as well as their coreps have been derived in the framework of Wigner theory.

In addition, the exact symmetries of phonons involved in S.Or.Ph.Tr. were determined. A comparison of non magnetic and magnetic crystals yielding the phonon degeneracies were determined. These findings are supported by the experimental Raman spectra of Cobalt and manganese doped ZnO.

It is crucial to take into account the hidden time reversal symmetry in magnetic crystals described by antiunitary operator such as time reversal symmetry. This is a clear evidence of the effect of time reversal symmetry on the coreps of phonons inducing structural phase transitions.

Therefore, this thesis opened up the investigation of elementary excitations

in magnetic crystals and their further applications.

Also the symmetrized and antisymmetrized Konecker products are still to be considered. They play a role in understanding the interactions like spin-spin, spin lattice, pressure and temperature induced phase transitions.

The special selection rules in magnetic crystals for optical and structural transitions need to be considered.

Appendices

Appendix A

Vector representations for hexagonal crystallographic point groups

Table A.1: Vector representations for Hexagonal crystallographic point groups

M & L	B & C			M & L	B & C		
1	E	x, y, z	$\begin{pmatrix}1&0&0\\0&1&0\\0&0&1\end{pmatrix}$	13	I	$-x, -y, -z$	$\begin{pmatrix}-1&0&0\\0&-1&0\\0&0&-1\end{pmatrix}$
2	C_6^+	x-y,x,z	$\begin{pmatrix}1&-1&0\\1&0&0\\0&0&1\end{pmatrix}$	14	S_3^-	-x+y,-x,-z	$\begin{pmatrix}-1&1&0\\-1&0&0\\0&0&-1\end{pmatrix}$
3	C_3^+	-y,x-y,z	$\begin{pmatrix}0&-1&0\\1&-1&0\\0&0&1\end{pmatrix}$	15	S_6^-	y,-x+y,-z	$\begin{pmatrix}0&1&0\\-1&1&0\\0&0&-1\end{pmatrix}$
4	C_2	-x,-y,z	$\begin{pmatrix}-1&0&0\\0&-1&0\\0&0&1\end{pmatrix}$	16	σ_h	x,y,-z	$\begin{pmatrix}1&0&0\\0&1&0\\0&0&-1\end{pmatrix}$
5	C_3^-	-x+y,-x,z	$\begin{pmatrix}-1&+1&0\\-1&0&0\\0&0&1\end{pmatrix}$	17	S_6^+	x-y,x,-z	$\begin{pmatrix}1&-1&0\\1&0&0\\0&0&-1\end{pmatrix}$
6	C_6^-	y,-x+y,z	$\begin{pmatrix}0&1&0\\-1&1&0\\0&0&1\end{pmatrix}$	18	S_3^+	-y,x-y,-z	$\begin{pmatrix}0&-1&0\\1&-1&0\\0&0&-1\end{pmatrix}$
7	C_{21}''	x-y,-y,-z	$\begin{pmatrix}1&-1&0\\0&-1&0\\0&0&-1\end{pmatrix}$	19	σ_{v1}	-x+y,y,z	$\begin{pmatrix}-1&1&0\\0&1&0\\0&0&1\end{pmatrix}$
8	C_{22}'	x,x-y,-z	$\begin{pmatrix}1&0&0\\1&-1&0\\0&0&-1\end{pmatrix}$	20	σ_{d2}	-x,-x+y,z	$\begin{pmatrix}-1&0&0\\-1&1&0\\0&0&1\end{pmatrix}$
9	C_{23}''	y,x,-z	$\begin{pmatrix}0&1&0\\1&0&0\\0&0&-1\end{pmatrix}$	21	σ_{v3}	-y,-x,z	$\begin{pmatrix}0&-1&0\\-1&0&0\\0&0&1\end{pmatrix}$
10	C_{21}'	-x+y,y,-z	$\begin{pmatrix}-1&1&0\\1&0&0\\0&0&-1\end{pmatrix}$	22	σ_{d1}	x-y,-y,z	$\begin{pmatrix}1&-1&0\\-1&0&0\\0&0&1\end{pmatrix}$
11	C_{22}''	-x,-x+y,-z	$\begin{pmatrix}-1&0&0\\-1&1&0\\0&0&-1\end{pmatrix}$	23	σ_{v2}	x,x-y,z	$\begin{pmatrix}1&0&0\\1&-1&0\\0&0&1\end{pmatrix}$
12	C_{23}'	-y,-x,-z	$\begin{pmatrix}0&-1&0\\-1&0&0\\0&056&-1\end{pmatrix}$	24	σ_{d3}	y,x,z	$\begin{pmatrix}0&1&0\\1&0&0\\0&0&1\end{pmatrix}$

Table A.2: Example of basis functions for C_6^6 a subgroup of C_{6v}^4 at Γ point of the Brillouin zone; $w = \exp\left(\frac{-i2\pi}{3}\right)$.

	E (1)	$C_6(2)$	$C_3(3)$	$C_2(4)$	$C_3^2(5)$	$C_6^5(6)$	Basis ψ
Γ_1	1	1	1	1	1	1	z^2 (Γ_1)
Γ_2	1	-1	1	-1	1	-1	z(x $\pm iy)^3$ (Γ_2)
Γ_3	1	w	w^2	1	w	w^2	$(x+iy)^2$ (Γ_3)
Γ_4	1	w^2	w	1	w^2	w	$(x-iy)^2$ (Γ_4)
Γ_5	1	-w	w^2	-1	w	$-w^2$	$z(x-iy)$ (Γ_5)
Γ_6	1	$-w^2$	w	-1	w^2	-w	$z(x+iy)$ (Γ_6)

Appendix B

Table of hexagonal and trigonal ordinary space groups in 3 dimensions (CDML)

Table B.1: Crystal system:Trigonal (25)

Group number	Schonflies notation	International notation
143-146	C_3	P3,$P3_1$,$P3_2$,R3
147-148	S_6	P3,R3
149-155	D_3	P312,P312,$P3_112$,$P3_121$,$P3_212$,$P3_221$,R32
156-161	C_{3v}	P3m1,P31m,P3c1,P31c,R3m,R3c
162-167	D_{3d}	P31m,P31c,P3m1,P3c1,R3m,R3c

Table B.2: Crystal system:Hexagonal (27)

Group number	Schonflies notation	International notation
168-173	C_6	P6,$P6_1$,$P6_5$,$P6_2$,$P6_4$,$P6_3$
174	C_{3h}	P6
175-176	C_{6h}	P6/m,$P6_3/m$
177-182	D_6	P622,$P6_122$,$P6_522$,$P6_222$,$P6_422$,$P6_322$
183-186	C_{6v}	P6mm,P6cc,$P6_3cm$,$P6_3mc$
187-190	D_{3h}	P6m2,P6c2,P62m,P62c
191-194	D_{6h}	P6/mmm,P6/mcc,$P6_3/mcm$,$P6_3/mmc$

Appendix C

Symmetrized and antisymmetrized squares of irreps for ZnO at Γ, A, H, K, L, and M points and lines in the BZ

$\Gamma \ominus \Gamma = \Gamma$
Channel 1: $(1)k_\Gamma + (1)k_\Gamma = k_\Gamma$
$\Gamma_1 \otimes \Gamma_1 = \Gamma_2 \otimes \Gamma_2 = \Gamma_3 \otimes \Gamma_3 = \Gamma_4 \otimes \Gamma_4 = [\Gamma_1] \oplus \{\}$
$\Gamma_5 \otimes \Gamma_5 = \Gamma_6 \otimes \Gamma_6 = [\Gamma_1 \oplus \Gamma_5] \oplus \{\Gamma_2\}$
$\Gamma_7 \otimes \Gamma_7 = \Gamma_8 \otimes \Gamma_8 = [\Gamma_2 \oplus \Gamma_6] \oplus \{\Gamma_1\}$
$\Gamma_9 \otimes \Gamma_9 = [\Gamma_2 \oplus \Gamma_3 \oplus \Gamma_4] \oplus \{\Gamma_1\}$

$A \otimes A = \Gamma$

Channel 1: $(1)k_A + (1)k_A = k_\Gamma$
$A_1 \otimes A_1 = A_2 \otimes A_2 = A_3 \otimes A_3 = A_4 \otimes A_4 = [\Gamma_4] \oplus \{\}$
$A_5 \otimes A_5 = A_6 \otimes A_6 = [\Gamma_4 \oplus \Gamma_6] \oplus \{\Gamma_3\}$
$A_7 \otimes A_7 = A_8 \otimes A_8 = [\Gamma_3 \oplus \Gamma_5] \oplus \{\Gamma_4\}$
$A_9 \otimes A_9 = [\Gamma_1 \oplus \Gamma_2 \oplus \Gamma_3] \oplus \{\Gamma_4\}$

$H \otimes H = \Gamma \oplus K$

Channel 1: $(1)k_H + (2)k_H = k_\Gamma$	Channel 2: $(2)k_H + (2)k_H = k_K$
$H_1 \otimes H_1 = H_2 \otimes H_2 = [] \oplus \{\}$	$[K_2] \oplus \{\}$
$H_3 \otimes H_3 = [\Gamma_4] \oplus \{\Gamma_2\}$	$[K_2 \oplus K_3] \oplus \{K_1\}$
$H_4 \otimes H_4 = H_5 \otimes H_5 = [\Gamma_2] \oplus \{\Gamma_4\}$	$[K_1] \oplus \{\}$
$H_6 \otimes H_6 = [\Gamma_2 \oplus \Gamma_3 \oplus \Gamma_5] \oplus \{\Gamma_1 \oplus \Gamma_4 \oplus \Gamma_6\}$	$[K_1 \oplus K_3] \oplus \{K_2\}$

$K \otimes K = \Gamma \oplus K$

Channel 1: $(1)k_K + (1)k_K = k_\Gamma$	Channel 2: $(2)k_K + (2)k_K = k_K$
$K_1 \otimes K_1 = K_2 \otimes K_2 = [\Gamma_1] \oplus \{\Gamma_3\}$	$[K_1] \oplus \{\}$
$K_3 \otimes K_3 = [\Gamma_1 \oplus \Gamma_4 \oplus \Gamma_5] \oplus \{\Gamma_2 \oplus \Gamma_3 \oplus \Gamma_6\}$	$[K_1 \oplus K_3] \oplus \{K_1\}$
$K_4 \otimes K_4 = K_5 \otimes K_5 = [\Gamma_3] \oplus \{\Gamma_1\}$	$[K_2] \oplus \{\}$
$K_6 \otimes K_6 = [\Gamma_2 \oplus \Gamma_3 \oplus \Gamma_6] \oplus \{\Gamma_1 \oplus \Gamma_4 \oplus \Gamma_5\}$	$[K_2 \oplus K_3] \oplus \{K_1\}$

$L \otimes L = \Gamma \oplus M$
Channel 1: $(1)k_L + (1)k_L = k_\Gamma$
$L_1 \otimes L_1 = L_2 \otimes L_2 = L_3 \otimes L_3 = L_4 \otimes L_4 = [\Gamma_4 \oplus \Gamma_6] \oplus \{\}$
$L_5 \otimes L_5 = [\Gamma_1 \oplus \Gamma_2 \oplus \Gamma_3 \oplus 2\Gamma_5 \oplus \Gamma_6] \oplus \{\Gamma_4 \oplus \Gamma_6\}$
Channel 2: $(2)k_L + (3)k_L = k_M$
$[M_4] \oplus \{M_3\}$
$[M_1 \oplus M_2 \oplus 3M_3] \oplus \{M_1 \oplus M_2 \oplus 2M_4\}$

$M \otimes M = \Gamma \oplus M$
Channel 1: $(1)k_M + (1)k_M = k_\Gamma$
$M_1 \otimes M_1 = M_2 \otimes M_2 = M_3 \otimes M_3 = M_4 \otimes M_4 = [\Gamma_1 \oplus \Gamma_5] \oplus \{\}$
$M_5 \otimes M_5 = [\Gamma_1 \oplus \Gamma_3 \oplus \Gamma_4 \oplus \Gamma_5 \oplus 2\Gamma_6] \oplus \{\Gamma_1 \oplus \Gamma_5\}$
Channel 2: $(2)k_M + (3)k_M = k_M$
$[M_1] \oplus \{M_2\}$
$[2M_2 \oplus M_3 \oplus M_4] \oplus \{2M_1 \oplus M_3 \oplus M_4\}$

Appendix D

Irreps of $C_{6v}^4, C_6^6, C_{3v}^4$ and C_{3v}^1 at Γ, A, H, K, L and M point of Brillouin zone (BZ); with $w = -\frac{1}{2} + \frac{\sqrt{3}}{2}i$

Table D.1: Irreducible representations of C_{6v}^4 for G^{k_Γ}

	1	2.1	3	4.1	5	6.1
Γ_1	1	1	1	1	1	1
Γ_2	1	1	1	1	1	1
Γ_3	1	-1	1	-1	1	-1
Γ_4	1	-1	1	-1	1	-1
Γ_5	$\begin{pmatrix} 1 & 0 \\ 0 & 1 \end{pmatrix}$	$\begin{pmatrix} w^* & 0 \\ 0 & w \end{pmatrix}$	$\begin{pmatrix} w & 0 \\ 0 & w^* \end{pmatrix}$	$\begin{pmatrix} 1 & 0 \\ 0 & 1 \end{pmatrix}$	$\begin{pmatrix} w & 0 \\ 0 & w \end{pmatrix}$	$\begin{pmatrix} w & 0 \\ 0 & w^* \end{pmatrix}$
Γ_6	$\begin{pmatrix} 1 & 0 \\ 0 & 1 \end{pmatrix}$	$\begin{pmatrix} -w^* & 0 \\ 0 & -w \end{pmatrix}$	$\begin{pmatrix} w & 0 \\ 0 & w^* \end{pmatrix}$	$\begin{pmatrix} -1 & 0 \\ 0 & -1 \end{pmatrix}$	$\begin{pmatrix} w^* & 0 \\ 0 & w \end{pmatrix}$	$\begin{pmatrix} -w & 0 \\ 0 & -w^* \end{pmatrix}$

Continued.Irreducible representations of C_{6v}^4 for G^{k_Γ}

	19	20.1	21	22.1	23	24.1
Γ_1	1	1	1	1	1	1
Γ_2	-1	-1	-1	-1	-1	-1
Γ_3	-1	1	-1	1	-1	1
Γ_4	1	-1	1	-1	1	-1
Γ_5	$\begin{pmatrix} 0 & 1 \\ 1 & 0 \end{pmatrix}$	$\begin{pmatrix} 0 & w^* \\ w & 0 \end{pmatrix}$	$\begin{pmatrix} 0 & w \\ w^* & 0 \end{pmatrix}$	$\begin{pmatrix} 0 & 1 \\ 1 & 0 \end{pmatrix}$	$\begin{pmatrix} 0 & w^* \\ w & 0 \end{pmatrix}$	$\begin{pmatrix} 0 & w \\ w^* & 0 \end{pmatrix}$
Γ_6	$\begin{pmatrix} 0 & -1 \\ -1 & 0 \end{pmatrix}$	$\begin{pmatrix} 0 & w^* \\ w & 0 \end{pmatrix}$	$\begin{pmatrix} 0 & -w \\ -w^* & 0 \end{pmatrix}$	$\begin{pmatrix} 0 & 1 \\ 1 & 0 \end{pmatrix}$	$\begin{pmatrix} 0 & -w^* \\ -w & 0 \end{pmatrix}$	$\begin{pmatrix} 0 & w \\ w^* & 0 \end{pmatrix}$

Table D.2: Irreducible representations of C_{6v}^4 for G^{k_A}

	1	2.1	3	4.1	5	6.1
A_1	1	i	1	i	1	i
A_2	1	i	1	i	1	i
A_3	1	-i	1	-i	1	-i
A_4	1	-i	1	-i	1	-i
A_5	$\begin{pmatrix} 1 & 0 \\ 0 & 1 \end{pmatrix}$	$\begin{pmatrix} w^*i & 0 \\ 0 & wi \end{pmatrix}$	$\begin{pmatrix} w & 0 \\ 0 & w^* \end{pmatrix}$	$\begin{pmatrix} i & 0 \\ 0 & i \end{pmatrix}$	$\begin{pmatrix} w^* & 0 \\ 0 & w \end{pmatrix}$	$\begin{pmatrix} wi & 0 \\ 0 & w^*i \end{pmatrix}$
A_6	$\begin{pmatrix} 1 & 0 \\ 0 & 1 \end{pmatrix}$	$\begin{pmatrix} -wi & 0 \\ 0 & -w^*i \end{pmatrix}$	$\begin{pmatrix} w^* & 0 \\ 0 & w \end{pmatrix}$	$\begin{pmatrix} -i & 0 \\ 0 & -i \end{pmatrix}$	$\begin{pmatrix} w & 0 \\ 0 & w^* \end{pmatrix}$	$\begin{pmatrix} -w^*i & 0 \\ 0 & -wi \end{pmatrix}$

Continued.Irreducible representations of C_{6v}^4 for G^{k_A}

	19	20.1	21	22.1	23	24.1
A_1	1	i	1	i	1	i
A_2	-1	-i	-1	-i	-1	-i
A_3	-1	i	-1	i	-1	i
A_4	1	-i	1	-i	1	-i
A_5	$\begin{pmatrix} 0 & -i \\ i & 0 \end{pmatrix}$	$\begin{pmatrix} 0 & -w^* \\ w & 0 \end{pmatrix}$	$\begin{pmatrix} 0 & -wi \\ w^*i & 0 \end{pmatrix}$	$\begin{pmatrix} 0 & -i \\ i & 0 \end{pmatrix}$	$\begin{pmatrix} 0 & -w^*i \\ wi & 0 \end{pmatrix}$	$\begin{pmatrix} 0 & -w \\ w^* & 0 \end{pmatrix}$
A_6	$\begin{pmatrix} 0 & i \\ -i & 0 \end{pmatrix}$	$\begin{pmatrix} 0 & -w \\ w^* & 0 \end{pmatrix}$	$\begin{pmatrix} 0 & w^*i \\ -wi & 0 \end{pmatrix}$	$\begin{pmatrix} 0 & i \\ -i & 0 \end{pmatrix}$	$\begin{pmatrix} 0 & wi \\ -w^*i & 0 \end{pmatrix}$	$\begin{pmatrix} 0 & -w^* \\ w & 0 \end{pmatrix}$

Table D.3: Irreducible representations of C_{6v}^4 for G^{k_H}

	1	3	5	20.1	22.1	24.1
H_1	1	1	1	i	i	i
H_2	1	1	1	-i	-i	-i
H_3	$\begin{pmatrix} 1 & 0 \\ 0 & 1 \end{pmatrix}$	$\begin{pmatrix} w & 0 \\ 0 & w^* \end{pmatrix}$	$\begin{pmatrix} w^* & 0 \\ 0 & w \end{pmatrix}$	$\begin{pmatrix} 0 & -w^* \\ w & 0 \end{pmatrix}$	$\begin{pmatrix} 0 & -1 \\ 1 & 0 \end{pmatrix}$	$\begin{pmatrix} 0 & -w \\ w^* & 0 \end{pmatrix}$

Table D.4: Irreducible representations of C_{6v}^4 for G^{k_K}

	1	3	5	20.1	22.1	24.1
K_1	1	1	1	1	1	1
K_2	1	1	1	-1	-1	-1
K_3	$\begin{pmatrix} 1 & 0 \\ 0 & 1 \end{pmatrix}$	$\begin{pmatrix} w & 0 \\ 0 & w^* \end{pmatrix}$	$\begin{pmatrix} w^* & 0 \\ 0 & w \end{pmatrix}$	$\begin{pmatrix} 0 & w^* \\ w & 0 \end{pmatrix}$	$\begin{pmatrix} 0 & 1 \\ 1 & 0 \end{pmatrix}$	$\begin{pmatrix} 0 & w \\ w^* & 0 \end{pmatrix}$

Table D.5: Irreducible representations of C_{6v}^4 for G^{k_L} and G^{k_M}

	G^{k_L}					G^{k_M}			
	1	4.1	20.1	23		1	4.1	20.1	23
L_1	1	i	i	1	M_1	1	1	1	1
L_2	1	i	-i	-1	M_2	1	1	-1	-1
L_3	1	-i	i	-1	M_3	1	-1	1	-1
L_4	1	-i	-i	1	M_4	1	-1	-1	1

Table D.6: Physically irreducible representations of C_{6v}^4 for G^{k_A}

	1	2.1	3	4.1	5	6.1
$A_1 \oplus A_4$	$\begin{pmatrix} 1 & 0 \\ 0 & 1 \end{pmatrix}$	$\begin{pmatrix} i & 0 \\ 0 & -i \end{pmatrix}$	$\begin{pmatrix} 1 & 0 \\ 0 & 1 \end{pmatrix}$	$\begin{pmatrix} i & 0 \\ 0 & -i \end{pmatrix}$	$\begin{pmatrix} 1 & 0 \\ 0 & 1 \end{pmatrix}$	$\begin{pmatrix} i & 0 \\ 0 & -i \end{pmatrix}$
$A_2 \oplus A_3$	$\begin{pmatrix} 1 & 0 \\ 0 & 1 \end{pmatrix}$	$\begin{pmatrix} i & 0 \\ 0 & -i \end{pmatrix}$	$\begin{pmatrix} 1 & 0 \\ 0 & 1 \end{pmatrix}$	$\begin{pmatrix} i & 0 \\ 0 & -i \end{pmatrix}$	$\begin{pmatrix} 1 & 0 \\ 0 & 1 \end{pmatrix}$	$\begin{pmatrix} i & 0 \\ 0 & -i \end{pmatrix}$
$A_5 \oplus A_6$	$\begin{pmatrix} E & 0 \\ 0 & E \end{pmatrix}$	$\begin{pmatrix} P^*i & 0 \\ 0 & -P^*i \end{pmatrix}$	$\begin{pmatrix} P & 0 \\ 0 & P^* \end{pmatrix}$	$\begin{pmatrix} I & 0 \\ 0 & -I \end{pmatrix}$	$\begin{pmatrix} P^* & 0 \\ 0 & P \end{pmatrix}$	$\begin{pmatrix} Pi & 0 \\ 0 & -Pi \end{pmatrix}$

Continued.Physically irreducible representations of C_{6v}^4 for G^{k_A}

	19	20.1	21	22.1	23	24.1
$A_1 \oplus A_4$	$\begin{pmatrix} 1 & 0 \\ 0 & 1 \end{pmatrix}$	$\begin{pmatrix} i & 0 \\ 0 & -i \end{pmatrix}$	$\begin{pmatrix} 1 & 0 \\ 0 & 1 \end{pmatrix}$	$\begin{pmatrix} i & 0 \\ 0 & -i \end{pmatrix}$	$\begin{pmatrix} 1 & 0 \\ 0 & 1 \end{pmatrix}$	$\begin{pmatrix} i & 0 \\ 0 & -i \end{pmatrix}$
$A_2 \oplus A_3$	$\begin{pmatrix} -1 & 0 \\ 0 & -1 \end{pmatrix}$	$\begin{pmatrix} -i & 0 \\ 0 & i \end{pmatrix}$	$\begin{pmatrix} -1 & 0 \\ 0 & -1 \end{pmatrix}$	$\begin{pmatrix} -i & 0 \\ 0 & i \end{pmatrix}$	$\begin{pmatrix} -1 & 0 \\ 0 & -1 \end{pmatrix}$	$\begin{pmatrix} -i & 0 \\ 0 & i \end{pmatrix}$
$A_5 \oplus A_6$	$\begin{pmatrix} J & 0 \\ 0 & J^* \end{pmatrix}$	$\begin{pmatrix} Q^* & 0 \\ 0 & Q^* \end{pmatrix}$	$\begin{pmatrix} Qi & 0 \\ 0 & Q^*i \end{pmatrix}$	$\begin{pmatrix} j & 0 \\ 0 & J^* \end{pmatrix}$	$\begin{pmatrix} iQ^* & 0 \\ 0 & -Pi \end{pmatrix}$	$\begin{pmatrix} Q & 0 \\ 0 & Q^* \end{pmatrix}$

Table D.7: Physically irreducible representations of C_{6v}^4 for G^{k_L}

	1	4.1	20.1	23
$L_1 \oplus L_4$	$\begin{pmatrix} 1 & 0 \\ 0 & 1 \end{pmatrix}$	$\begin{pmatrix} i & 0 \\ 0 & -i \end{pmatrix}$	$\begin{pmatrix} i & 0 \\ 0 & -i \end{pmatrix}$	$\begin{pmatrix} 1 & 0 \\ 0 & 1 \end{pmatrix}$
$L_2 \oplus L_3$	$\begin{pmatrix} 1 & 0 \\ 0 & 1 \end{pmatrix}$	$\begin{pmatrix} i & 0 \\ 0 & -i \end{pmatrix}$	$\begin{pmatrix} -i & 0 \\ 0 & i \end{pmatrix}$	$\begin{pmatrix} -1 & 0 \\ 0 & -1 \end{pmatrix}$

Table D.8: Induced full representations C_{6v}^4 at M point

	1	2.1	3	4.1
M_2	$\begin{pmatrix}1&0&0\\0&1&0\\0&0&1\end{pmatrix}$	$\begin{pmatrix}0&0&1\\1&0&0\\0&1&0\end{pmatrix}$	$\begin{pmatrix}0&1&0\\0&0&1\\1&0&0\end{pmatrix}$	$\begin{pmatrix}1&0&0\\0&1&0\\0&0&1\end{pmatrix}$
M_3	$\begin{pmatrix}1&0&0\\0&1&0\\0&0&1\end{pmatrix}$	$\begin{pmatrix}0&0&-1\\1&0&0\\0&1&0\end{pmatrix}$	$\begin{pmatrix}0&-1&0\\0&0&-1\\1&0&0\end{pmatrix}$	$\begin{pmatrix}-1&0&0\\0&-1&0\\0&0&-1\end{pmatrix}$
M_4	$\begin{pmatrix}1&0&0\\0&1&0\\0&0&1\end{pmatrix}$	$\begin{pmatrix}0&0&-1\\1&0&0\\0&1&0\end{pmatrix}$	$\begin{pmatrix}0&-1&0\\0&0&-1\\1&0&0\end{pmatrix}$	$\begin{pmatrix}-1&0&0\\0&-1&0\\0&0&-1\end{pmatrix}$
	5	6.1	19	20.1
M_2	$\begin{pmatrix}0&0&1\\1&0&0\\0&1&0\end{pmatrix}$	$\begin{pmatrix}0&1&0\\0&0&1\\1&0&0\end{pmatrix}$	$\begin{pmatrix}0&0&-1\\0&-1&0\\-1&0&0\end{pmatrix}$	$\begin{pmatrix}-1&0&0\\0&0&-1\\0&-1&0\end{pmatrix}$
M_3	$\begin{pmatrix}0&0&1\\-1&0&0\\0&-1&0\end{pmatrix}$	$\begin{pmatrix}0&1&0\\0&0&1\\-1&0&0\end{pmatrix}$	$\begin{pmatrix}0&0&-1\\0&-1&0\\-1&0&0\end{pmatrix}$	$\begin{pmatrix}1&0&0\\0&0&-1\\0&-1&0\end{pmatrix}$
M_4	$\begin{pmatrix}0&0&1\\-1&0&0\\0&-1&0\end{pmatrix}$	$\begin{pmatrix}0&1&0\\0&0&1\\-1&0&0\end{pmatrix}$	$\begin{pmatrix}0&0&1\\0&1&0\\1&0&0\end{pmatrix}$	$\begin{pmatrix}-1&0&0\\0&0&1\\0&1&0\end{pmatrix}$
	21	22.1	23	24
M_2	$\begin{pmatrix}0&-1&0\\-1&0&0\\0&0&-1\end{pmatrix}$	$\begin{pmatrix}0&0&-1\\0&-1&0\\-1&0&0\end{pmatrix}$	$\begin{pmatrix}-1&0&0\\0&0&-1\\0&-1&0\end{pmatrix}$	$\begin{pmatrix}0&-1&0\\-1&0&0\\0&0&-1\end{pmatrix}$
M_3	$\begin{pmatrix}0&1&0\\1&0&0\\0&0&-1\end{pmatrix}$	$\begin{pmatrix}0&0&1\\0&1&0\\1&0&0\end{pmatrix}$	$\begin{pmatrix}-1&0&0\\0&0&1\\0&1&0\end{pmatrix}$	$\begin{pmatrix}0&-1&0\\-1&0&0\\0&0&1\end{pmatrix}$
M_4	$\begin{pmatrix}0&-1&0\\-1&0&0\\0&0&1\end{pmatrix}$	$\begin{pmatrix}0&0&-1\\0&-1&0\\-1&0&0\end{pmatrix}$	$\begin{pmatrix}1&0&0\\0&0&-1\\0&-1&0\end{pmatrix}$	$\begin{pmatrix}0&0&1\\1&0&0\\0&0&-1\end{pmatrix}$

Table D.9: Induced full representations of C_{6v}^4 at K point

	1	2.1	3	4.1	5	6.1
K_1	$\begin{pmatrix}1&0\\0&1\end{pmatrix}$	$\begin{pmatrix}0&1\\1&0\end{pmatrix}$	$\begin{pmatrix}1&0\\0&1\end{pmatrix}$	$\begin{pmatrix}0&1\\1&0\end{pmatrix}$	$\begin{pmatrix}1&0\\0&1\end{pmatrix}$	$\begin{pmatrix}0&1\\1&0\end{pmatrix}$
K_2	$\begin{pmatrix}1&0\\0&1\end{pmatrix}$	$\begin{pmatrix}0&1\\1&0\end{pmatrix}$	$\begin{pmatrix}0&1\\1&0\end{pmatrix}$	$\begin{pmatrix}0&1\\1&0\end{pmatrix}$	$\begin{pmatrix}1&0\\0&1\end{pmatrix}$	$\begin{pmatrix}0&1\\0&1\end{pmatrix}$

Table D.10: Irreducible representations of $C_6^6(P6_3)$ space group for G^{k_Γ}

C_6^6	**1**	**2.1**	**3**	**4.1**	**5**	**6.1**
$\mathbf{\Gamma_1}$	1	1	1	1	1	1
$\mathbf{\Gamma_2}$	1	-1	1	-1	1	-1
$\mathbf{\Gamma_3}$	1	w^*	w	1	w^*	w
$\mathbf{\Gamma_4}$	1	$-w^*$	w	-1	w^*	-w
$\mathbf{\Gamma_5}$	1	w	w^*	1	w	w^*
$\mathbf{\Gamma_6}$	1	-w	w^*	-1	w	$-w^*$

Table D.11: Physically Irreducible representations of $C_6^6(P6_3)$ space group at point Γ where $\Gamma_3 \oplus \Gamma_3^* = \Gamma_{3,5}$ and $\Gamma_4 \oplus \Gamma_4^* = \Gamma_{4,6}$

C_6^6	**1**	**2.1**	**3**	**4.1**	**5**	**6.1**
$\mathbf{\Gamma_1}$	1	1	1	1	1	1
$\mathbf{\Gamma_2}$	1	-1	1	-1	1	-1
$\mathbf{\Gamma_{3,5}}$	$\begin{pmatrix}1&0\\0&1\end{pmatrix}$	$\begin{pmatrix}w^*&0\\0&w\end{pmatrix}$	$\begin{pmatrix}w&0\\0&w^*\end{pmatrix}$	$\begin{pmatrix}1&0\\0&1\end{pmatrix}$	$\begin{pmatrix}w^*&0\\0&w\end{pmatrix}$	$\begin{pmatrix}w&0\\0&w^*\end{pmatrix}$
$\mathbf{\Gamma_{4,6}}$	$\begin{pmatrix}1&0\\0&1\end{pmatrix}$	$\begin{pmatrix}-w^*&0\\0&-w\end{pmatrix}$	$\begin{pmatrix}w&0\\0&w^*\end{pmatrix}$	$\begin{pmatrix}-1&0\\0&-1\end{pmatrix}$	$\begin{pmatrix}w^*&0\\0&w\end{pmatrix}$	$\begin{pmatrix}-w&0\\0&-w^*\end{pmatrix}$

Table D.12: Irreducible representations of $C_6^6(P6_3)$ for G^{k_A}

	1	2.1	3	4.1	5	6.1
A_1	1	i	1	i	1	i
A_2	1	-i	1	-i	1	-i
A_3	1	u^*	w	i	w^*	-u
A_4	1	$-u^*$	w	-i	w^*	u
A_5	1	-u	w^*	i	w	u^*
A_6	1	u	w^*	-i	w	$-u^*$

Table D.13: Irreducible representations of $C_6^6(P6_3)$ for G^{k_H}, G^{k_K}, G^{k_L} and G^{k_M}

G^{k_H}				G^{k_K}				G^{k_L}			G^{k_M}		
	1	3	5		1	3	5		1	4.1		1	4.1
H_1	1	1	1	K_1	1	1	1	L_1	1	i	M_1	1	1
H_2	1	w	w^*	K_2	1	w	w^*	L_2	1	-i	M_2	1	-1
H_3	1	w^*	w	K_3	1	w^*	w						

Table D.14: Irreducible representations of C_{3v}^4 for G^{k_Γ}

	1	3	5	20.1	22.1	24.1
Γ_1	1	1	1	1	1	1
Γ_2	1	1	1	-1	-1	-1
$\mathbf{\Gamma_3}$	$\begin{pmatrix}1&0\\0&1\end{pmatrix}$	$\begin{pmatrix}w&0\\0&w^*\end{pmatrix}$	$\begin{pmatrix}w^*&0\\0&w\end{pmatrix}$	$\begin{pmatrix}0&w^*\\w&0\end{pmatrix}$	$\begin{pmatrix}0&1\\1&0\end{pmatrix}$	$\begin{pmatrix}0&w\\w^*&0\end{pmatrix}$

Table D.15: Irreducible representations of C_{3v}^4 for G^{k_A}

	1	3	5	20.1	22.1	24.1
A_1	1	1	1	i	i	i
A_2	1	1	1	-i	-i	-i
A_3	$\begin{pmatrix} 1 & 0 \\ 0 & 1 \end{pmatrix}$	$\begin{pmatrix} w & 0 \\ 0 & w^* \end{pmatrix}$	$\begin{pmatrix} w^* & 0 \\ 0 & w \end{pmatrix}$	$\begin{pmatrix} 0 & -w^* \\ w & 0 \end{pmatrix}$	$\begin{pmatrix} 0 & -1 \\ 1 & 0 \end{pmatrix}$	$\begin{pmatrix} 0 & -w \\ w^* & 0 \end{pmatrix}$

Table D.16: Irreducible representations of C_{3v}^4 for G^{k_H}

	1	3	5	20.1	22.1	24.1
H_1	1	1	1	i	i	i
H_2	1	1	1	-i	-i	-i
$\mathbf{H_3}$	$\begin{pmatrix}1 & 0\\0 & 1\end{pmatrix}$	$\begin{pmatrix}w & 0\\0 & w^*\end{pmatrix}$	$\begin{pmatrix}w^* & 0\\0 & w\end{pmatrix}$	$\begin{pmatrix}0 & -w^*\\w & 0\end{pmatrix}$	$\begin{pmatrix}0 & -1\\1 & 0\end{pmatrix}$	$\begin{pmatrix}0 & -w\\w^* & 0\end{pmatrix}$

Table D.17: Irreducible representations of C_{3v}^1 for G^{k_Γ}

	1	3	5	19	21	23
Γ_1	1	1	1	1	1	1
Γ_2	1	1	1	-1	-1	-1
$\mathbf{\Gamma_3}$	$\begin{pmatrix}1 & 0\\0 & 1\end{pmatrix}$	$\begin{pmatrix}w & 0\\0 & w^*\end{pmatrix}$	$\begin{pmatrix}w^* & 0\\0 & w\end{pmatrix}$	$\begin{pmatrix}0 & 1\\1 & 0\end{pmatrix}$	$\begin{pmatrix}0 & w\\w^* & 0\end{pmatrix}$	$\begin{pmatrix}0 & w^*\\w & 0\end{pmatrix}$

Table D.18: Irreducible representations of C_{3v}^1 for G^{k_A}

	1	3	5	19	21	23
A_1	1	1	1	1	1	1
A_2	1	1	1	-1	-1	-1
$\mathbf{A_3}$	$\begin{pmatrix}1 & 0\\0 & 1\end{pmatrix}$	$\begin{pmatrix}w & 0\\0 & w^*\end{pmatrix}$	$\begin{pmatrix}w^* & 0\\0 & w\end{pmatrix}$	$\begin{pmatrix}0 & 1\\1 & 0\end{pmatrix}$	$\begin{pmatrix}0 & w\\w^* & 0\end{pmatrix}$	$\begin{pmatrix}0 & w^*\\w & 0\end{pmatrix}$

Table D.19: Irreducible representations of C_{3v}^1 for G^{k_H}, G^{k_K}, G^{k_L} and G^{k_M}

G^{k_H}				G^{k_K}				G^{k_L}			G^{k_M}		
	1	3	5		1	3	5		1	4.1		1	4.1
H_1	1	1	1	K_1	1	1	1	L_1	1	1	M_1	1	1
H_2	1	w	w^*	K_2	1	w	w^*	L_2	1	-1	M_2	1	-1
H_3	1	w^*	w	K_3	1	w^*	w						

Appendix E

Corepresentations of the magnetic space groups:$C_{6v}^4(C_6^6)$, $C_{6v}^4(C_{3v}^4)$ and $C_{6v}^4(C_{3v}^1)$, originating from C_{6v}^4 non magnetic.

Table E.1: Corepresentations for $C_{6v}^4(C_6^6)$ magnetic space group at point Γ

where

$$\begin{pmatrix} 1 & 0 \\ 0 & 1 \end{pmatrix} = E, and \begin{pmatrix} w & 0 \\ 0 & w^* \end{pmatrix} = P.$$

	1	**2.1**	**3**	**4.1**	**5**	**6.1**
$\mathbf{C\Gamma_1}$	1	1	1	1	1	1
$\mathbf{C\Gamma_2}$	1	-1	1	-1	1	-1
$\mathbf{C\Gamma_{3,5}}$	$\begin{pmatrix} E & 0 \\ 0 & E \end{pmatrix}$	$\begin{pmatrix} P^* & 0 \\ 0 & P^* \end{pmatrix}$	$\begin{pmatrix} P & 0 \\ 0 & P \end{pmatrix}$	$\begin{pmatrix} E & 0 \\ 0 & E \end{pmatrix}$	$\begin{pmatrix} P^* & 0 \\ 0 & P^* \end{pmatrix}$	$\begin{pmatrix} P & 0 \\ 0 & P \end{pmatrix}$
$\mathbf{C\Gamma_{4,6}}$	$\begin{pmatrix} E & 0 \\ 0 & E \end{pmatrix}$	$\begin{pmatrix} -P^* & 0 \\ 0 & -P \end{pmatrix}$	$\begin{pmatrix} P & 0 \\ 0 & P \end{pmatrix}$	$\begin{pmatrix} -E & 0 \\ 0 & -E \end{pmatrix}$	$\begin{pmatrix} P^* & 0 \\ 0 & P^* \end{pmatrix}$	$\begin{pmatrix} -P & 0 \\ 0 & -P \end{pmatrix}$

(Continued): Corepresentations for $C_{6v}^4(C_6^6)$ magnetic space group at point Γ

	θ19	**θ20.1**	**θ21**	**θ22.1**	**θ23**	**θ24.1**
$\mathbf{C\Gamma_1}$	1	1	1	1	1	1
$\mathbf{C\Gamma_2}$	1	-1	1	-1	1	-1
$\mathbf{C\Gamma_{3,5}}$	$\begin{pmatrix} 0 & E \\ E & 0 \end{pmatrix}$	$\begin{pmatrix} 0 & P^* \\ P & 0 \end{pmatrix}$	$\begin{pmatrix} 0 & P \\ P^* & 0 \end{pmatrix}$	$\begin{pmatrix} 0 & E \\ E & 0 \end{pmatrix}$	$\begin{pmatrix} 0 & P^* \\ P & 0 \end{pmatrix}$	$\begin{pmatrix} 0 & P \\ P^* & 0 \end{pmatrix}$
$\mathbf{C\Gamma_{4,6}}$	$\begin{pmatrix} 0 & E \\ E & 0 \end{pmatrix}$	$\begin{pmatrix} 0 & -P^* \\ -P & 0 \end{pmatrix}$	$\begin{pmatrix} 0 & P \\ P^* & 0 \end{pmatrix}$	$\begin{pmatrix} 0 & -E \\ -E & 0 \end{pmatrix}$	$\begin{pmatrix} 0 & P^* \\ P & 0 \end{pmatrix}$	$\begin{pmatrix} 0 & -P \\ -P^* & 0 \end{pmatrix}$

Table E.2: Corepresentations for $C_{6v}^4(C_6^6)$ magnetic space group at point A

where

$$\begin{pmatrix}1 & 0\\ 0 & 1\end{pmatrix} = E, \begin{pmatrix}w & 0\\ 0 & w^*\end{pmatrix} = P \begin{pmatrix}i & 0\\ 0-i & \end{pmatrix} = I and \begin{pmatrix}u & 0\\ 0 & u^*\end{pmatrix} = U$$

	1	**2.1**	**3**	**4.1**	**5**	**6.1**
$\mathbf{CA_1}$	1	i	1	i	1	i
$\mathbf{CA_2}$	1	-i	1	-i	1	-i
$\mathbf{CA_{3,6}}$	$\begin{pmatrix}E & 0\\ 0 & E\end{pmatrix}$	$\begin{pmatrix}U^* & 0\\ 0 & U^*\end{pmatrix}$	$\begin{pmatrix}P & 0\\ 0 & P\end{pmatrix}$	$\begin{pmatrix}I & 0\\ 0 & I\end{pmatrix}$	$\begin{pmatrix}P^* & 0\\ 0 & P^*\end{pmatrix}$	$\begin{pmatrix}-U & 0\\ 0 & -U\end{pmatrix}$
$\mathbf{CA_{4,5}}$	$\begin{pmatrix}E & 0\\ 0 & E\end{pmatrix}$	$\begin{pmatrix}-U^* & 0\\ 0 & -U^*\end{pmatrix}$	$\begin{pmatrix}P & 0\\ 0 & P\end{pmatrix}$	$\begin{pmatrix}-I & 0\\ 0 & -I\end{pmatrix}$	$\begin{pmatrix}P^* & 0\\ 0 & P^*\end{pmatrix}$	$\begin{pmatrix}-U & 0\\ 0 & -U\end{pmatrix}$

(Continued): Corepresentations for $C_{6v}^4(C_6^6)$ magnetic space group at point A

	θ**19**	θ**20.1**	θ**21**	θ**22.1**	θ**23**	θ**24.1**
$\mathbf{CA_1}$	1	i	1	i	1	i
$\mathbf{CA_2}$	1	-i	1	-i	1	-i
$\mathbf{CA_{3,6}}$	$\begin{pmatrix}0 & E\\ E & 0\end{pmatrix}$	$\begin{pmatrix}0 & -U^*\\ -U^* & 0\end{pmatrix}$	$\begin{pmatrix}0 & P^*\\ P & 0\end{pmatrix}$	$\begin{pmatrix}0 & I\\ I^* & 0\end{pmatrix}$	$\begin{pmatrix}0 & P\\ P^* & 0\end{pmatrix}$	$\begin{pmatrix}0 & U^*\\ U & 0\end{pmatrix}$
$\mathbf{CA_{4,5}}$	$\begin{pmatrix}0 & E\\ E & 0\end{pmatrix}$	$\begin{pmatrix}0 & U^*\\ U^* & 0\end{pmatrix}$	$\begin{pmatrix}0 & P^*\\ P & 0\end{pmatrix}$	$\begin{pmatrix}0 & -I\\ -I^* & 0\end{pmatrix}$	$\begin{pmatrix}0 & P\\ P^* & 0\end{pmatrix}$	$\begin{pmatrix}0 & -U^*\\ -U & 0\end{pmatrix}$

Table E.3: Corepresentations for $C_{6v}^4(C_6^6)$ magnetic space group at point H where

$$\begin{pmatrix}1 & 0\\ 0 & 1\end{pmatrix} = E, \begin{pmatrix}w & 0\\ 0 & w^*\end{pmatrix} = P \begin{pmatrix}i & 0\\ 0 & -i\end{pmatrix} = I and \begin{pmatrix}u & 0\\ 0 & u^*\end{pmatrix} = U$$

	1	**3**	**5**	**θ20.1**	**θ22.1**	**θ24.1**
$\mathbf{CH_1}$	1	1	1	1	1	1
$\mathbf{CH_{2,3}}$	$\begin{pmatrix}E & 0\\ 0 & E\end{pmatrix}$	$\begin{pmatrix}P & 0\\ 0 & P\end{pmatrix}$	$\begin{pmatrix}P^* & 0\\ 0 & P^*\end{pmatrix}$	$\begin{pmatrix}0 & 1\\ 1 & 0\end{pmatrix}$	$\begin{pmatrix}0 & P^*\\ p & 0\end{pmatrix}$	$\begin{pmatrix}0 & P\\ P & 0\end{pmatrix}$

Table E.4: Corepresentations for $C_{6v}^4(C_6^6)$ magnetic space group at point K where

$$\begin{pmatrix}1 & 0\\ 0 & 1\end{pmatrix} = E, \begin{pmatrix}w & 0\\ 0 & w^*\end{pmatrix} = P \begin{pmatrix}i & 0\\ 0 & -i\end{pmatrix} = I and \begin{pmatrix}u & 0\\ 0 & u^*\end{pmatrix} = U$$

	1	**3**	**5**	**θ20.1**	**θ22.1**	**θ24.1**
$\mathbf{CK_1}$	1	1	1	1	1	1
$\mathbf{CK_{2,3}}$	$\begin{pmatrix}E & 0\\ 0 & E\end{pmatrix}$	$\begin{pmatrix}P & 0\\ 0 & P\end{pmatrix}$	$\begin{pmatrix}P^* & 0\\ 0 & P^*\end{pmatrix}$	$\begin{pmatrix}0 & 1\\ 1 & 0\end{pmatrix}$	$\begin{pmatrix}0 & P^*\\ p & 0\end{pmatrix}$	$\begin{pmatrix}0 & P\\ P & 0\end{pmatrix}$

Table E.5: Corepresentations of the magnetic space group $C_{6v}^4(C_{3v}^4)$ at point A

	1	**3**	**5**	**20.1**	**22.1**	**24.1**
CA_1	1	1	1	1	1	1
CA_2	1	1	1	-1	-1	-1
$\mathbf{CA_3}$	$\begin{pmatrix}1 & 0\\ 0 & 1\end{pmatrix}$	$\begin{pmatrix}w & 0\\ 0 & w^*\end{pmatrix}$	$\begin{pmatrix}w^* & 0\\ 0 & w\end{pmatrix}$	$\begin{pmatrix}0 & -w^*\\ w & 0\end{pmatrix}$	$\begin{pmatrix}0 & -1\\ 1 & 0\end{pmatrix}$	$\begin{pmatrix}0 & -w\\ w^* & 0\end{pmatrix}$

(Continued): Corepresentations for $C_{6v}^4(C_{3v}^4)$ magnetic space group at point A

	θ**2.1**	θ**4.1**	θ**6.1**	θ**19**	θ**21**	θ**23**
CA_1	1	1	1	1	1	1
CA_2	1	1	1	-1	-1	-1
$\mathbf{CA_3}$	$\begin{pmatrix}1&0\\0&1\end{pmatrix}$	$\begin{pmatrix}w&0\\0&w^*\end{pmatrix}$	$\begin{pmatrix}w^*&0\\0&w\end{pmatrix}$	$\begin{pmatrix}0&w\\w^*&0\end{pmatrix}$	$\begin{pmatrix}0&w^*\\w&0\end{pmatrix}$	$\begin{pmatrix}0&1\\1&0\end{pmatrix}$

Table E.6: Corepresentations for $C_{6v}^4(C_{3v}^4)$ magnetic space group at point Γ

	1	**3**	**5**	**20.1**	**22.1**	**24.1**
$C\Gamma_1$	1	1	1	1	1	1
$C\Gamma_2$	1	1	1	-1	-1	-1
$\mathbf{C\Gamma_3}$	$\begin{pmatrix}1&0\\0&1\end{pmatrix}$	$\begin{pmatrix}w&0\\0&w^*\end{pmatrix}$	$\begin{pmatrix}w^*&0\\0&w\end{pmatrix}$	$\begin{pmatrix}0&w^*\\w&0\end{pmatrix}$	$\begin{pmatrix}0&1\\1&0\end{pmatrix}$	$\begin{pmatrix}0&w\\w^*&0\end{pmatrix}$

(Continued): Corepresentations for $C_{6v}^4(C_{3v}^4)$ magnetic space group at point Γ

	θ**2.1**	θ**4.1**	θ**6.1**	θ**19**	θ**21**	θ**23**
$C\Gamma_1$	1	1	1	1	1	1
$C\Gamma_2$	1	1	1	-1	-1	-1
$\mathbf{C\Gamma_3}$	$\begin{pmatrix}1&0\\0&1\end{pmatrix}$	$\begin{pmatrix}w&0\\0&w^*\end{pmatrix}$	$\begin{pmatrix}w^*&0\\0&w\end{pmatrix}$	$\begin{pmatrix}0&-w\\w^*&0\end{pmatrix}$	$\begin{pmatrix}0&-w^*\\w&0\end{pmatrix}$	$\begin{pmatrix}0&-1\\1&0\end{pmatrix}$

Table E.7: Corepresentations for $C_{6v}^4(C_{3v}^4)$ magnetic space group at point M

	120.1	θ**4.1**	θ**23**	
CM_1	1	1	1	1
CM_2	1	-1	1	-1

Table E.8: Corepresentations for $C_{6v}^4(C_{3v}^4)$ magnetic space group at point L

	1	**20.1**	θ**4.1**	θ**23**
CL_1	1	1	1	1
CL_2	$\begin{pmatrix}1 & 0\\0 & 1\end{pmatrix}$	$\begin{pmatrix}-i & 0\\0 & i\end{pmatrix}$	$\begin{pmatrix}0 & 1\\1 & 0\end{pmatrix}$	$\begin{pmatrix}0 & -i\\i & 0\end{pmatrix}$

Table E.9: Corepresentations for $C_{6v}^4(C_{3v}^1)$ magnetic space group at point Γ

	1	**3**	**3**	**19**	**21**	**23**
$C\Gamma_1$	1	1	1	1	1	1
$C\Gamma_2$	1	1	1	-1	-1	-1
$\mathbf{C\Gamma_3}$	$\begin{pmatrix}1 & 0\\0 & 1\end{pmatrix}$	$\begin{pmatrix}w & 0\\0 & w^*\end{pmatrix}$	$\begin{pmatrix}w^* & 0\\0 & w\end{pmatrix}$	$\begin{pmatrix}0 & 1\\1 & 0\end{pmatrix}$	$\begin{pmatrix}0 & w\\w^* & 0\end{pmatrix}$	$\begin{pmatrix}0 & w^*\\w & 0\end{pmatrix}$

(Continued): Corepresentations for $C_{6v}^4(C_{3v}^1)$ magnetic space group at point Γ

	θ**2.1**	θ**4.1**	θ**6.1**	θ**20.1**	θ**22.1**	θ**24.1**
$C\Gamma_1$	1	1	1	1	1	1
$C\Gamma_2$	1	1	1	-1	-1	-1
$\mathbf{C\Gamma_3}$	$\begin{pmatrix}1&0\\0&1\end{pmatrix}$	$\begin{pmatrix}w&0\\0&w^*\end{pmatrix}$	$\begin{pmatrix}w^*&0\\0&w\end{pmatrix}$	$\begin{pmatrix}0&w\\w^*&0\end{pmatrix}$	$\begin{pmatrix}0&w^*\\w&0\end{pmatrix}$	$\begin{pmatrix}0&1\\1&0\end{pmatrix}$

Table E.10: Corepresentations for $C_{6v}^4(C_{3v}^1)$ magnetic space group at point A

	1	**3**	**3**	**19**	**21**	**23**
CA_1	1	1	1	1	1	1
CA_2	1	1	1	-1	-1	-1
$\mathbf{CA_3}$	$\begin{pmatrix}1&0\\0&1\end{pmatrix}$	$\begin{pmatrix}w&0\\0&w^*\end{pmatrix}$	$\begin{pmatrix}w^*&0\\0&w\end{pmatrix}$	$\begin{pmatrix}0&1\\1&0\end{pmatrix}$	$\begin{pmatrix}0&w\\w^*&0\end{pmatrix}$	$\begin{pmatrix}0&w^*\\w&0\end{pmatrix}$

(Continued): Corepresentations for $C_{6v}^4(C_{3v}^1)$ magnetic space group at point A

	θ**2.1**	θ**4.1**	θ**6.1**	θ**20.1**	θ**22.1**	θ**24.1**
CA_1	1	1	1	1	1	1
CA_2	1	1	1	-1	-1	-1
$\mathbf{CA_3}$	$\begin{pmatrix}1&0\\0&1\end{pmatrix}$	$\begin{pmatrix}w&0\\0&w^*\end{pmatrix}$	$\begin{pmatrix}w^*&0\\0&w\end{pmatrix}$	$\begin{pmatrix}0&w\\w^*&0\end{pmatrix}$	$\begin{pmatrix}0&w^*\\w&0\end{pmatrix}$	$\begin{pmatrix}0&1\\1&0\end{pmatrix}$

Table E.11: Corepresentations for $C_{6v}^{4}(C_{3v}^{1})$ magnetic space group at point H

	1	3	5	θ**20.1**	θ**22.1**	θ**24.1**
CH_1	1	1	1	1	1	1
$CH_{2,3}$	$\begin{pmatrix} E & 0 \\ 0 & E \end{pmatrix}$	$\begin{pmatrix} P & 0 \\ 0 & P \end{pmatrix}$	$\begin{pmatrix} P^* & 0 \\ 0 & P^* \end{pmatrix}$	$\begin{pmatrix} 0 & E \\ E & 0 \end{pmatrix}$	$\begin{pmatrix} 0 & P \\ P & 0 \end{pmatrix}$	$\begin{pmatrix} 0 & P^* \\ P & 0 \end{pmatrix}$

Table E.12: Corepresentations for $C_{6v}^4(C_{3v}^1)$ magnetic space group at point K

	1	3	5	θ**20.1**	θ**22.1**	θ**24.1**
CK_1	1	1	1	1	1	1
$CK_{2,3}$	$\begin{pmatrix} E & 0 \\ 0 & E \end{pmatrix}$	$\begin{pmatrix} P & 0 \\ 0 & P \end{pmatrix}$	$\begin{pmatrix} P^* & 0 \\ 0 & P^* \end{pmatrix}$	$\begin{pmatrix} 0 & E \\ E & 0 \end{pmatrix}$	$\begin{pmatrix} 0 & P \\ P & 0 \end{pmatrix}$	$\begin{pmatrix} 0 & P^* \\ P & 0 \end{pmatrix}$

Bibliography

[1] A. P Cracknell, B.L. Davies, S.C. Miller, and W.F. Love, Kronecker product Tables. Vols. **1-4** (IFI/Plenum, New York, Washington, London, 1979).

[2] L.D. Landau and E.M Lifshitz, *Statistical physics*, (Pergamon press, London, 1958).

[3] G.Ya. Luybarskii, *The application of Group Theory in Physics*, translated by S. Dedijer, Pergamon Press (1960).

[4] J. Birman, Phys. Rev. Letters, **17** 1216 (1966).

[5] C.J. Bradley, B.L. Davies, Reviews of Modern Physics, Vol **40** N0 2. (1968).

[6] A.P. Cracknell, *Magnetism in crystalline materials*, Pergamon Press, Oxford, Toronto, New York, (1965).

[7] ,Arthur P. Cracknell, Progress of theoretical Physics, Vol.**38**, N0.6 (1967).

[8] E.P. Wigner, *Group theory and its application to quantum mechanics of atomic spectra*, (Academic Press, New York, London, 1959).

[9] Morton Hamermesh; *Group theory and its application to physical problems*, Addison-Wesley, (1962).

[10] J. Kocinski, *Theory of symmetry changes at continuous phase transitions*, Amsterdam, Oxford, New York, (1983).

[11] L.D. Landau, Zh.eksp.teor. Fiz.7, 19; translated in Collected papers of L.D. Landau (ed. D. ter Haar), Gordon and Breach, New York, (1965).

[12] G. Fröbenius and I. Schur, Berl. Ber.186 (1906).

[13] H.W. Kunert, The European physical journal of applied physics, **27**, 309-312 (2004).

[14] G. L. Bir, G.E. Pikus, *Symmetry and strain-induced effects in semiconductors*, Jerusalem, London, (1974).

[15] Rhoda Berenson, J. Phys. Chem. Solids Vol **42**, 391-404 (1981).

[16] J. Pankove, T.D. Moustakas, *Semiconductors and semimetals, Gallium Nitride* (GaN),(Academic Press, San Diego, London, Boston, New York, Sydney, Tokyo, Toronto 1999).

[17] H.W. Kunert, Cryst. Res. Technol. **38**, 366 (2003).

[18] H.W. Kunert, Appl. Surf. Sci. **212-213** 890 (2003).

[19] S.P.S. Porto, R. S. Krishnan, J. Chem. Phys. **47**, 1009 (1967).

[20] M. R. Wagner, H.W. Kunert, A. G. J. Machatine, P. Niyongabo, A. Hoffiman, J. Malherbe, and J. Barnas, Micro-electron. J. **40**, 289 (2009).

[21] Herbert W. Kunert, Markus R. Wagner, Augusto G. J. Machatine, Prime Niyongabo, Johan B. Malherbe, Axel Hoffmann, Jozef Barnas, and Wojciech Florek, Phy. Status Solidi B **247**, NO.7, 1802-1806 (2010).

[22] H.W. Kunert, A.G.J. Machatine, P. Niyongabo, M. Govender, and B.W Mwakikunga, Status Solidi C **9**, NO.10-11, 1974-1977 (2012).

[23] A.G.J. Machatine, H.W.Kunert, A. Hoffman, J.B. Malherbe, J. Barnas, M.R. Wagner, P. Niyongabo, and N. Nephale, Journal of physics: Conference Series **92** (2007).

[24] H.W. Kunert, A.G.J. Machatine, P. Niyongabo, M. Govender, and B.W Mwakikunga, Status Solidi C **9**, NO.10-11, 1978-1980 (2012).

[25] H.W. Kunert, A.G.J. Machatine, P. Niyongabo, M. Govender, and B.W Mwakikunga, Status Solidi A **211**, NO.2, 435-439 (2014).

[26] G.F. Koster, J.O. Dimmock, R.C. Wheeler, H. Statz, *Properties of the thirty-two point groups*, MIT Press, Cambridge. MA.(1963).

[27] W.F. Karavaev, Soviet Phys.-Solid State, **6**, 2943 (1965).

[28] H.W. Kunert, Journal of physics: Conference Series **30**, 290-301 (2006).

[29] L. Molnar, *An algebraic approach to wigner's unitary-antiunitary theorem*, J. Austral. Math. soc. **65**, 354-369 (1998).

[30] A. Mouchet, An alternative proof of Wigner theorem om quantum transformation based on elementary complex analysis, Physics letters A, **377**, 2709-2711 (2013).

[31] HE Qing, Xu Jia-Yue, Li Xin-Hua, A. Kamzin, L. Kamzina, CHIN. PHYS.LETT., **24**. N0. 12 (2007)3499.

[32] C.Y.Lin, W.H. Wang, C.S. Lee, K.W.Sun, and Y.W.Suen, Applied physics letters **94**, 151909 (2009).

[33] M. Millot, J. Gonzalez, I. Molina, B. Salas, Z. Golacki, J. M. Broto, H. Rakoto, M. Goiran, Journal of alloys and compounds **423** 224-227 (2006).

Appendix F

Articles

Microelectronics Journal 40 (2009) 289–292

Contents lists available at ScienceDirect

Microelectronics Journal

journal homepage: www.elsevier.com/locate/mejo

Bound and free excitons in ZnO. Optical selection rules in the absence and presence of time reversal symmetry

M.R. Wagner [a,*], H.W. Kunert [b], A.G.J. Machatine [b], A. Hoffmann [a], P. Niyongabo [b], J. Malherbe [b], J. Barnas [c]

[a] Institut für Festkörperphysik, Technische Universität Berlin, Hardenbergstr. 36, 10623 Berlin, Germany
[b] Department of Physics, University of Pretoria, 0002, South Africa
[c] Department of Physics, Adam Mickiewicz University, ul. Ulmutowska 85, 61-614 Poznan, Poland

ARTICLE INFO

Available online 24 September 2008

Keywords:
ZnO
Lithium
Magneto-photoluminescence
Excitons
Symmetry

ABSTRACT

The correlation between ionized donor bound exciton recombinations and neutral donor bound exciton recombinations in ZnO has been investigated. The experimental data obtained by means of magneto-photoluminescence (MPL) concerning charge state and localization energies of ionized and neutral donor bound excitons are in good agreement with theoretical predictions. The optical selection rules in absence and presence of time reversal symmetry (TRS) are investigated. It is shown that the inclusion of extra degeneracy due to TRS reveals a number of new states of the same symmetries and essentially does not change the existing optical selection rules.

1. Neutral and ionized donor bound excitons

Lithium-doped ZnO epilayers were grown by chemical vapor deposition on ZnO substrates. Photoluminescence (PL) and magneto-photoluminescence (MPL) measurements were performed using a 325 nm HeCd laser. Fig. 1 displays the PL at 4.2 K in the energetic range of the free and bound excitons. The most prominent excitonic transition lines are the I_9 (3.3567 eV), I_8 (3.3598 eV), I_{6a} (3.3604 eV), I_2 (3.3674 eV), I_1 (3.3720 eV), and I_0 (3.3726 eV).

Previous studies have shown that I_9, I_8, and I_{6a} are neutral exciton complexes bound to an indium [1], gallium [2], and aluminum impurity, respectively [3]. These lines are accompanied by the higher energetic lines I_2, I_1, and I_0 [4]. The neutral bound exciton line I_9 is correlated to I_2, I_8–I_1, and I_{6a}–I_0. In fact, all investigated samples exhibit only I_0–I_2 excitons if the related excitons I_{6a}–I_9 are present as well. Due to a similar scaling in intensity and energetic position, it is likely that these correlated pairs of transition lines are excitons bound to an impurity of the same chemical identity but in a different charge state. Consequently, we attribute I_0, I_1, and I_2 to ionized donor bound excitons related to Al, Ga, and In impurities, respectively. Concerning the I_1 complex, this correlation is in agreement with the data published by Johnston et al. [2], who reported a simultaneous decrease in the I_8 and I_1 intensity for ZnO crystals doped with a radioactive Ga isotope. The various bound exciton complexes with their localization energies and suggested chemical identities are summarized in Table 1.

The charge states of the bound exciton complexes are investigated by MPL spectroscopy. Excitons bound to ionized impurities can be distinguished from those bound to neutral impurities by a nonlinear splitting of energy levels in the magnetic field perpendicular to the *c*-axis of the crystal, while excitons bound to neutral impurities exhibit a linear splitting behavior for $\mathbf{B} \perp \mathbf{c}$ [5]. For ionized bound excitons at low magnetic fields, only a high energy Zeeman component, resulting from a Γ_5 state is visible, whereas the low energy component, originating from Γ_1 to Γ_6 transition is forbidden by selection rules (SRs). However, for larger magnetic fields, the SRs can be relaxed due to a spin–spin interaction of Γ_5 states with anti-parallel spin, mixed with Γ_6 states with parallel spin, thus allowing the appearance of a new line associated with the Γ_6 state. The extrapolation of the peak positions to $B = 0$ T reveals the presence of the zerofield splitting, ascribed to the spin–spin interaction energy. Such an interaction cannot occur in transition lines originating from excitons bound to neutral impurities, since the spin of the two equal particles are anti-parallel.

Evidently, we observe a linear Zeeman splitting for the I_{6a}–I_8 lines, whereas this is not the case for the bound excitons I_0 and I_1 (Fig. 2). Furthermore, an additional low energy transition due to the zerofield splitting appears for I_0 and I_1 if a magnetic field is applied. Similar results (not shown) were obtained for I_9 (linear Zeeman splitting) and I_2 (zerofield splitting) in accordance with the previously published measurements [6]. Consequently, following the previous discussion, the transition lines I_{6a}–I_9 originate from recombinations of neutral bound excitons, whereas I_0–I_2 are related to ionized bound exciton complexes.

* Corresponding author.
E-mail address: Markus.wagner@physik.tu-berlin.de (M.R. Wagner).

0026-2692/$ - see front matter © 2008 Elsevier Ltd. All rights reserved.
doi:10.1016/j.mejo.2008.07.025

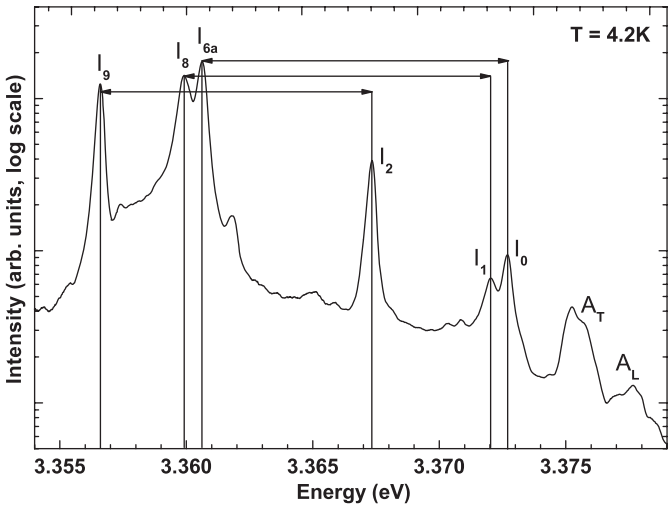

Fig. 1. PL spectra of lithium-doped high quality ZnO grown by CVD at a temperature of 4.2 K.

Table 1
Bound exciton complexes in ZnO

Line	E (eV)	E_b (meV)	Complex	Chem. element
I_9	3.3567	19.2	D^0X	In
I_8	3.3598	16.1	D^0X	Ga
I_{6a}	3.3604	15.5	D^0X	Al
I_2	3.3674	8.5	D^+X	In
I_1	3.3718	4.1	D^+X	Ga
I_0	3.3726	3.3	D^+X	Al

Energetic positions are given for $T = 4.2$ K.

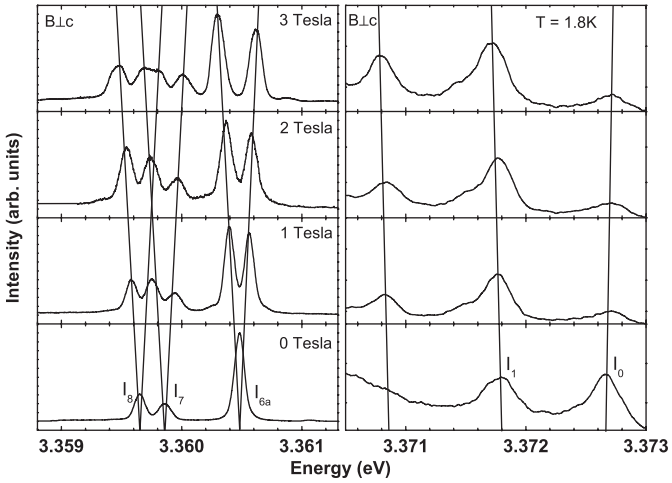

Fig. 2. Zeeman splitting of neutral and ionized donor bound excitons for magnetic fields of 0–3 T. Spectra are taken at 1.8 K in Voigt geometry ($\vec{\mathbf{B}} \perp \mathbf{c}$).

2. Band structure and SRs for optical transitions in the absence and presence of time reversal symmetry

Large magnetic fields and high spectral resolutions better than 50–100 μeV reveal the presence of additional transition lines due to the lifting of degeneracy [7]. The new transitions are related to the absorption and emission of free and bound excitons, which depend on the structure and symmetry of the conduction band (CB) and valence band (VB). In order to understand the origin of the optical transitions, we recall and modify the theory of band structures and SRs for wurtzite compounds with the C_{6v}^4 space group. Possible reason for additional transition lines could be related to excited states, non-zero hole g-values, hyperfine structure splittings, or time reversal symmetry (TRS) splittings. The following theoretical discussion intends to clarify, if the inclusion of TRS in the group theoretical consideration can explain the additional degeneracy and optical transitions.

2.1. Band structure

The band structure of wurtzite compounds has been investigated by many authors [8,9]. However, to our best knowledge the effect of TRS has not been considered. Disregarding the spin–orbit (S–O) interaction, crystalline field (CF) and TRS effect, the free electrons occupy S-like CB states and free holes P (P_x, P_y, P_z) VB states. The S-like states transform according to irreducible representation (irrp) Γ_1^c of the C_{6v}-ZnO point group, while the P (P_x, P_y, P_z) hydrogenic-like orbitals transform like X, Y, Z according to the so-called vector representation $V(x, y, z)$.

The CF splits the P_x, P_y, P_z states into $P_x, P_y(\Gamma_5(x, y))$ and $P_z(\Gamma_1(z))$ states. The vector representation for ZnO is reducible to Γ_1 and Γ_5 irrps $V = \Gamma_1(z) \oplus \Gamma_5(x, y)$.

The inclusion of the S–O interaction results in further splittings: $\Gamma_1^c \otimes D_{1/2} = \Gamma_7^c$, $\Gamma_5^v \otimes D_{1/2} = \Gamma_7^v \oplus \Gamma_9^v$, and $\Gamma_1^v \otimes D_{1/2} = \Gamma_7^v$. The free electrons in the CB and holes in VBs are classified according to double-valued irrps [10].

2.2. The effect of TRS on band structure and classification of states

Replacing t by $-t$ and taking the complex conjugate of any time-dependent Schrödinger equation we obtain $\Psi_i^\star(\vec{r}, -t)$ wave functions which are also eigenfunctions of $\hat{H}_{\mathrm{Sch}}$ together with the $\Psi_i(\vec{r}, t)$. The Ψ_i are the basis of the D irrp of the group of $\hat{H}_{\mathrm{Sch}}$ while $\Psi_i^\star$ are the basis of $D^\star$. When D and $D^\star$ are complex [11] the state of a system (energy term) will be classified by the joint $D \oplus D^\star$ irrps. Clearly, the degeneracy of a state increases twice. In order to determine whether or not the TRS is present in a system, one has to find all complex irrps of a symmetry group of a Hamiltonian. Fröbenius and Schur [12] showed that it is sufficient to know only the characters of irrps to determine whether a representation (rep) is real or complex. The characters of the 32 crystallographic point groups and 230 space groups are readily available in CDML tables [13]. We have tested all irrps of the C_{6v}-ZnO group. The following irrps are TRS degenerate:

Single-valued irrps for classification of spinless particle states (like phonons): $A_{1,2,3,4,5,6}$, $\Delta_{1,2,3,4,5,6}$, $H_{1,2}$, $L_{1,2,3,4}$, $U_{1,2,3,4}$, $P_{1,2,3}$, and $S_{1,2}$ of high symmetry points.

Double-valued irrps for particles with $S = \frac{1}{2}, \frac{3}{2}, \ldots$ (spinors): $\Gamma_{6,7,8}$ of point and space groups. The double-valued irrps of the 32 crystallographic point groups and 230 space groups are normally complex and therefore TR degenerated. Consequently, the states of free electrons and holes at $\mathbf{k} = \mathbf{0}$ in ZnO suppose to be classified by joint irrps: $\Gamma_7^c \oplus (\Gamma_7^c)^\star, \Gamma_9^v \oplus (\Gamma_9^v)^\star$, and $\Gamma_7^v \oplus (\Gamma_7^v)^\star$. Fig. 3 displays the effect of TRS on the band structure.

2.3. SRs for optical transitions in wurtzite structure in the absence of TRS

In the absence of accidental degeneracy and TRS, the matrix elements of a perturbation $\hat{f}$ between CB and VB states is of the form: $\int (\Psi_i^c)^\star \hat{f} \varphi_j^v \, \mathrm{d}\vec{r}$, which is non-zero when the corresponding Kronecker product $\Gamma^c \otimes D^f \otimes \Gamma^v$ contains the unit rep normally denoted as Γ_1 or A_1 [13].

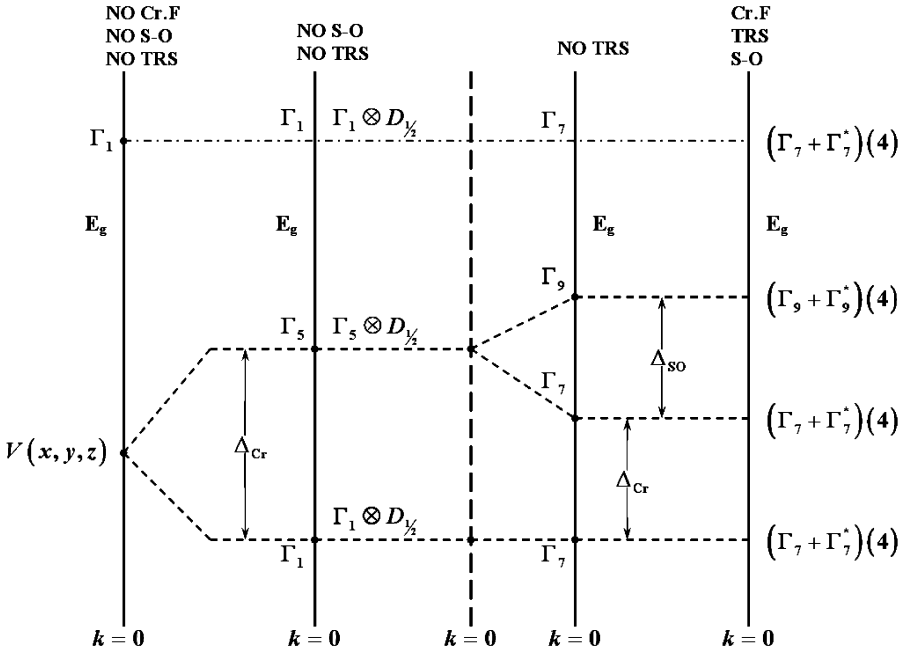

Fig. 3. Band structure and selection rules for wurtzite compounds at the Γ symmetry point ($\mathbf{k}=\mathbf{0}$). The V stands for 3×3 dimensional vector representation, which is reducible to $\Gamma_1(z)+\Gamma_5(x,y)$. There are a number of wurtzite compounds for which the above band structure is valid. In some of them the crystalline field is rather negligible. For them the very first left diagram of band structure can be relevant. Our figure can be directly compared with Fig. 1 in Ref. [8]. Birman assigned the top VB of a zinc-blende structure by Γ_4' rep. The Γ_4' rep is one of the irrps of the zinc-blende space group and it is simultaneously vector representation of the group. For wurtzite structures, a similar assignment on Birman's figure is missing. It should be mentioned that for the here used valence band structure of ZnO, the ordering of the uppermost valence bands has to be reversed.

The D^f is a rep (not necessary irreducible) according to which the perturbation operator transforms. In case of absorption (emission) of electromagnetic radiation, the dipole moment operator $\hat{f}=\hat{d}$ for the electric dipole radiation transforms like X,Y,Z (vector rep $V=\Gamma_1(z)\oplus\Gamma_5(x,y)$) in ZnO. In order to discuss the SRs we have to establish the ordering of the VBs. Following the ordering of Thomas and Hopfield [14] in agreement with recent MPL studies [6] we attribute the uppermost A VB to consist of hole states with Γ_7 symmetry.

For $\tilde{\mathbf{E}}\|\mathbf{c}$ (c-hexagonal axis along z) the SRs are:

$\Gamma_7^c\otimes\Gamma_1(z)\otimes\Gamma_7^v=\Gamma_1\oplus\Gamma_2\oplus\Gamma_5$ (allowed transitions for A- and C-excitons).
$\Gamma_7^c\otimes\Gamma_1(z)\otimes\Gamma_9^v=\Gamma_5\oplus\Gamma_6$ (B-excitons, forbidden transition since the Kronecker product does not contain Γ_1 rep).

For $\tilde{\mathbf{E}}\perp\mathbf{c}$, we have:

$\Gamma_7^c\otimes\Gamma_5(x,y)\otimes\Gamma_7^v=\Gamma_1\oplus\Gamma_2\oplus 2\Gamma_5\oplus\Gamma_6$.
$\Gamma_7^c\otimes\Gamma_5(x,y)\otimes\Gamma_9^v=\Gamma_1\oplus\Gamma_2\oplus\Gamma_6\oplus\Gamma_3\oplus\Gamma_4\oplus\Gamma_5$.

For $\tilde{\mathbf{E}}\perp\mathbf{c}$ polarization all transitions for A-, B-, and C-excitons are allowed and observed experimentally [15,16].

2.4. SRs in the presence of TRS

As mentioned the electron and hole states are TR degenerated and therefore their states are classified according to the joint reps: $D\oplus D^\star$. Consequently, the respective SRs are:

For $\tilde{\mathbf{E}}\|\mathbf{c}$: $(\Gamma_7^c\oplus(\Gamma_7^c)^\star)\otimes\Gamma_1(z)\otimes(\Gamma_9^v\oplus(\Gamma_9^v)^\star)$. The decomposition of the KPs reveals $4\Gamma_5$ and $4\Gamma_6$ states. All the states have different basis functions and those can be obtained by Clebsch–Gordon coefficients methods. The B-excitons are still forbidden as in the absence of TRS.

For $\tilde{\mathbf{E}}\|\mathbf{c}$: $(\Gamma_7^c\oplus(\Gamma_7^c)^\star)\otimes\Gamma_1(z)\otimes(\Gamma_7^v\oplus(\Gamma_7^v)^\star)=4\Gamma_1\oplus 4\Gamma_2\oplus 4\Gamma_5$. The transitions are also allowed as in the absence of TRS.

For $\tilde{\mathbf{E}}\perp\mathbf{c}$: $(\Gamma_7^c\oplus(\Gamma_7^c)^\star)\otimes\Gamma_5(x,y)\otimes(\Gamma_9^v\oplus(\Gamma_9^v)^\star)=(\Gamma_5\oplus\Gamma_6)\otimes\Gamma_5\oplus\cdots$. The transition is allowed for an B-exciton, since the KP $\Gamma_1\in\Gamma_5\otimes\Gamma_5$.

For $\tilde{\mathbf{E}}\perp\mathbf{c}$: $(\Gamma_7^c\oplus(\Gamma_7^c)^\star)\otimes\Gamma_5(x,y)\otimes(\Gamma_7^v)\oplus(\Gamma_7^v)^\star=4(\Gamma_1\oplus\Gamma_2\oplus\Gamma_3\oplus\Gamma_4\oplus\Gamma_5\oplus\Gamma_6)$. Again these transitions are allowed.

Clearly the TRS does not change the existing SRs. It introduces only a number of new states of the same symmetries. All the states are based on different wave functions, which correspond to different energy levels. Further splitting due to TRS is possible. The effect of TRS on phonons and TR splitting has been experimentally observed [18]. Recent studies of the electronic band structure of ZnO by means of first-principles calculations and density-functional theory [17] clearly evidence the existence of TRS on high symmetry point A and Δ line in ZnO and other wurtzite compounds.

3. Discussions and conclusion

From the first part of this paper, it follows that magneto-photoluminescence studies can clearly identify the origin of the neutral and ionized bound exciton transitions shown in Figs. 1 and 2. We observe a linear splitting of I_{6a}–I_8 corresponding to neutral excitonic complexes and a non-linear zero-field splitting for the ionized donor bound excitons I_0–I_2. It is suggested, that these ionized donor bound excitons are related to the same chemical impurity as their correlated neutral donor bound excitons I_{6a}, I_8, and I_9.

The selections rules discussed in Section 2 are related to absorption (emission) transitions observed by reflectivity measurements [19,20]. Our results are in good agreement with early and recently reported experimental data [21]. The ordinary photoluminescence (PL) technique can only probe A-excitons at $\mathbf{k}=0$ of symmetries Γ_5 and Γ_6 ($\Gamma_7^c\otimes\Gamma_9^v=\Gamma_5(\uparrow\downarrow)\oplus\Gamma_6(\uparrow\uparrow)$). The shoulder lines at around 3.3750 and 3.3775 eV might be

related to the Γ_5 (anti-parallel spins) and Γ_6 (parallel spins) free excitons.

As discussed in Section 1, the transition lines I_{6a}, I_8, and I_9 originate from the recombination of bound excitons at neutral donor complexes such as Al, Ga, and In. The atomic ground states of the elements listed in Table 1, including Li, are: Li ($n=2$, $^2S_{1/2}$), Al ($n=3$, $^2P_{1/2}$), Ga ($n=4$, $^2P_{1/2}$), In ($n=5$, $^2P_{1/2}$); see Fig. 5.2, p. 87 and Fig. 8.1, p. 115 in Ref. [22], where n is the principal quantum number. These states are doublets ($2S+1=2$) and therefore exhibit anomalous Zeeman splitting. Their spectral terms can also be found in [22]. In ZnO these dopants become shallow donors to which the excitons of symmetries $\Gamma_7^c \oplus \Gamma_7^v$(A), $\Gamma_7^c \oplus \Gamma_9^v$(B), and $\Gamma_7^c \oplus \Gamma_7^v$(C) are bound. The excitons bound to the dopant states do not contribute to the spin states of complexes. Therefore, these complexes remain doublets ($S=\frac{1}{2}$, $2S+1=2$), $m_s=-1/2, +1/2$. In a magnetic field, the Zeeman effect of these states can be observed and the g-values obtained.

For phonons in ZnO and GaN the extra time reversal degeneracy has already been proven by experiments [19,20]. Clearly, the phonons at the high symmetry line Δ and point A experience time reversal symmetry (TRS) degeneracy. However, the time reversal splitting of electronic states has, to the best of our knowledge, never been observed. Since the inclusion of TRS has no effect on the optical selection rules, but only introduces additional states of the same symmetry, this fact is in agreement with our theoretical calculations.

In conclusion we have demonstrated a correlation between ionized and neutral donor bound excitons of the same chemical identity. For high resolution and high magnetic field spectra additional transition lines can be observed. Rigidly derived selection rules are in good agreement with the experimental data. The inclusion of TRS as possible origin has been studied. It could be proven that the inclusion of TRS does not change the existing selection rules compared to those in the absence of TRS. It only introduces new states of the same symmetry. By the strict derivation of the selection rules, it could be concluded that the inclusion of TRS should not affect the observable optical transition.

References

[1] S. Müller, D. Stichtenoth, M. Uhrmacher, H. Hofsäss, C. Ronning, J. Röder, Appl. Phys. Lett. 90 (2007) 012107.
[2] K. Johnston, M.O. Henry, D. McCabe, E. McGlynn, M. Dietrich, E. Alves, M. Xi, Phys. Rev. B 73 (2006) 165212.
[3] B.K. Meyer, H. Alves, D.M. Hofmann, W. Kriegseis, D. Forster, F. Bertram, J. Christen, A. Hoffmann, M. Straburg, M. Dworzak, U. Haboeck, A.V. Rodina, Phys. Status Solidi 241 (2004) 231.
[4] B.K. Meyer, J. Sann, S. Lautenschläger, M.R. Wagner, A. Hoffmann, Phys. Rev. B 76 (2007) 184120.
[5] D.G. Thomas, J.J. Hopfield, Phys. Rev. Lett. 7 (1961) 316.
[6] A.V. Rodina, M. Strassburg, M. Dworzak, U. Haboeck, A. Hoffmann, A. Zeuner, H.R. Alves, D.M. Hofmann, B.K. Meyer, Phys. Rev. B 69 (2004) 125206.
[7] M.R. Wagner, A. Hoffmann, A. Rodina, B.K. Meyer, to be published, 2008.
[8] J. Birman, Phys. Rev. Lett. 2 (1959) 4.
[9] W.R.L. Lambrecht, A.V. Rodina, S. Limpijumnong, B. Segall, B.K. Meyer, Phys. Rev. B 65 (2002) 075207.
[10] M. Hammermesh, Group Theory and its Application to Physical Problems, Pergamon Press, New York, 1962.
[11] G.F. Koster, J.O. Dimmock, R.G. Wheeler, H. Statz, Properties of the Thirty-Two Point Groups, MIT Press, Cambridge, MA, 1963.
[12] G. Frobenius, I. Schur, Berl. Ber. 186 (1906).
[13] A.P. Cracknell, B.L. Davis, S.C. Miller, W.F. Love, Kronecker Product Tables, vol. 4. IFI/Plenum Press, New York, Washington, London, 1979.
[14] J.J. Hopfield, J. Phys. Chem. Solids 15 (1960) 97.
[15] Y.S. Park, C.W. Litton, T.C. Collins, D.C. Reynolds, Phys. Rev. 143 (1966) 512.
[16] P. Erhart, K. Albe, A. Klein, Phys. Rev. B 73 (2006) 205203.
[17] J. Serrano, A.H. Romero, F.J. Manjon, R. Lauck, M. Cardona, Rubio, Phys. Rev. B 69 (2004) 094306.
[18] D.C. Thomas, J.J. Hopfield, Phys. Rev. 128 (1962) 2135.
[19] K. Thoma, B. Dorner, G. Duesing, W. Wegener, Solid State Commun. 15 (1974) 11111.
[20] A.W. Hewat, Solid State Commun. 8 (1974) 187.
[21] D.C. Reynolds, C.W. Litton, T.C. Collins, Phys. Rev. 140 (1965) A1726.
[22] H.E. White, Introduction to Atomic Spectra, McGraw-Hill, New York, London, 1934.

Journal of Physics: Conference Series **92** (2007) 012071 doi:10.1088/1742-6596/92/1/012071

Phonons and electronic states of ZnO, Al_2O_3 and Ge in the presence of time reversal symmetry

A G J Machatine[1], H W Kunert[1], A Hoffmann[2], J B Malherbe[1], J Barnas[3], R Seguin[2], M R Wagner[2], P Niyongabo[1] and N Nephale[1]

[1]Department of Physics, University of Pretoria, 0002 Pretoria, South Africa
[2]Institut für Festkörperphysik, Technische Universität Berlin, Hardenbergerstr. 6 10-623 Berlin, Germany
[3]Department of Physics, Adam Mickiewicz University, ul. Umultowska 85, 61-614 Poznan, Poland

E-mail: augusto.machatine@up.ac.za

Abstract. Using group theoretical techniques we have investigated all single valued representations as well as double valued, these follow from the inclusion of spin, of wurtzite (e.g. ZnO) , trigonal (e.g. Al_2O_3) and cubic (e.g. Ge) structures, with the C_{6v}^4, D_{3d}^6 and O_h^7 space groups, respectively, with regard to the presence or absence of Time Reversal Symmerty (TRS). We have found a number of phonons in wurtzite and trigonal structures to be time reversal degenerate, whereas in the cubic Si, Ge and diamond the vibrational modes are not time reversal degenerate. Electronic band structure also experience extra TRS degeneracy. Therefore, the selections rules for optical radiative transitions need modification.

1. Introduction

Wurtzite (C_{6v}^4-space group) wide band semiconductors: ZnO, GaN, 6H-SiC, etc., have received considerable attention owing to their opto-electronic properties. Phonons are the primary excitations that influence the thermodynamics and the transport properties of materials. In order to understand materials phenomena we study phonons thouroughly.

Sapphire Al_2O_3 is a very common material on the Earth's crust that crystallizes in the trigonal space group D_{3d}^6. The excellent mechanical and optical properties of sapphire in its pure and dopped form makes it a material of choice for various physical and technological applications. It is frequently used as substrate for growing thin films of semiconductor such as GaN, ZnO, ZnS, etc.

Ge, Si and Diamond with the space group O_h^7 are well known compounds with a large variety of technological applications.

The effect of time reversal symmetry on vibrational modes, electronic states and optical properties of these compounds is still not well understood. It is our aim to comprehesively investigate the impact of TRS on the properties of these materials. TRS has also has an impact on scattering processes of semiconductors. We shall briefly indicate some consequences of TRS on optical transistions.

2. Space and Time Reversal Symmetry. Phonons and Electronic States of Quasiparticles in Wurtzite, Trigonal and Cubic Crystals.

States of quasiparticles such as phonons, electrons in conduction band (CB), holes in the valence band (VB), excitons, plasmons, polaritons, magnons, etc., in the absence of the TRS are classified according to the irreducible representations (irrps) $D_j^{\mathbf{k}}$ of the space group $G^{\mathbf{k}}$. The wave vector $\mathbf{k}$ runs over the entire first Brillouin zone (BZ) and determines the high symmetry points and lines. In wurtzite BZ they are Γ, A, M, K, L, H, R, Q, S, Δ, Σ, Λ, U and P; in trigonal crystals: Γ, T, P, F, Y, L, Λ and Σ and in cubic crystal structures Γ, $W, X, Z(V), Q, S, A$, Λ, Δ and Σ. All these high symmetry points and lines have own set of irrps. The irrps of the 230 space groups and their characters are well established and available in CDML tables [1]. In the tables the generators of single and double valued irrps are given. The states of phonon-spinless quasiparticles are classified according to the single valued (SV) irrps, while states of electrons, holes, and therefore excitons according to double valued (DV) irrps. Frobenius and Schur (F-Sch.) showed that when an irrp is complex an extra degeneracy may occur. They derived the so-called reality test for irrps which is of the form:

$$R = \frac{f}{h} \sum_{g \in G^{\mathbf{k}}} \chi_{\mathbf{k}}(g^2)\, \delta_{k,-gk} = +1(a), \quad -1(c), \quad 0(b) \tag{1}$$

where all the quantities have their usual meaning [2, 3]. In the case (a) the irrps are real and there is no extra degeneracy, while in (b) and (c) cases an extra degeneracy occurs. In these cases the states of quasiparticles will be classified according to the direct sum of $D_j^{\mathbf{k}}$ and $(D_j^{\mathbf{k}})^\star$ irrps $\Rightarrow D_j^{\mathbf{k}} \oplus (D_j^{\mathbf{k}})^\star$. This classification of the states reflects both space and time reversal symmetry. Consequently, the degeneracy (the dimension of $D_j^{\mathbf{k}}$) doubles.

In this paper we shall investigate irrps of a space group using F-Sch. criterion (equation (1)) to determine whether or not the TRS is present in a crystal. Using the equation (1) we have investigated all SV and DV irrps of wurtzite, trigonal and cubic cyrstals.

2.1. Single Valued irrps. Phonons

As mentioned above SV irrps are used for the classification of spinless quasiparticles.
The following irrps belong to (b) or (c) cases of equation (1). All others not listed belong to case (a).

wurtzite	A_{1-6}, Δ_{1-6}, $P_{1,2,3}$, L_{1-4}, $H_{1,2,3}$
trigonal	Λ_i , P_i, T_i $(i = 1, 2, 3)$
cubic	None. All irrps are real (case (a)). There is no TRS degeneracy.

The resulting classification of the vibrational states in these crystals subjected to TRS is:

wurtzite	$A_i \oplus A_i^\star$, $\Delta_i \oplus \Delta_i^\star$, $P_j \oplus P_j^\star$; $L_i \oplus L_i^\star$, $H_j \oplus H_j^\star$ $(i = 1-4, j = 1-3)$
trional	$\Lambda_i \oplus \Lambda_i^\star$, $P_i \oplus P_i^\star$, $T_i \oplus T_i^\star$; $(i = 1-3)$
cubic	The phonons in Si, Ge, and diamond are not subject to TRS. They are classified according to the $D_j^{\mathbf{k}}$ tabulated in CDML[1].

2.2. Discussion of line $\Gamma - \Delta - A$ for wurtzite

The displacement representation [4, 5, 6] provides the number of normal modes and their symmetries in the entire BZ. In the wurtzite structure the normal modes spanned by displacement representation at critical points Γ, A and line Δ are:

$$\begin{aligned} \Gamma &: \quad 2\Gamma_1 \oplus 2\Gamma_4 \oplus 2\Gamma_5 \oplus 2\Gamma_6 \\ A &: \quad 2A_1 \oplus 2A_4 \oplus 2A_5 \oplus 2A_6 \\ \Delta &: \quad 2\Delta_1 \oplus 2\Delta_4 \oplus 2\Delta_5 \oplus 2\Delta_6 \end{aligned}$$

Using compatibility relations, the resulting modes assignment along the $\Gamma - \Delta - A$ axis is:

Point Γ : $\Gamma_1 \oplus \Gamma_5$, Γ_6, Γ_4, Γ_5, Γ_6, Γ_4 and Γ_1
Point A : $A_5 \oplus A_5^\star$, $A_1 \oplus A_1^\star$, $A_5 \oplus A_5^\star$ and $A_1 \oplus A_1^\star$
Line Δ : the dispersion curves connect the points Γ and A when going from the bottom to the top on the A axis side: Δ_5, $\Delta_5^\star$, Δ_1, $\Delta_1^\star$, Δ_5, $\Delta_5^\star$, Δ_1 and $\Delta_1^\star$.

Using CDML tables we have derived all Γ, Δ and A irrps. We have found the following relations. $A_1^\star = A_4$, $A_5^\star = A_6$, $\Delta_1^\star = \Delta_4$, $\Delta_5^\star = \Delta_6$. Figure 1 displays assignment of the schematic dispersion curves of the $\Gamma - \Delta - A$ region of the BZ subjected to TRS for wurtzite compounds in terms of joint irrps. For simplicity we used straight lines for connectivity.

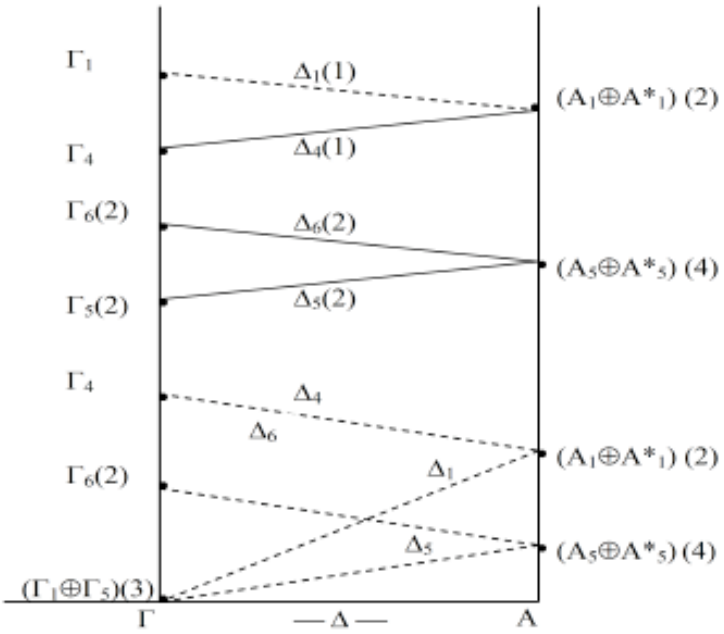

Fig.1 Phonon assignment along the $\Gamma - \Delta - A$ axis.

2.3. Experimental Evidence

The very first experimental proof of the existence of TRS have been provided by Hewat and Thoma [7, 8] and reference herein. by inelastic neutron scattering. They observed experimental data on a $\Delta-$ line phonon dispersion curve TR degenerate. More recently Ruf [9] et. al. studied the phonon dispersion curves in GaN by inelastic X-ray scattering in Fig.2 in [9]. Their data gave evidence of the existence of TRS. With the help of our Figure 1 it is easy to understand experimental evidence of TRS obtained by Hewat, Thoma, Ruf and others [7, 8, 9]. A number of lattice dynamics calculations by means of density functional theory and ab initio theory have been reported [10, 11, 12], providing further evidence of TRS degeneracy. Sapphire has similar features on high the symmetry $\Lambda-$ line which have been proven theoretically and experimentally by Heid, Schrober and Ossowski [12, 13, 14, 15].

2.4. Double Valued irrps. Electrons, holes and excitons

Inclusion of spin results in DV irrps (spinors) for electron and hole states. These states transform according to DV irrps. We have briefly discussed the selection rules for the excitons symmetries in the presence of TRS with respect to phonon scattering processes, previously discussed by Birman and Ganguly [16] without consideration of the effect of TRS on the exciton symmetry. For the Hamiltonian of the exciton-phonon interaction one needs the exact symmetry for the exciton and phonon. The exciton symmetry results from the product of electrons and holes symmetries. For

ZnO the A-exciton has the symmetry $\Gamma_7^{CB} \otimes \Gamma_9^{VB} = \Gamma_5 \oplus \Gamma_6$. The spilitting onto two single states Γ_5 and Γ_6 is due to exchange interaction. The irrps Γ_7^{CB} and Γ_9^{VB} are DV irrps (spinors) and belong to case (c) in equation (1). Therefore, the TRS must be taken into account. The resulting A-exciton symmetry due to TRS is $\left[\Gamma_7^{CB} \oplus \left(\Gamma_7^{CB}\right)^\star\right] \otimes \left[\Gamma_9^{VB} \oplus \left(\Gamma_9^{VB}\right)^\star\right] = 4\Gamma_5 \oplus 4\Gamma_6$, and in this case the exchange interaction splits the exciton state into four Γ_5 and Γ_6 states. Clearly, the inclusion of TRS results in three more states of Γ_5 and Γ_6 symmetries, with different energy levels, compared to the selection rules without TRS. In other words, the TRS does not introduce states of new symmetries, but introduces more states of the same symmetries. Consequently, TRS does not change the existing optical selection rules tabulated in many books [1], but it may affect the enhanced Raman scattering processes in crystals. These involve a creation and destruction of intermediate states of crystals. The interaction of excitons with phonons is determined by Kronecker product of exciton and phonon symmetry $D_j^{Exciton} \otimes D_j^{Phonon}$. These KPs have to be evaluated by the standard group theoretical decomposition of the reducible rep onto irrps.

3. Conclusion

We have investigated the effect of TRS on vibrational modes in wurtzite, trigonal and cubic structures. For these structures the single valued representations of time reversal degenerate states are given. The symmetry of excitons in wurtzite time reversal subjected is discussed. Inclusion of TRS may result in an increase of time reversal degenerate phonon states of the exciton-phonon interaction for enhanced Raman scattering processes. A need of modification of existing optical selection rules (Kronecker Products) in the presence of TRS is indicated. Our results are valid for the following compounds: wurzite: ZnO, ZnS, ZnSe, ZnTe, GaN, AlN, InN, BP, BeO, CdS, CdSe, CdTe, CuI, 2H-SiC, 3H-SiC, 4H-SiC, 6H-SiC, etc.; Trigonal: Al_2O_3, Cr_2O_3, Fe_2O_3, V_2O_3, Ti_2O_3, $AlBO_3$, $FeBO_3$, $NaNO_3$, $CaCO_3$, $ZnCO_3$, $MgCO_3$ MgTe, $MnCO_3$, $CdCO_3$, $FeCO_3$, etc.; Cubic : Ge, Si, Diamond, etc.

References

[1] Cracknell A P, Davies B L, Miller S C and Love W F 1979 *Kronecker Product Tables* vol 4 (IFI/Plenum Press, New York, Washington, London)
[2] Frobenuis G and Schur I 1906 *Berl. Ber.* 186
[3] Bir G L and Pikus G E 1974 *Symmetry and Strain-Induced Effects in Semiconductors* (John Wiley & Sons, New York, Toronto)
[4] Kunert H W 2004 *Eur. Phys. J. Appl. Phys.* **27** 251
[5] Kunert H W 2003 *Appl. Surf. Sci.* **212-213** 890
[6] Birman J 1963 *Phys. Rev* **131** 1489
[7] Hewat A W 1970 *Solid State Comm.* **8** 187
[8] Thomas K, Dorner B, Duesing G and Wegener W 1974 *Solid State Comm.* **15** 1111
[9] Ruf T, Serrano J, Cardona M, Pavone P, Past M, Krisch M, D' Astuto M, Suski T, Grezegory I and Leszczynski M 2001 *Phys. Rev. Lett.* **86** 906
[10] Parlinski K and Kawazoe Y 1999 *Phys. Rev. B* **60** 15511
[11] Karch K, Wagner J-M and Bechstedt F 1998 *Phys. Rev. B* **57** 7043
[12] Ossowski M M, Boyer L L and Mehl M J 2002 *Phys. Rev. B* **66** 224302
[13] Schrober H, Strauch D and Dorner B 1993 *Z. Phys. B* **92** 273
[14] Schrober H, Strauch D and Dorner B 1984 *Z. Phys. B* **29** 2190
[15] Heid R, Strauch D and Bohnen K P 2000 *Phys. Rev. B* **61** 8625
[16] Birman J and Ganguly A K 1966 *Phys. Rev. Lett.* **17** 647

Phys. Status Solidi B **247**, No. 7, 1802–1806 (2010) / **DOI** 10.1002/pssb.200945583

physica status solidi b
www.pss-b.com
basic solid state physics

Clebsch–Gordan coefficients for scattering tensors in ZnO and other wurtzite semiconductors

Herbert W. Kunert*[,1], Markus R. Wagner[2], Augusto G. J. Machatine[1], Prime Niyongabo[1], Johan B. Malherbe[2], Axel Hoffmann[2], Jozef Barnaś[3], and Wojciech Florek[3]

[1] Department of Physics, University of Pretoria, 0001 Pretoria, South Africa
[2] Institute of Solid State Physics, Technische Universität Berlin, Hardenbergstr. 36, 10623 Berlin, Germany
[3] Faculty of Physics, Adam Mickiewicz University, ul. Umultowska 85, 61-614 Poznań, Poland

Received 4 December 2009, revised 8 February 2010, accepted 10 February 2010
Published online 17 May 2010

Keywords II–VI semiconductors, Clebsch–Gordan coefficients, scattering tensor

* Corresponding author: e-mail Herbert.Kunert@up.ac.za, Phone: +27 4202636, Fax: +27(0)12-362-5288

Selection rules for inter- and intra-valley scattering processes between the minima of the lowest conduction band Γ, L, M, and A are investigated in wurtzite ZnO. The knowledge of the selection rules is required for the determination of the Clebsch–Gordon coefficients (CGCs). These coefficients diagonalize the Kronecker products (KPs) of relevant irreducible representations of quasi particles participating in scattering processes. The elements of the scattering tensors are the linear combinations of the CGCs. Within this work, the CGCs for ZnO belonging to the space group C_{6v}^4 are determined.

1 Introduction The study of scattering processes involving phonons provides important information about various physical properties of semiconductors. These processes are usually described by the different scattering tensors which are determined by appropriate experimental techniques. Applying electrical (transport) measurements, tensors like the second rank conductivity, capacitance, and resistivity tensor can be determined. The inelastic light scattering is described by a symmetric second rank tensor which can be derived with high accuracy using Raman spectroscopy. The mechanical properties of crystals depend on tensors like surface stiffness constants, determined by, e.g., Brillouin scattering, or the third rank piezoelectric tensor which involves electron–acoustic–phonon interactions. Particularly, in non-centro-symmetric crystals (zinc blende and wurtzite) the strain tensor and induced electric fields can be expressed as a third rank electromechanical tensor (see, e.g., Ref. [1]).

In this contribution we investigate scattering processes in the wide band gap semiconductor ZnO which is attracting much attention due to potential applications in, e.g., short-wavelength optoelectronic devices and surface acoustic wave modulators [2, 3]. In particular, possible inter- and intra-valley scattering processes at local extrema in the electronic band structure of ZnO are studied by Clebsch–Gordan coefficients (CGCs). These scattering processes can occur at high symmetry points due to the interaction of carriers with phonons, impurities, and dislocations. The mechanisms have been studied in a wide variety of different semiconductors. Lax and Hopfield [4] and Birman et al. [5] have investigated the selection rules for direct and indirect radiative transitions by intra- and inter-valley scattering in Si and Ge. The Raman scattering tensors in cubic Cu_2O (O_h^4) were analyzed by Birman [6]. The mathematical theory of the CGCs was derived by Berenson and Birman [7] who calculated CGCs for diamond (O_h^7) and rocksalt (O_h^5) [8]. Birman et al. [9] have shown that the matrix elements of the Luttinger–Bir–Picus $\boldsymbol{k}\cdot\boldsymbol{p}$ effective Hamiltonian can be constructed as products of the CGCs times symmetrized tensorial field quantities. They applied the method to the β-wolfram structure (O_h^3). Kunert and Suffczyński [10, 11] developed the theory of the CGCs related to the wave vector selection rules (WVSRs) in terms of block structures. They computed the CGCs for the O_h^3 space group. Finally, Berenson [12] discussed the scattering tensors for crystals limited to the point groups T_d and C_{6v}. However, the coefficients for ZnO have not been studied up to now. In principal, the here presented results can also be applied to

Original Paper

Table 1 Clebsch–Gordan coefficient matrix for $L_1 \otimes M_1 = A_1 \oplus A_5 \oplus L_1 \oplus L_2$, $a = 1/\sqrt{2}$, $b = 1/\sqrt{3}$, $w = -1/2 + i\sqrt{3}/2$.

WVSRs	block $\sigma\sigma'\sigma''$	A_1	A_5	L_1			L_2		
$\boldsymbol{k}_L + \boldsymbol{k}_M = \boldsymbol{k}_A$	111	b	b	b	0	0	0	0	0	0
$2\boldsymbol{k}_L + 2\boldsymbol{k}_M = \boldsymbol{k}_A$	221	b	$-iwb$	$-iw^*b$	0	0	0	0	0	0
$3\boldsymbol{k}_L + 3\boldsymbol{k}_M = \boldsymbol{k}_A$	331	b	w^*b	wb	0	0	0	0	0	0
$2\boldsymbol{k}_L + 3\boldsymbol{k}_M = \boldsymbol{k}_L$	231	0	0	0	ia	0	0	$-ia$	0	0
$3\boldsymbol{k}_L + 2\boldsymbol{k}_M = \boldsymbol{k}_L$	321	0	0	0	$-ia$	0	0	ia	0	0
$\boldsymbol{k}_L + 3\boldsymbol{k}_M = 2\boldsymbol{k}_L$	132	0	0	0	0	$-ia$	0	0	ia	0
$3\boldsymbol{k}_L + \boldsymbol{k}_M = 2\boldsymbol{k}_L$	312	0	0	0	0	ia	0	0	$-ia$	0
$\boldsymbol{k}_L + 2\boldsymbol{k}_M = 3\boldsymbol{k}_L$	123	0	0	0	0	0	ia	0	0	$-ia$
$2\boldsymbol{k}_L + \boldsymbol{k}_M = 3\boldsymbol{k}_L$	213	0	0	0	0	0	$-ia$	0	0	ia

$$U^{-1}(L_1 \otimes M_1)U = \begin{pmatrix} A_1 & 0 & 0 & 0 \\ 0 & A_5 & 0 & 0 \\ 0 & 0 & L_1 & 0 \\ 0 & 0 & 0 & L_2 \end{pmatrix}$$

other wide band gap semiconductors like GaN, CdS, 6H-SiC, BeO, and ZnS which crystallize in the same hexagonal C_{6v}^4 structure.

2 Symmetry of ZnO band structure The states of spin less quasi-particles like phonons and excitons are classified according to the single-valued irreducible representations (SV-irrps) of the crystal space group. Recently, Lambrecht et al. [13] calculated the band structure of ZnO using first principles linear muffin-tin orbital density functional theory. In their computation the spin of electrons and holes was disregarded. However, the effect of the time reversal symmetry along the high symmetry line Δ and at point A was taken into account.

Figure 1 in Ref. [13] gives an overview of the ZnO band structure throughout the entire Brillouin zone (BZ). Several minima of conduction bands at high symmetry points can be distinguished, e.g., for Γ, M, A, L, and X. The corresponding symmetries are Γ_1, M_1, A_1, L_1, and X_1. The valley A_1 is time reversal degenerate. Therefore, its symmetry is supposed to be $A_1 \oplus (A_1)^* = A_1 \oplus A_4$ [14]. The maxima of the valence bands at the Γ point and A point have the symmetries Γ_5 and A_5, respectively.

For direct optical transitions in semiconductors, which preserve the $\boldsymbol{k}$ vector, an electron can be scattered by a phonon. In such a case the scattering processes can be described by group theoretical scattering selection rules regarding only the SVirrps [4, 5]. In most semiconductors, however, there is also an appreciable and measurable spin–orbit interaction. Consequently, the electron and hole states must be assigned by spinor representations. For ZnO, these are Γ_7 for the conduction band and Γ_{7+}, Γ_9, Γ_{7-} for the upper valence bands. The spinor representations are also referred to as double-valued irrps (DV-irrps).

3 The wave vector selection rules: Kronecker product and Clebsch–Gordan coefficients In this section we discuss the consequences of the momentum conservation principle, when an electron in the state $\boldsymbol{k}$ is scattered into another state with $\boldsymbol{k}'$ due to a phonon in the $\boldsymbol{k}''$ state. The momentum conservation determines the WVSRs. In ZnO as well as many other hexagonal crystals with the space group C_{6v}^4, there are three minima at the L and M points in the BZ. The first minimum at each of these points is characterized by the wave vectors $\boldsymbol{k}_L(101)$ and $\boldsymbol{k}_M(010)$ in the fundamental domain of the BZ [15]. The remaining two minima are derived from the $\boldsymbol{k}_L$ and $\boldsymbol{k}_M$ wave vectors to $2\boldsymbol{k}_L(011)$, $3\boldsymbol{k}_L(-111)$ and $2\boldsymbol{k}_M(100)$, $3\boldsymbol{k}_M(010)$, where 1, 2, and 3 are the symmetry operators according to the CDML labeling [15]. Together with $\boldsymbol{k}_L(101)$ and $\boldsymbol{k}_M(010)$, the wave vectors form so-called stars of the high symmetry points L and M. Combining these six wave vectors, we obtain the WVSRs of momenta conservation which are listed in Table 1 together with the calculated coupling coefficients. The U matrices for all tables are created from the elements of the Tables 1–5. For an example, see the listed U matrix of Table 3.

The description of any scattering process is given by the Kronecker product (KP) of irrps which corresponds to the particles involved in such processes. For example, for

Table 2 Clebsch–Gordan coefficient matrix for $(A_1 \oplus A_1^*) \otimes M_1 = [L_1 \oplus L_2]$.

WVSRs	block $\sigma\sigma'\sigma''$	aa'	L_1 1	2	3	L_2 1	2	3
$\boldsymbol{k}_A + \boldsymbol{k}_M = \boldsymbol{k}_L$	111	11	0	0	0	$\pm i$	0	0
		11	$\pm i$	0	0	0	0	0
$\boldsymbol{k}_A + 2\boldsymbol{k}_M = 2\boldsymbol{k}_L$	122	12	0	0	0	0	$\pm i$	0
		21	0	$\pm i$	0	0	0	0
$\boldsymbol{k}_A + 3\boldsymbol{k}_M = 3\boldsymbol{k}_L$	133	13	0	0	0	0	0	$\pm i$
		31	0	0	$\pm i$	0	0	0

$$U^{-1}((A_1 + A_1^*) \otimes M_1)U = \begin{pmatrix} L_1 & 0 \\ 0 & L_2 \end{pmatrix}$$

physica status solidi b

Table 3 Clebsch–Gordan coefficient matrix $M_1 \otimes M_1 = [\Gamma_1 \oplus \Gamma_5]$, $b = 1/\sqrt{3}, w = -1/2 + i\sqrt{3}/2$.

	block			Γ_1	Γ_5	
WVSRs	$\sigma\sigma'\sigma''$	aa'	$a'' =$	1	1	2
$\boldsymbol{k}_M + \boldsymbol{k}_M = \boldsymbol{k}_\Gamma$	111	11		b	b	$b\sqrt{w^*}$
$2\boldsymbol{k}_M + 2\boldsymbol{k}_M = \boldsymbol{k}_\Gamma$	221	12		b	bw	$bw^*\sqrt{w^*}$
$3\boldsymbol{k}_M + 3\boldsymbol{k}_M = \boldsymbol{k}_\Gamma$	331	13		b	bw^*	$bw\sqrt{w^*}$

$$U^{-1}(M_1 \otimes M_1)U = \begin{pmatrix} \Gamma_1 & 0 \\ 0 & \Gamma_5 \end{pmatrix}$$

$$U = b\begin{pmatrix} 1 & 1 & \sqrt{w^*} \\ 1 & w & w^*\sqrt{w^*} \\ 1 & w^* & w\sqrt{w^*} \end{pmatrix}$$

the scattering of an electron from the L valley into the M valley, the KP $L \otimes M$ must be decomposed into irrps of phonons. For this purpose, we use the comprehensive tables for KPs of the 230 space groups by Crackenell et al. [15] (CDML). The CGCs are the elements of a unitary matrix that reduces the direct KP of two reducible or irrps onto a sum of blocks of irrps contained in the product $D^{\{^*\boldsymbol{k}\}l} \otimes D^{\{^*\boldsymbol{k}'\}l'}$ with

$$U^{-1}D^{\{^*\boldsymbol{k}\}l} \otimes D^{\{^*\boldsymbol{k}'\}l'}U = \sum_{l''} c_{ll',l''}D^{\{^*\boldsymbol{k}''\}l''}, \qquad (1)$$

where all quantities have their usual meaning [7]. The KP reflects different kinds of interactions like electron–hole, electron–phonon, phonon–phonon, etc. which are normally treated as perturbation of an unperturbed Hamiltonian. In other words, the CGCs matrix diagonalizes the perturbation terms. Selected CGCs for ZnO are listed in Tables 1–5. For detailed calculations of CGCs in other space groups, please refer to the Berenson–Birman–Kunert method [7, 10, 11].

4 Scattering processes in ZnO Despite the fact that ZnO is a direct band gap semiconductor, inter- and intra-valley scattering processes are possible. Carriers in semiconductors are scattered by their interaction with many different defects, like stacking faults, dislocations, surfaces, interfaces, and impurities. Very common impurities with high concentrations in ZnO are, e.g., the group III donors Al, Ga, and In in the neutral (I_6, I_8, I_9) and ionized charge state (I_0, I_1, $I_{2/3}$) [16, 17]. Raman scattering in resonance with excitonic states results in a strong increase of the Raman cross-section due to the exciton–phonon interaction in ZnO [18]. In terms of electrical transport, the Boltzmann kinetic equation includes the effects on the distribution function $f(\boldsymbol{k})$ due to the applied field, diffusion of carriers, and scattering by phonons and impurities [19, 20]. The scattering processes are determined by appropriate matrix elements of the relevant Hamiltonian. These matrix elements, in turn, depend on the symmetry and obey certain selection rules. From the band structure of ZnO [13], we can easily derive the symmetries of the valence bands and conduction bands at the high symmetry points M, L, and A. Here, we determine the CGCs for the intra- and inter-valley scattering processes involving the emission of phonons in ZnO. These CGCs are listed in Tables 1–4. For an excitation energy $E > 3.8$ eV, the creation of excitons at the high symmetry point A is possible. The symmetries for these excitons are listed in Table 5.

Table 4 Clebsch–Gordan coefficient matrix $M_1 \otimes M_1 = [M_4]$, $c = 1/\sqrt{2}$, $w = -1/2 + i\sqrt{3}/2$.

	block			M_4		
WVSRs	$\sigma\sigma'\sigma''$	aa'	$a'' =$	1	2	3
$\boldsymbol{k}_M + 2\boldsymbol{k}_M = 3\boldsymbol{k}_M$	111	11		c	0	0
$\boldsymbol{k}_M + 3\boldsymbol{k}_M = 2\boldsymbol{k}_M$	123	12		0	w	0
$2\boldsymbol{k}_M + \boldsymbol{k}_M = 3\boldsymbol{k}_M$	231	13		0	0	w^*
$2\boldsymbol{k}_M + 3\boldsymbol{k}_M = \boldsymbol{k}_M$	222	21		$-c$	0	0
$3\boldsymbol{k}_M + \boldsymbol{k}_M = 2\boldsymbol{k}_M$	333	22		0	w^*	0
$3\boldsymbol{k}_M + 2\boldsymbol{k}_M = \boldsymbol{k}_M$	312	23		0	0	w

$U^{-1}(M_1 \otimes M_1)U = [M_4]$

Table 5 Clebsch–Gordan coefficient matrix for exciton wave functions originating from high symmetry point A, $A_7^{\mathrm{CB}} \otimes A_9^{\mathrm{VB}} = [\Gamma_5 \oplus \Gamma_6]$.

	block			Γ_5		Γ_6	
WVSRs	$\sigma\sigma'\sigma''$	aa'	$a'' =$	1	2	1	2
$\boldsymbol{k}_A + \boldsymbol{k}_A = \boldsymbol{k}_\Gamma$	111	11		0	$\pm i$	0	0
		12		0	0	$\pm i$	0
		21		0	0	0	$\pm i$
		22		$\pm i$	0	0	0

$$U^{-1}((A_7)^{\mathrm{CB}} \otimes (A_9)^{\mathrm{VB}})U = \begin{pmatrix} \Gamma_5 & 0 \\ 0 & \Gamma_6 \end{pmatrix}$$

5 Tables of coefficient matrices Following the general introduction about scattering processes in ZnO, we now provide detailed tables of CGCs for various scattering processes. For scattering processes between different valleys of the conduction band, the following KPs are required: $L \otimes M, L \otimes \Gamma, L \otimes A, M \otimes \Gamma, M \otimes A$, and $\Gamma \otimes A$. In Table 1, we list the CGCs for electron scattering between the L_1 and M_1 valleys resulting in large phonon momenta of A_1, A_5, L_1, and L_2 symmetries ($L_1 \otimes M_1 = A_1 \oplus A_5 \oplus L_1 \oplus L_2$).

Table 2 displays the CGCs for linear combinations of wave functions of phonons with large momenta $\hbar k_{L_1}$ and $\hbar k_{L_2}$ which originate from the scattering of electrons occupying the conduction band minima of A_1 and M_1 symmetry ($(A_1 \oplus A_1^*) \otimes M_1 = [L_1 \oplus L_2]$).

Tables 3 and 4 consist of CGCs for scattering processes of electrons occupying three different sub-valleys with momenta $\hbar k_M$, $2\hbar k_M$, and $3\hbar k_M$ which belong to one minimum of the CB valley M_1. The scattering processes resulting in low momentum ($\hbar k_\Gamma \approx 0$) of Γ_1 and Γ_5 phonons are shown in Table 3 ($M_1 \otimes M_1 = [\Gamma_1 \oplus \Gamma_5]$). The CGCs

Original Paper

for M_4 phonons with large momentum are listed in Table 4 ($M_1 \otimes M_1 = [M_4]$).

In Table 5, we display an example of the symmetries and CGCs of possible excitons at the A point for $(A_7)^{\mathrm{CB}} \otimes (A_9)^{\mathrm{VB}}$. The conceivable excitons of A symmetries have low momentum and the same symmetries as the Γ excitons. It should be noted that the valence band symmetry at the A point in Table 5 describes a hole state from the B valence band as has be proven in a recent magneto-optical study of the valence band ordering in ZnO by Wagner et al. [21].

6 Discussion The CGCs provided in this work have several important applications. Principally, they are defined as coefficients between basis functions of the irrps contained in the KP and the basis functions of the product of two irrps [7, 11]

$$\Psi_{a''}^{\boldsymbol{k}''\sigma''l''\gamma} = \sum_{\sigma a}\sum_{\sigma' a'} \left(\begin{array}{cccc|cc|c} \boldsymbol{k} & l & \boldsymbol{k}' & l' & \boldsymbol{k}'' & l'' & \gamma \\ \sigma & a & \sigma' & a' & \sigma'' & a'' & \end{array}\right) \Phi_a^{\boldsymbol{k}\sigma l} \Phi_{a'}^{\boldsymbol{k}'\sigma' l'}, \tag{2}$$

where

$$\left(\begin{array}{cccc|cc|c} \boldsymbol{k} & l & \boldsymbol{k}' & l' & \boldsymbol{k}'' & l'' & \gamma \\ \sigma & a & \sigma' & a' & \sigma'' & a'' & \end{array}\right) = U_{aa';a''}^{\sigma l \sigma' l';\sigma'' l'' \gamma} \tag{3}$$

are the matrix elements of the CGCs. The symbols a, a', and a'' indicate the matrix elements of the KP $l \otimes l'$ and the representation contained in the KP (l''). These symbols a, a', and a'' enumerate also the basis wave functions of the irrps l, l', and l'', respectively (see Eq. (4)). The $\boldsymbol{k}$, $\boldsymbol{k}'$ and $\boldsymbol{k}''$ stand for wave vectors (momenta $\hbar k$) of quasi particles involved in scattering processes such as electrons and phonons. The U matrix (CGC matrix) has two important physical meanings. On the one hand, it yields suitable linear combinations of the appropriate symmetry allowed basis functions of irrps (l'') contained in the KP in terms of product wave functions of $l \otimes l'$ (see Eqs. (2) and (3)). On the other hand, the U matrix diagonalizes any KP of two irrps ($l \otimes l'$) and brings the irrps l'' to the matrix diagonal block form (see Eq. (1) and the equations below the Tables 1–5).

For example, using our coefficients listed in Table 3, the appropriate symmetries of the Γ_5 wave functions contained in $M_1 \otimes M_1$ can be determined to:

$$\psi_{11}^{\Gamma_5} = \frac{1}{\sqrt{3}}\left\{\psi_{11}^{\boldsymbol{k}_M M_1} + w\psi_{22}^{2\boldsymbol{k}_M M_1} + w^*\psi_{33}^{3\boldsymbol{k}_M M_1}\right\},$$

$$\psi_{22}^{\Gamma_5} = \frac{1}{\sqrt{3}}\sqrt{w^*}\left\{\psi_{11}^{\boldsymbol{k}_M M_1} + w^*\psi_{22}^{2\boldsymbol{k}_M M_1} + w^*\psi_{33}^{3\boldsymbol{k}_M M_1}\right\}. \tag{4}$$

Next, the CGCs can also be used in the determination of the scattering tensors $\boldsymbol{P}$. When expanded in powers of kQ, we have [20]:

$$\boldsymbol{P}_{\alpha\beta} = \boldsymbol{P}_{\alpha\beta}^0 + \sum_{\mu\nu} \boldsymbol{P}_{\alpha\beta}^{j\nu} \boldsymbol{k}^j \cdot Q(\mu\nu) + \cdots \tag{5}$$

and in terms of CGCs they are

$$\boldsymbol{P}_{\alpha\beta}^{j\nu} = \sum_{\mu\nu} c(\mu\nu m) U_{\nu j,mn}^{l\otimes l'} \boldsymbol{P}_{\alpha\beta}^{(1)}(\mu\nu), \tag{6}$$

where $\boldsymbol{P}$ is the first order scattering tensor, and U is the matrix of the CGCs. The quantities in the above equations have their usual meanings [20]. The CGCs can also be used in the description of morphic effects [12], higher infrared order moment expansion, diagonalization of phonon dynamical matrices, as well as in the description of Gunn effect (inter-valley electron–phonon interaction) (see Ref. [1] and references therein). The coefficients can essentially be utilized in the construction of the effective Luttinger–Bir–Picus Hamiltonian matrix elements [9]:

$$H(K) = \sum_{\kappa} a_\kappa \delta_{\kappa,jj^*} \sum_l X_l^{(\kappa)} K_l^{(\kappa)^*}, \tag{7}$$

where a is the constant and K_l is Hermitian. The X_l span the l-dimensional linear vector space consisting of independent matrices. Birman et al. [9] have shown that the matrices are exactly the CGCs and therefore each element of an effective Hamiltonian matrix is a sum of symmetry adapted components of invariants times a CGC with the reduced matrix given by means of the Wigner–Eckart theorem:

$$H_{\alpha\beta}(K) = \sum_\kappa a_\kappa \sum_l (U^{-1})_{\alpha\beta l}^{j^* j\kappa} K_l^{(\kappa)^*}. \tag{8}$$

Using the CGCs and invariants, Birman et al. [9] constructed the effective Hamiltonian matrix for Diamond (O_h^7) with the $\boldsymbol{k}\cdot\boldsymbol{p}$ expansion method to the second order degree in k of the twofold degenerate Γ_{12+} state. With the here provided CGCs, a similar approach can be applied to construct the effective Hamiltonians for ZnO.

7 Conclusion In summary, we have studied the scattering tensors in ZnO by means of CGCs. Starting from existing band structure calculations, the CGCs were derived from selection rules for inter- and intra-valley scattering processes. For scattering processes in the same valley, both cases of low and large momentum of the quasi-particles were considered. In addition, the symmetries and CGCs of excitons at the high symmetry point A were determined.

Acknowledgements The work is supported by the RSA-Poland exchange program.

References

[1] P. Y. Yu and M. Cardona, Fundamentals of Semiconductors, Physics and Materials Properties (Springer-Verlag, Berlin, Heidelberg, New York, 1996).

physica status solidi b

[2] T. Makino, C. H. Chia, N. T. Tuan, H. O. Sun, and Y. Seguwa, Appl. Phys. Lett. **77**, 975 (2000).
[3] C. R. Gorda, N. W. Emanetoglu, S. Liang, W. E. Mayo, Y. Lu, M. Wraback, and H. Shen, J. Appl. Phys. **85**, (1999).
[4] M. Lax and J. J. Hopfield, Phys. Rev. **124**, 115 (1961).
[5] J. L. Birman, M. Lax, and R. Loudon, Phys. Rev. **142**, 620 (1966).
[6] J. L. Birman, Phys. Rev. B **9**, 4518 (1974).
[7] R. Berenson and J. L. Birman, J. Math. Phys. **16**, 227 (1975).
[8] R. Berenson, I. Itzkan, and J. L. Birman, J. Math. Phys. **16**, 236 (1975).
[9] J. L. Birman, T. K. Lee, and R. Berenson, Phys. Rev. B **14**, 318 (1976).
[10] M. Suffczyński and H. W. Kunert, J. Phys. (France) **38**, 1187 (1978).
[11] H. W. Kunert and M. Suffczyński, J. Phys. (France) **40**, 199 (1979).
[12] R. Berenson, Phys. Chem. Solids **42**, 391 (1981).
[13] W. R. L. Lambrecht, A. V. Rodina, S. Limpijummon, B. Segau, and B. K. Meyer, Phys. Rev. B **65**, 0752071 (2002).
[14] H. W. Kunert, J. Phys.: Conf. Ser. **30**, 290 (2006).
[15] A. P. Crackenell, B. L. Davis, S. C. Miller, and W. F. Love, Kronecker Product Tables Vol. 1–4 (IFI/Plenum Press, New York, Washington, London,1979).
[16] M. R. Wagner, H. W. Kunert, A. G. J. Machatine, A. Hoffmann, P. Niyongabo, J. Malherbe, and J. Barnaś, Microelectron. J. **40**, 289 (2009).
[17] B. K. Meyer, J. Sann, S. Lautenschläger, M. R. Wagner, and A. Hoffmann, Phys. Rev. B **76**, 184120 (2007).
[18] M. R. Wagner, P. Zimmer, A. Hoffmann, and C. Thomsen, Phys. Status Solidi RRL **1**, 169 (2007).
[19] H. W. Kunert, Eur. Phys. J.: Appl. Phys. **27**, 309 (2004).
[20] N. E. Christensens and P. Parlin, in: Semiconductors and Semimetals, Gallium Nitride (GaN), edited by I. Pankowe, and T. D. Moustakas (Academic Press, San Diego, London, Boston, 1999), p. 415.
[21] M. R. Wagner, J. H. Schulze, R. Kirste, M. Cobet, A. Hoffmann, C. Rauch, A. V. Rodina, B. K. Meyer, U. Röder, and K. Thonke, Phys. Rev. B **80**, 205203 (2009).

Phys. Status Solidi C **9**, No. 10–11, 1978–1980 (2012) / **DOI** 10.1002/pssc.201200097

physica status solidi c
www.pss-c.com
current topics in solid state physics

Clebsch-Gordan coefficients for scattering processes in Si and Ge

H. W. Kunert[1], A. G. J. Machatine[*,1], P. Niyongabo[1], M. Govender[1,2], and B. W. Mwakikunga[2]

[1] Department of Physics, University of Pretoria, Pretoria 0002, South Africa
[2] CSIR National Centre for Nano-Structured Materials, P.O.Box 395, Pretoria 0001, South Africa

Received 29 April 2012, revised 30 May 2012, accepted 7 June 2012
Published online 30 July 2012

Keywords symmetrized Kronecker product, scattering processes, Si,Ge, Clebsch-Gordan coefficients, spin-orbit interaction

[*] Corresponding author: e-mail augusto.machatine@up.ac.za, Phone: +27-12-4202652, Fax: +27-362-5288

Scattering matrix for two phonon processes at $\mathbf{k} = 0$ in Si and Ge of O_h^7 symmetry is given. Also diagonalization of spin-orbit interaction Hamiltonian has been computed by means of Clebsh-Gordan coefficients.

1 Introduction The Raman active modes (RAM's) with $\mathbf{k} = 0$ in two-phonon processes are determined by irreducible representations (irreps) contained in symmetrized Kronecker product (SKP) of single valued (SV) vector representation (VR). For Si and Ge the VR is Γ_{4-} [1] with the basis $xf(r)$, $yf(r)$ and $z(fr)$ and we have $[\Gamma_{4-} \otimes \Gamma_{4-}]$. The irreps contained in the SKP determine the RAM's symmetry allowed. The Clebsch-Gordan coefficients (CGC's) matrix which diagonalizes the Kronecker product (KP), yields correct linear combinations of allowed phonon basis wave functions.
The spin-orbit (SO) interaction represented by KP, $\Gamma_{4-} \otimes D_{\frac{1}{2}}$, involves double valued (DV) spinor irreps. Here we diagonalize the SO matrix by means of suitable CGC's matrix.

2 The simplified coupling coefficients theory The KP of two irreps l and l' is equivalent to the sum of l'' irreps contained in the product

$$D^l \otimes D^{l'} \cong \sum_R (ll' \mid l'') D^{l''} \tag{1}$$

and the basis of l'' are of the form :

$$\psi_\alpha^{l''} = \sum U_{\alpha\beta}^{ll'} \psi_\alpha^l \psi_\beta^{l'} \tag{2}$$

The matrix elements of U are determined by

$$U_{aa',a''}^{ll',l''} U_{\bar{a}\bar{a}'\bar{a}''}^{ll',l''*} = \frac{l''}{g} \sum_R D^l(R)_{a\bar{a}} D^{l'}(R)_{a'\bar{a}'} D^{l''*}(R)_{a''\bar{a}''} \tag{3}$$

and putting $a = \bar{a} = a_0, a' = \bar{a}' = \bar{a}'_0, a'' = \bar{a}'' = \bar{a}''_0$

we calculate non-zero coefficients of $U_{a_0,a'_0a''_0} . U^*_{a_0,a'_0a''_0} = |U_{a_0,a'_0a''_0}|^2$.

Then all other matrix elements of $U_{a_0a'_0a''_0}$ are obtained from

$$U_{a_0a'_0a''_0} = \frac{1}{U^*_{a_0a'_0a''_0}} . \frac{l''}{g} \sum_R D^l(R)_{aa_0} D^{l'}(R)_{a'a'_0} D^{l''*}(R)_{a''a''_0} \tag{4}$$

3 Diagonalization of SKP for Raman active modes In this section we want to diagonalize the KP $[\Gamma_{4-} \otimes \Gamma_{4-}] \cong \Gamma_{1+} + \Gamma_{3+} + \Gamma_{5+}$.
The CGC's U matrix brings the above KP to the block diagonal form:
$U^{-1}[\Gamma_{4-} \otimes \Gamma_{4-}]U = \Gamma_{1+} \oplus \Gamma_{3+} \oplus \Gamma_{5+}$.

For SKP of identical irreps, $l = l' = \Gamma_{4-}$ we reformu-

Contributed Article

late the standard Eq. (3) in the following manner:

$$U^{\Gamma_{4-}\Gamma_{4-},l''}_{aa',a''} U^{\Gamma_{4-}\Gamma_{4-},l''*}_{\bar{a}\bar{a}'\bar{a}''} = \frac{dim(l'')}{2g} \sum_R [(\Gamma_{4-})_{aa'}(\Gamma_{4-})_{\bar{a}\bar{a}'} + (\Gamma_{4-})_{\bar{a}a'}(\Gamma_{4-})_{a\bar{a}'}] .\Gamma^{l''*}_{a''\bar{a}''} \quad (5)$$

where the irreps l'' are $\Gamma_{1+}, \Gamma_{2+}, \Gamma_{5+}$.

The diagonal elements of SKP $[\Gamma_{4-} \otimes \Gamma_{4-}]^s_{a\bar{a},a'\bar{a}'}$ are obtained using the index relation: $a\bar{a}, a'\bar{a}' \longrightarrow (aa'\bar{a}\bar{a}' + \bar{a}a'a\bar{a}')$ and
$U_s^{-1}[\Gamma_{4-} \otimes \Gamma_{4-}]_2 U_s = \Gamma_{1+} \oplus \Gamma_{3+} \oplus \Gamma_{5+}$

For calculation of non-zero diagonal elements we have: $a = \bar{a} = a_0, a' = \bar{a}' = a'_0, a'' = \bar{a}'' = a''_0$

$$U_{aa'a''} U^*_{a_0 a'_0 a''} = \frac{dim(l'')}{2g} \sum_R [(\Gamma_{4-}(R))_{a\bar{a}_0}(\Gamma_{4-}(R))_{a'\bar{a}'_0} + (\Gamma_{4-}(R))_{a''\bar{a}''_0}(\Gamma_{4-}(R))_{a''\bar{a}''_0}] .\Gamma^{l''*}_{a''\bar{a}''_0}(R) \quad (6)$$

Having the non-zero diagonal matrix elements, we calculate the remaining matrix elements of U as follows.

$$U_{aa'a''} = \frac{dim(l'')}{2g} \frac{1}{U^*_{a_0 a'_0 a''_0}} \sum_R [(\Gamma_{4-})_{a\bar{a}_0}(\Gamma_{4-})_{a'\bar{a}_0'} + (\Gamma_{4-})_{a''\bar{a}_0''}(\Gamma_{4-})_{a''\bar{a}_0''}] .D^{l''*}_{a''\bar{a}_0''} \quad (7)$$

The obtained U matrix is:

$$U = \begin{bmatrix} \pm b & \pm b & \pm b & 0 & 0 & 0 \\ 0 & 0 & 0 & 0 & 0 & \pm a \\ 0 & 0 & & 0 & \pm a & 0 \\ 0 & 0 & 0 & 0 & 0 & \pm a \\ \pm b & \pm w^\star b & \pm w b & 0 & 0 & 0 \\ 0 & 0 & 0 & \pm a & 0 & 0 \\ 0 & 0 & 0 & 0 & \pm a & 0 \\ 0 & 0 & 0 & \pm a & 0 & 0 \\ \pm b & \pm w b & \pm w^\star b & 0 & 0 & 0 \end{bmatrix} \quad (8)$$

where: $a = \frac{1}{\sqrt{2}}, b = \frac{1}{\sqrt{3}}$, and $w = -\frac{1}{2} + i\frac{\sqrt{3}}{2}$.
The matrix U diagonalizes the SKP

$$U^{-1}[\Gamma_{4-} \otimes \Gamma_{4-}] U = \Gamma_{1+} \oplus \Gamma_{3+} \oplus \Gamma_{5+} \quad (9)$$

The coefficients of the first column give an appropriate combination of phonon Γ_{1+} wave function: $\varphi^{\Gamma_{1+}}_{ph} = \pm bf(r)(x^2 + y^2 + z^2)$. Similarly the $\varphi^{\Gamma_{3+}}_{ph}$ and $\varphi^{\Gamma_{5+}}_{ph}$ can be constructed.

4 Diagonalization of spin-orbit interaction In this section we give second example of diagonalization of SO effective Hamiltonian frequently needed for band structure calculation in semiconductor. Particularly the $\bar{k}.\hat{p}$ perturbation method is very useful in the determination of $E(\bar{k})$. In the $\bar{\mathbf{k}}.\hat{\mathbf{p}}$ expansion to second degree in $\bar{k}$ the inclusion of SO interaction leads to 6×6 matrix: $\Gamma_{4-} \otimes D_{\frac{1}{2}}$ where $D_{\frac{1}{2}}(\alpha, \beta, \gamma)$ for full rotational group O_h^7 space group operators becomes Γ_{6+}[1] and therefore again we deal with KP; $\Gamma_{4-} \otimes \Gamma_{6+}$ which decomposed takes a form $\Gamma_{4-} \otimes \Gamma_{6+} \cong \Gamma_{8-} \oplus \Gamma_{6-}$. It means the top of three fold degenerate valence band of Γ_{4-} in Si and Ge splits onto Γ_{8-}(four fold degenerate hole states) and Γ_{6-}(two fold degenerate). The energy distance between Γ_{8-} and Γ_{6-} is the energy of SO interaction. The SO matrix elements can be straight forward computed using general formula:

$$\mathbf{H}_{so} = \frac{\hbar}{4m_0^2 c^2} (\nabla U \times \hat{\mathbf{p}}) \hat{\sigma} \quad (10)$$

The $\sigma_x, \sigma_y, \sigma_z$ are Pauli matrices. Choosing the basis:

$$\varphi_1 = yzf(r) \begin{pmatrix} 1 \\ 0 \end{pmatrix}, \varphi_2 = zxf(r) \begin{pmatrix} 1 \\ 0 \end{pmatrix}$$
$$\varphi_3 = xyf(r) \begin{pmatrix} 1 \\ 0 \end{pmatrix}, \varphi_4 = yzf(r) \begin{pmatrix} 0 \\ 1 \end{pmatrix}$$
$$\varphi_5 = zxf(r) \begin{pmatrix} 0 \\ 1 \end{pmatrix}, \varphi_6 = xyf(r) \begin{pmatrix} 0 \\ 1 \end{pmatrix}$$

one obtains:

$$H_{so} = -\frac{\Delta}{3} \begin{bmatrix} 0 & i & 0 & 0 & 0 & -1 \\ -i & 0 & 0 & 0 & 0 & i \\ 0 & 0 & 0 & 1 & -i & 0 \\ 0 & 0 & 1 & 0 & -i & 0 \\ 0 & 0 & i & i & 0 & 0 \\ -1 & -i & 0 & 0 & 0 & 0 \end{bmatrix} \quad (11)$$

where Δ is the SO energy distance between $P_{\frac{3}{2}}$ and $P_{\frac{1}{2}}$ hole states. In the Kane's Jm_s base [3] the matrix is diagonalized

$$H_{11} = H_{22} = H_{44} = H_{55} = \frac{\Delta}{3},$$
$$H_{33} = H_{66} = \frac{-2\Delta}{3}$$

where the new basis functions are given in terms of the old φ_i (i = 1 - 6) by CGC's matrix [3].

$$\varphi_j = \sum_{j=1}^{6} U_{ji} \varphi_i \quad (12)$$

The matrix U in Eq. (11) is the CGC's matrix that must be calculated by rigid group theoretical method using Eqs.

(3), (4), (9) in our paper.
The SO Hamiltonian transforms according to the KP: $\Gamma_{4-} \otimes \Gamma_{6+}$ which contains the symmetry of heavy holes Γ_{8-} and the symmetry of light holes Γ_{6-}.

$$U^{-1}(\Gamma_{4-} \otimes \Gamma_{6+})U = \Gamma_{8-} \oplus \Gamma_{6-} \tag{13}$$

In order to perform calculations we have computed the 96 matrices of following irreps $\Gamma_{4-}, \Gamma_{6+}, \Gamma_{8-}$ and Γ_{6-} using augmenters from [1]. The resulting U matrix is:

$$U = \frac{1}{2}\begin{bmatrix} -1 & i & 0 & 0 & 0 & -1 \\ -i & -1 & 0 & 0 & 0 & i \\ 0 & 0 & -1 & 1 & -i & 0 \\ 0 & 0 & 1 & -1 & -i & 0 \\ 0 & 0 & i & i & -1 & 0 \\ -1 & -i & 0 & 0 & 0 & -1 \end{bmatrix} \tag{14}$$

Clearly our group theoretical diagonalization method by means of Eqs. (3), (4) is the most rigid and correct way.

5 Discussion Our diagonalization of SKP regarded to two-phonon processes can be used in analysis of Raman spectra [2]. From the Eqs. (5), (6) the correct linear combinations of RAM's wave functions follow. To our best knowledge, it is the first time that SKP is used for computing symmetrized Raman scattering tensors.
Concerning SO matrix the energy parameter Δ can not be calculated theoretically. It is measured by several experimental methods. Queisser and Panish were the first who measured Δ by photoluminescence (PL) spectroscopy from heavily doped by Zn- holes in GaAs [4]. They observed second PL band originating from transition between the lowest conduction band and split-off light hole valence band Γ_6 in GaAs with T_d^2 space group.
For Ge, $\Delta = 0.26$ meV and Si, $\Delta = 0.044$ meV have been measured by Ghosh [5].

6 Conclusion We have used group theoretical method for diagonalization of two-phonon using symmetrized Kronecker product. We also have diagonalized SO matrices. Our method can be extended to three-phonon processes as well as to other interactions like spin-spin, inter- and intravalley scattering. Our results are valid for all compounds with O_h^7 symmetry.

References

[1] A. P. Cracknell, B. L. Davies, S. C.Miller, and W. F. Love, Kronecker Product Tables, Vol. 1-4 (New York, 1979).
[2] J. L Birman, Theory of Crystal Space Groups and Lattice Dynamics (New York, 1984).
[3] A. O. Kane, Energy Band Structure in p-type Germanium and Silicon (New York, 1956), p. 82.
[4] H. J Queisser and M. B. Panish, J. Phys. Chem. Solids **28**, 1177 (1967).
[5] A. K Ghosh, Phys. Rev. **165**, 888 (1968).

Phys. Status Solidi C **9**, No. 10–11, 1974–1977 (2012) / **DOI** 10.1002/pssc.201200068

physica status solidi c
www.pss-c.com
current topics in solid state physics

Scattering tensors and optical transitions in Si and Ge

H. W. Kunert[**,1], **A. G. J. Machatine**[*,1], **P. Niyongabo**[1], **M. Govender**[1,2], **and B. W. Mwakikunga**[2]

[1] Department of Physics, University of Pretoria, Pretoria 0002, South Africa
[2] CSIR National Centre for Nano-Structured Materials, P. O. Box 395, Pretoria 0001, South Africa

Received 24 April 2012, revised 24 May 2012, accepted 27 May 2012
Published online 24 August 2012

Keywords scattering tensors, selection rules, Clebsch-Gordan coefficients, Si, Ge

[*] Corresponding author: e-mail augusto.machatine@up.ac.za, Phone: +27 124202652, Fax: +27 865466898
[**] e-mail herbert.kunert@up.ac.za, Phone: +27 12 420 3536, Fax: +27 865466898

The selection rules (SR's) for the Kronecker product (KP) of Si and Ge irreducible representations (irreps) are required to determine the intervalley scattering processes. The SR's for transitions between the lowest conduction band minima at Γ, X and L high symmetry points and the highest maximum of the valence band (VB) in the Brillouin zone of O_h^7 space group symmetry are determined. The symmetry of phonons due to electron-phonon (El-Ph) interaction follows from the KP's: $L_1 \otimes \Gamma_{12}(\Gamma_{2-})$, $\Delta_1 \otimes \Gamma_{12}(\Gamma_{2-})$, $L_1(L_{1+}) \otimes \Delta_1$ for Ge and $L_1 \otimes \Gamma_{15}(\Gamma_{4-})$, $\Delta_1 \otimes \Gamma_{15}(\Gamma_{4-})$, $L_1(L_{1+}) \otimes \Delta_1$ for Si. The elements of El-Ph scattering tensors are linear combinations of the Clebsch-Gordon coefficients (CGC's). Here we have computed the coupling coefficients relevant to scattering tensors. Our theoretical results confirm the available experimental data.

1 Introduction The scattering tensors (Sc.T's) are of great interest to experimentalists. Historically many authors have used polarized measurements to interpret and assign vibrational modes of Raman spectra and most recently this technique have become powerful research tool in many areas due to availability of lasers [1-3]. The CGC's can also be used to obtain the polarization SR's for dipole and quadrupole resonant Raman and Brillouin scattering, as well as in morphic effects. They are useful in interpretation of infrared absorption spectra in optical transitions in higher order optical processes. They also play a major role in determination of effective Hamiltonians. Birman showed [4] that the matrix elements of any Hamiltonian is prescribed as a sum of symmetry adapted components of symmetrised base times CGC's. The utility of CGC's can also be extended to second order phase transition phenomena where the so-called active representations (AR's) are needed. The antisymmetrized square and symmetrised cube of AR's involve CGC's. In this work we focus on intravalleys (Intra.V) and intervalleys (Inter.V) scattering of quasiparticles by phonons in Si and Ge, those were discussed by Lax et al. [5] and Birman et al. [6].

In order to establish the SR's associated with scattering processes the Wave Vector Selection Rules (WVSR's) have to be determined. The WVSR's are a primary step in finding the appropriate scattering tensors. The El-Ph interaction in Si and Ge is represented by the KP of the following irreps:

Ge: $\Gamma_{2-} \otimes L_1$, $\Gamma_{2-} \otimes \Delta_1$, $L_1 \otimes \Delta_1$

Si: $\Gamma_{4-} \otimes L_1$, $\Gamma_{4-} \otimes \Delta_1$, $L_1 \otimes \Delta_1$.

In general, the KP is reducible to the irreps of phonons $D^{*\mathbf{k}''l''}$, according to

$$D^{*\mathbf{k}l} \otimes D^{*\mathbf{k}'l'} \cong \sum c_{ll'l''}(j) D^{*\mathbf{k}''l''}. \quad (1)$$

The CGC's matrix diagonalises the El-Ph perturbation determined by the KP of irreps in a given Hamiltonian $\boldsymbol{H}$, and following from Eq. (1):

$$U^{-1}\left[D^{*\mathbf{k}l} \otimes D^{*\mathbf{k}'l'}\right]U = \sum c_{ll'l''}(j) D^{*\mathbf{k}''l''}. \quad (2)$$

In Eq. (2), the matrices of irreps l'' have diagonal block form. For calculations of U matrices we use the Birman

Contributed Article

method [7] and the CDML reps labelling [8]. It is the aim of this paper to obtain the U matrices for several scattering processes in Si and Ge.

2 The wave vector selection rules In this section we discuss the WVSR's for Inter.V and Intra.V scattering processes. In Ge there are four equivalent minima at the L point which are obtained from the star of the first wave vector denoted by $\mathbf{k}_L = \frac{\pi}{a}(1,1,1)$ of the little group $G^{\mathbf{k}_L}$. The star $\mathbf{k}_L$ is $\{{}^*\mathbf{k}_L\} = \{E\mathbf{k}_L, C_{2x}\mathbf{k}_L, C_{2y}\mathbf{k}_L, C_{2z}\mathbf{k}_L\}$ with $C_{2x}\mathbf{k}_L = \frac{\pi}{a}(-1,0,0)$, $C_{2y}\mathbf{k}_L = \frac{\pi}{a}(0,-1,0)$ and $C_{2z}\mathbf{k}_L = \frac{\pi}{a}(0,0,-1)$, where the symmetry operators transforms the $\mathbf{k}_L = \frac{\pi}{a}(1,1,1)$ into the remaining valleys. The WVSR for these scattering processes are listed in Tables 1 and 2 and the symmetry operators $E(1)$, $C_{2x}(2)$, $C_{2y}(3)$, $C_{2z}(4)$ and $C_{31}^{-}(5)$, $C_{31}^{+}(9)$ are labelled in CDML notation [8].

In Ge for Intra.V and Inter.V scattering processes within the four *L*-valleys and three *X*-valleys, the WVSR's and the CGC's are presented in Tables 1 and 2.

In Silicon the Inter.V scattering between the one Γ-valley and six Δ-valleys are governed by SR's listed in Table 3 $(\mathbf{k}_\Delta + \mathbf{k}_\Gamma = \mathbf{k}_\Delta)$ together with appropriate CGC's for these scattering processes. Empty places in the tables mean zero matrix elements.

Table 1 Clebsch-Gordan coeffiecients for scattering within valleys of the same symmetry type: $a = \frac{1}{2}$.

$L_{1+} \otimes L_{1+} =$	$\Gamma_{1+} \oplus$		Γ_{5+}	
WVSR's	1	1	2	3
$1\mathbf{k}_L + 1\mathbf{k}_L = \mathbf{k}_\Gamma$	*a*	*a*	*a*	*a*
$2\mathbf{k}_L + 2\mathbf{k}_L = \mathbf{k}_\Gamma$	*a*	*-a*	*a*	*-a*
$3\mathbf{k}_L + 3\mathbf{k}_L = \mathbf{k}_\Gamma$	*a*	*-a*	*-a*	*a*
$4\mathbf{k}_L + 4\mathbf{k}_L = \mathbf{k}_\Gamma$	*a*	*a*	*-a*	*a*

Table 2 Clebsch-Gordan coefficients for scattering between different valleys of the same symmetry type: $b = \frac{\sqrt{2}}{2}i$ and $c = \frac{\sqrt{2}}{2}$.

$[L_{1+} \otimes L_{1+}]_2$	X_1					
	1	2	3	4	5	6
$1\mathbf{k}_L + 3\mathbf{k}_L = \mathbf{k}_X$	*c*	*-b*				
$2\mathbf{k}_L + 4\mathbf{k}_L = \mathbf{k}_X$	*c*	*b*				
$1\mathbf{k}_L + 2\mathbf{k}_L = 5\mathbf{k}_X$			*c*	*b*		
$4\mathbf{k}_L + 3\mathbf{k}_L = 5\mathbf{k}_X$			*c*	*-b*		
$1\mathbf{k}_L + 4\mathbf{k}_L = 9\mathbf{k}_X$					*c*	*b*
$2\mathbf{k}_L + 3\mathbf{k}_L = 9\mathbf{k}_X$					*c*	*b*

Table 3 Clebsch-Gordon coefficients for scattering processes between different valleys Γ and Δ.

$\Gamma_{4-} \otimes \Delta_1 =$	Δ_1						$\oplus$				Δ_5							
	1	2	3	4	5	6	1	2	3	4	5	6	7	8	9	10	11	12
$\mathbf{k}_\Gamma + \mathbf{k}_\Delta = \mathbf{k}_\Delta$	0						1	0										
	0						0	*i*										
	i						0	0										
$\mathbf{k}_\Gamma + 2\mathbf{k}_\Delta = 2\mathbf{k}_\Delta$		0							-1	0								
		0							0	*i*								
		-i							0	0								
$\mathbf{k}_\Gamma + 3\mathbf{k}_\Delta = 3\mathbf{k}_\Delta$			*i*								1	0						
			0								0	*- i*						
			0								0	0						
$\mathbf{k}_\Gamma + 4\mathbf{k}_\Delta = 4\mathbf{k}_\Delta$				*- i*									0	0				
				0									1	0				
				0									0	*i*				
$\mathbf{k}_\Gamma + 5\mathbf{k}_\Delta = 5\mathbf{k}_\Delta$					*- i*										0	0		
					0										-1	0		
					0										0	*- i*		
$\mathbf{k}_\Gamma + 6\mathbf{k}_\Delta = 6\mathbf{k}_\Delta$						*i*											0	0
						0											-1	0
						0											0	*- i*

Table 4 Generating matrices for induced representations.

O_h^7	4	2	9	26	37
L_{1+}	0 0 0 1 0 0 1 0 0 1 0 0 1 0 0 0	0 1 0 0 1 0 0 0 0 0 0 1 0 0 1 0	1 0 0 0 0 0 0 1 0 1 0 0 0 0 1 0	0 -1 0 0 1 0 0 0 0 0 0 -1 0 0 1 0	1 0 0 0 0 0 1 0 0 1 0 0 0 0 0 1
L_{2-}	0 0 0 1 0 0 1 0 0 1 0 0 1 0 0 0	0 1 0 0 1 0 0 0 0 0 1 1 0 0 0 0	1 0 0 0 0 0 0 1 0 1 0 0 0 0 1 0	0 1 0 0 -1 0 0 0 0 0 0 1 0 0 -1 0	1 0 0 0 0 0 1 0 0 1 0 0 0 0 0 1

Generators=2.2, 4.1, 9, 26.2 and 37 and generating relations. 4.1x4.1=1, 11.3x5=3.3, 2,2x5=6.2, 5x4.1=7.3, 5x2.2=8.1, 9x4.1=10.2, 9x2.2=11.3, 4.1x9=12.1, 37x25=13, 2.2x13=14.2, 3.3x13=15.3, 4.1x13=16.1, 13x9=17, 2.2x17=19.2, 4.1x17=20.1, 13x5=21, 2.2x21=22.2, 3.3x21=23.3, 4.1x21=24.1, 2.2x26.2=25, 3.3x25=27.3, 4.1x25=28.1, 6.2x25=30.2, 7.3x25=31.3, 8.1x25=32.1, 10.2x25=34.2, 11.3x25=35.3, 12.1x25=36.1, 14.2x25=38.2, 15.3x25=39, 16.1x25=40.1, 17x25=41, 18.2x25=42.2, 19.3x25=43.3, 20,1x25=44.1, 21x25=45, 21.4x25=45.4, 22.2x25=46.2, 23.3x25=25=47.3 and 24.1x25=48.1.

3 Scattering processes in Ge and Si For scattering processes between different valleys belonging to the same star, the following symmetric KP's have to be considered:

- Ge: $[\Gamma_{2'}]_{(2)}$; $[L_{1'}]_{(2)}$; $[\Delta_1]_{(2)}$
  Si: $[\Gamma_{15}]_{(2)}$; $[L_1]_{(2)}$; $[\Delta_1]_{(2)}$ in Lax et al. [2]

- Ge: $[\Gamma_{2-}]_{(2)}$; $[L_{1+}]_{(2)}$; $[\Delta_1]_{(2)}$
  Si: $[\Gamma_4]_{(2)}$; $[L_{1+}]_{(2)}$; $[\Delta_1]_{(2)}$ in CDML [5]

For scattering between one valley Γ_{2-} and four L-valleys $\mathbf{k}_L$, $2\mathbf{k}_L$, $3\mathbf{k}_L$ and $4\mathbf{k}_L$, the phonon symmetry is L_{2-} (LA) and the CGC's of U are obtained from:

$$U^{-1}\left(\Gamma_{2-}\otimes\uparrow L_{1+}\right)U=\uparrow L_{2-}. \tag{3}$$

- The $\uparrow L_{2-}$ is the full induced 4×4-dimensional rep where U is given by:

$$U=\begin{pmatrix}\pm i & 0 & 0 & 0\\ 0 & \pm i & 0 & 0\\ 0 & 0 & \pm i & 0\\ 0 & 0 & 0 & \pm i\end{pmatrix}. \tag{4}$$

In order to prove the correctness of the U matrix, we have computed the matrix U by Sakata method [9], using:

$$F=\sum_{r\in H}D'(r)AD^{\dagger}(r). \tag{5}$$

where all quantities have their usual meaning. In this method one uses the full induced reps. We have computed the generators of L_{2-} full induced phonon representation. It is clear that the generating matrices are not diagonal, and so the matrix U diagonalizes the KP of Eq. (3) and the rep $\uparrow L_{2-}$ on the right-hand side has a block diagonal 4×4-form. The matrix calculated by Sakata method is identical to our U matrix.

4 Discussion In Table 1, we list the WVSR's for L-Inter.V and the corresponding CGC's. The scattering processes in all valleys are the same and the symmetry of the participating phonons is $\Gamma(\mathbf{k}\approx 0)$.

In Table 2 we present the WVSR and CGC's for $[L_1\otimes L_1]_2=X_1\oplus\ldots$ Inter.V scattering between four different L-valleys. It follows that the symmetry of phonons belongs to X-valley $(\mathbf{k}_X,5\mathbf{k}_X,9\mathbf{k}_X)$. We can estimate the energy lost by an electron in emitting an acoustic phonon. In our tables we list momentum conservation principles for scattering processes. The energy of these particles must also be conserved. For $\mathbf{k}'=\mathbf{k}_L$, $\mathbf{k}'=3\mathbf{k}_L$ and $\mathbf{k}'=9\mathbf{k}_L$, we read:

$$E_{\mathbf{k}'_L}-E_{\mathbf{k}_L}=E_{Ph}(\mathbf{k}_X);\ \hbar\mathbf{k}_L-\hbar 3\mathbf{k}_L=\hbar\mathbf{q}(\mathbf{k}_X) \tag{6}$$

where $\mathbf{k}$, $\mathbf{k}'$ and $\mathbf{q}$ runs through $\mathbf{k}_L$, $2\mathbf{k}_L$, $3\mathbf{k}_L$, $4\mathbf{k}_L$, $\mathbf{k}_X$, $5\mathbf{k}_X$ and $9\mathbf{k}_X$. An electron with initial energy $E_{\mathbf{k}}$ and wave vector $\mathbf{k}$ is scattered to another energy state with $E'_{\mathbf{k}}$ and wave vector $\mathbf{k}'$. Assuming that we deal with parabolic bands and where the effective mass is given, for example, $(m_e^*)_{\perp}=1.6m_0$ in Ge [10]. Obviously our $\mathbf{q}$ lies between minimum and $5\mathbf{k}_X$. For the backscattering we have:

$$E_{\mathbf{k}'_L}-E_{\mathbf{k}_L}=h\nu_s\mathbf{q}_{\max}=2\hbar\nu_s\left(k-2m\upsilon_s^2\right), \tag{7}$$

where $\upsilon_s\cong 10^6\ m/s$ is the phonon velocity.

For $k_L\approx 4\times10^6\,\mathrm{cm}^{-1}$, $k'_L\approx 4.2\times10^6\,\mathrm{cm}^{-1}$, $E_{\mathbf{k}_L}=(\hbar\mathbf{k})^2/2m_e^*\approx 47\,\mathrm{meV}$ and $k_q\approx 8.2\times10^{-6}\,\mathrm{cm}^{-1}$, we obtain 8 meV. In emitting a phonon with the same vector $(\mathbf{k}_X,5\mathbf{k}_X,9\mathbf{k}_X)$, the electron reverses its direction and energy changes by 10% [10].

5 Conclusion In this work, we focused on utilisation of group theory with regard to matrix elements of scattering tensors which are a linear combination of Clebsch-

Gordon coefficients. The required phonon symmetries are determined by irreps contained in KP. We have calculated the U matrix for the LA phonon which diagonalizes the intervalley scattering between the Γ_{2-} valley and the four L-valleys of the same star symmetry. We also have estimated an electron energy loss to X-valley acoustic phonon emission due to L-valleys electron scattering in a quasi-elastic process in agreement with available experimental data.

References

[1] A. Jorio, M. Dresselhaus, R. Siato, and G. Dresselhaus, Raman Spectroscopy in Graphene and Related Materials (Springer, 2011); ISBN 978-3-527-40811-5.
[2] S.-L. Zhang, Raman Spectroscopy and Its Applications in Nanostructures (Wiley, 2012); ISBN 978-0-470-68610-2.
[3] M. Govender, L. Shikwambana, B.W. Mwakikunga, E. Sideras-Haddad, R.M. Erasmus, and A. Forbes, Nanoscale Res. Lett. **6**, 166 (2011).
[4] J. L Birman and T. K. Lee, Phys. Rev. B **14**, 318 (1976).
[5] M. Lax and J. J. Hopfield, Phys. Rev. **124**, 115 (1961).
[6] J. L. Birman, M. Lax, and R. Loudon, Phys. Rev. **145**, 620 (1965).
[7] J. L. Birman, Theory of Space Groups and Lattice Dynamics (Springer, 1974); ISBN 3-540-13395-X.
[8] A. P. Cracknell, B. L. Davies, S. C. Miller, and W. F. Love, Kronecker Product Tables (Plenum, New York, Washington, 1979).
[9] I. Sakata, J. Math. Phys. **15**, 1702 (1974).
[10] P. Y. Yu and M. Cardona, Fundamentals of Semiconductors (Springer, 2010).

Phys. Status Solidi A **211**, No. 2, 435–439 (2014) / **DOI** 10.1002/pssa.201300187

physica status solidi a
www.pss-a.com
applications and materials science

Optical selection rules and scattering processes in rocksalt wide band gap ZnO

H. W. Kunert*[,1], M. Govender[1,2], A. G. J. Machatine[1], B. W. Mwakikunga[2], and P. Niyongabo[1]

[1] Department of Physics, University of Pretoria, Pretoria 0002, South Africa
[2] DST/CSIR National Centre for Nano-Structured Materials, CSIR, P. O. Box 395, Pretoria, 0001, South Africa

Received 6 June 2013, revised 15 January 2014, accepted 16 January 2014
Published online 12 February 2014

Keywords excitons, group theory, scattering processes, zinc oxide

* Corresponding author: e-mail herbert.kunert@up.ac.za, Phone: +27 12 4202636, Fax: +27 12 3625288

At sufficiently high pressures, wurtzite structure zinc oxide (*W*-ZnO) can be transformed to the cubic rocksalt (*R*-ZnO) structure. The *R*-ZnO exhibits semiconductor behavior with an indirect wide band gap of $E_g = 5.5$ eV. The maximum valence band is found far away from the center of the Brillouin zone (BZ) at high symmetry point *L* and line Σ, depending on the pressure. The unusual electronic band structure (EBS) of the *R*-ZnO leads to several direct and indirect optical transitions which find applications in ultraviolet optoelectronic devices. We have investigated radiative and non-radiative symmetry restricted selection rules, as well as inter- and intra-valley scattering processes.

1 Introduction The *R*-ZnO structure (*R*-O_h^5, $Fm3n$ space group) has recently attracted much attention due to an unconventional EBS that can be used in mechanical and optoelectronic applications [1–4]. Jaffe et al. [5] calculated the EBS of *R*-ZnO by the all-electron local-orbits Hartree–Fock method along some major symmetry lines and points, shown in Fig. 1a. Some symmetry assignments are contrary to that commonly accepted, for example, the band structure of R-ZnO in [5], which is presented in Fig. 1b, where one of the VB maximum has W_1 symmetry instead of W_5 symmetry, and the *K* point seems to be incorrectly assigned. Reference to group theoretical assignments has not yet been provided.

Segura et al. [6] reported on pressure dependence of the optical absorption edge in *R*-ZnO up to 20 GPa measured at room temperature. The low-energy tail of the absorption has been assigned to an indirect transition. Figure 2 shows the EBS of *R*-ZnO along some high symmetry directions of the BZ at several pressures. The minimum of the lowest conduction band (CB) remains at the center of the BZ (point Γ), while the highest maximum of the valence band (VB) occurs on the Σ-line and at the *L* point. No group theoretical assignments of electron and hole states have been discussed, and therefore no optical selection rules (OPSRs) have been considered. Based on pressure absorption dependence, the optical absorption leads to indirect transitions: *L*–Γ, Σ–Γ as well as direct transitions at *X*, *L*, and high symmetry points have been assigned by us using a group theoretical approach. In this paper, we provide rigidly calculated OPSRs for all transitions, as well as selection rules for possible inter- and intra-valley scattering processes.

In Section 2 of this paper, we discuss assignments of electrons and holes in CBs and VBs needed for determination of OPSRs. In Section 3, we deal with the general quantum mechanical rules needed for matrix element transitions. In Section 4, we discuss the wave vector selections rules (WVSRs) which follow from the momentum conservation principle. The direct radiative transition selection rules (DrTrSRs) and the symmetry of excitons are discussed in Section 5. The indirect transitions (InDrTrs) involving vibrational modes are considered in Section 6. In the last section we discuss our results and predictions regarding the splitting of *L* excitons.

2 Symmetry assignments of electron and hole states in the conduction and valence bands in *R*-ZnO The states of electrons and holes in a crystal are characterized by the wave vector $\boldsymbol{k}$ and the irreducible representations (irrps) of a space group $G(\boldsymbol{k})$. When the spin of a particle or quai-particle is disregarded, the states are classified according to the so-called single-valued irrps (SVirrps). The inclusion of spin leads to double-valued irrps (DVirrps) known as spinors. The EBS can be determined by several experimental techniques such as absorption, Raman, photoluminescence and reflectivity spectroscopies.

physica status solidi a

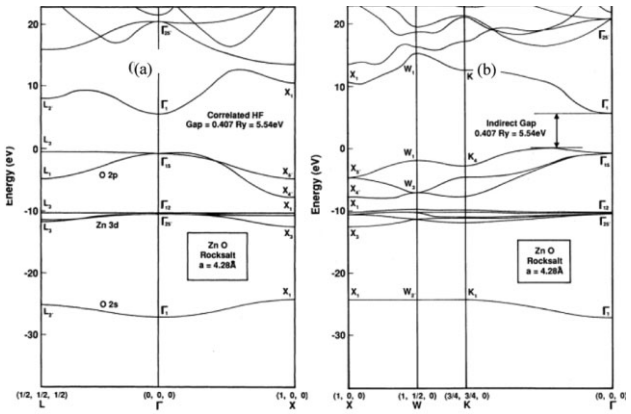

Figure 1 (a) Correlation-corrected Hartree–Fock band structure of ZnO in the rocksalt structure and (b) correlation-corrected Hartree–Fock band structure of ZnO in the rocksalt structure for some additional directions in reciprocal space. Diagrams adopted from Ref. [5].

Segura et al. [6] did not take into account SRs for their high symmetry points, so based on group theoretical techniques, we have determined the major high symmetry line and points of the respective BZ according to the irrps of O_h^5 space group using Cracknell, Davies, Miller and Love Tables (CDML) labeling [7]. In Table 1, we list the respective states of electron and holes in terms of CDML labeling of irrps in CBs and VBs. In Table 2, we show a correspondence of irrps labeling between Bouckaert, Smoluchowski and Wigner (BSW) [8] Jaffet and Koster (JK) [9], and CDML tables.

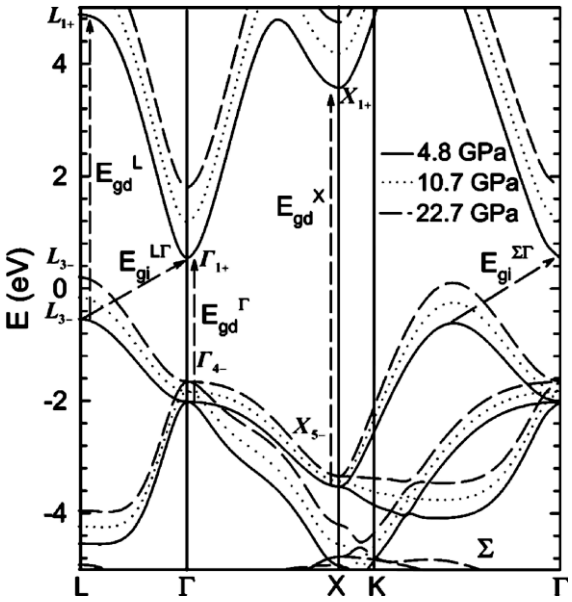

Figure 2 Electronic band structure of rocksalt ZnO along high-symmetry directions of the BZ at several pressures, as calculated through *ab initio* DFT-LDA pseudopotential method. Diagram adopted from Ref. [6].

Table 1 Symmetry assignment of high symmetry points in cubic *R*-ZnO.[a]

single-valued representations–spin excluded			
conduction bands	L_{1+}	Γ_{1+} (lowest)	X_{1+}
valence bands	L_{3-} (highest)	Γ_{4-}	X_{5-}
double-valued representations–spin included			
conduction bands	L_{6+}	Γ_{6+}	X_{6+}
valence bands[b]	L_{4-}, L_{5-}, L_{6-}	Γ_{8-}, Γ_{6-}	X_{7-}, X_{6-}

[a]The assignment is in terms of CDML irreducible representations. The double-valued representations have been obtained by multiplication of the single-valued representations by two-dimensional representations (spinor representation $D_{(1/2)}$ CDML [7], p. 9);
[b]Due to possible spin–orbit interactions, the valence band L_{3-} (two-dimensional, small representation) $\times D_{(1/2)}$ splits onto L_{4-} (one-dimensional), L_{5-} (one-dimensional) and L_{6-} (two-dimensional) representations. Similar effects happen for Γ_{6+} and X_{6+} representations.

Table 2 Labels of irreducible representations for the point Γ for O_h^5–*Fm3n* space group of *R*-ZnO.[a]

JK [8]	BSW [9]	CDML [7]
Γ_{1+}	Γ_1	Γ_{1+}
Γ_{2+}	Γ_2	Γ_{2+}
Γ_{3+}	Γ_{12}	Γ_{3+}
Γ_{4+}	$\Gamma_{15'}$	Γ_{4+}
Γ_{5+}	$\Gamma_{25'}$	Γ_{5+}
Γ_{1-}	$\Gamma_{1'}$	Γ_{1-}
Γ_{2-}	$\Gamma_{2'}$	Γ_{2-}
Γ_{3-}	Γ_{12+}	Γ_{3-}
Γ_{4-}	Γ_{15+}	Γ_{4-}
Γ_{5-}	Γ_{25}	Γ_{5-}

[a]For more details, see Ref. [10], p. 533.

3 Selection rules We first recall the basic theorems on SRs [9]. The study of an absorption or scattering cross section for a process involving the absorption or scattering of particles or quasi-particles with wave vector $\boldsymbol{k}$ in a crystal involves the calculation of transition probabilities, which in turn involves the calculation of quantum mechanical matrix elements. The matrix elements of a perturbation f between an initial and final state are of the form $V_{pq}^{\mu\nu} = \left\langle \psi_q^\mu | f | \psi_p^\nu \right\rangle$, where ψ_q^μ and ψ_p^ν are the wave functions (with respective basis functions for irrps D^μ and D^ν) of the particle or quasi-particles involved in the absorption or scattering processes.

Acting by symmetry operators of a given space group on the matrix elements (wave functions and perturbation operator f, we obtain the Kronecker product (KP) between three irrps $D^\mu \times D^f \times D^\nu$. When the KP contains the unit representation, normally denoted as Γ_1, Γ_{1+} or A_1, the transition between states due to perturbation f is allowed, otherwise it is forbidden. The square of any irrps always contains the identity representation. Therefore, it suffices to consider only single KPs between two irrps and check whether the third representation is in the decomposition. All

Original Paper

possible KPs for 230 space groups have been tabulated in CDML.

4 Momentum conservation principles: Wave vector selection rules An electron in a state $\boldsymbol{k}$ can be scattered into another state $\boldsymbol{k}'$ due to an interaction with a phonon at the $\boldsymbol{k}''$ state. The momentum conservation $\boldsymbol{k}+\boldsymbol{k}'=\boldsymbol{k}''$ determines the WVSRs. The WVSRs originate from appropriate combinations of arms of stars $*\boldsymbol{k}$, $*\boldsymbol{k}'$ and $*\boldsymbol{k}''$[11]. For face-centered cubic crystals with tetragonal and cubic symmetries (T_d^2, O_h^5, and others), the WVSRs have been tabulated in Table 2. In *R*-ZnO, there are three pronounced valleys at Γ, *L*, and *X* points. The star of the *L* valley is $*\boldsymbol{k}(L):\boldsymbol{k}L$, $2\boldsymbol{k}L$, $3\boldsymbol{k}L$, and $4\boldsymbol{k}L$, and the star of the *X* valley is $\boldsymbol{k}X$, $5\boldsymbol{k}X$, and $9\boldsymbol{k}X$. At the Γ point, we have only one wave vector $\boldsymbol{k}=0$. The numbers 1, 2, 3, 4, 5, and 9 denote the symmetry operators of O_h^5 group [7]. The first minima at each of these points are characterized by the first wave vectors $\boldsymbol{k}=0$, $\boldsymbol{k}L$, and $\boldsymbol{k}X$ in the fundamental domain of the BZ. It means that we deal with four non-equivalent *L* valleys, three *X* and one Γ valley. The inter- and intra-valley scattering processes are subjected to WVSRs and are discussed in Section 6.

5 Direct radiative transition selection rules in *R*-ZnO

5.1 Point Γ At point Γ, the momentum of the electron and hole are very small (almost zero). The respective KP of a radiative transition from the minimum CB of Γ_{1+} symmetry (spin of electron and hole excluded) to the maximum of the VB of Γ_{4-} symmetry (Table 1) due to the laser beam with electric field $\boldsymbol{E}=\boldsymbol{E}_0\exp(\boldsymbol{kr}-\omega t)$, (E_x,E_y,E_z) which transforms like an ordinary vector x,y,z. Therefore, according to Γ_{4-} representation (VR) is of the form: $\{(\Gamma_{1+})\times(\Gamma_{4-})\times(\Gamma_{4-})\}$. The KP contains the identity representation and therefore the direct transitions at Γ are in accordance with absorption measurements [6].

5.2 Points *L* and *X* The appropriate WVSR for direct transitions between the minimum of the *L*'s CB of L_{1+} symmetry and the maximum of VB of L_{3-} symmetry is $\boldsymbol{k}L+\boldsymbol{k}L=\boldsymbol{k}G$ in channel Γ and $\boldsymbol{k}L+3\boldsymbol{k}L=\boldsymbol{k}X$, $\boldsymbol{k}L+2\boldsymbol{k}L=5\boldsymbol{k}X$, and $\boldsymbol{k}L+4\boldsymbol{k}L=9\boldsymbol{k}X$ in the *X* channel. The SR is $\{L_{1+}(\mathrm{CB})\times L_{3-}(\mathrm{VB})\times\Gamma_{4-}\}=(\Gamma_{3-}+\Gamma_{4-}+\Gamma_{5-})\times(\Gamma_{4-})$ in the Γ channel and $(X_{1-}+X_{2-}+X_{3-}+X_{4-}+2X_{5-})$ in the *X* channel. Clearly the KP contains the identity representation Γ_{1+}. Consequently, the direct transitions at the *L* point are allowed in accordance with experimental data [6].

For point *X*, we have $\boldsymbol{k}X+\boldsymbol{k}X=\boldsymbol{k}G$ in the Γ channel and $\boldsymbol{k}X+5\boldsymbol{k}X=9\boldsymbol{k}X$ for the *X* channel, respectively. The respective KP is of the form $\{(X_{1+})\times(X_{5-})\times(\Gamma_{4-})\}=(\Gamma_{1-}+\Gamma_{5-})\times\Gamma_{4-}$, in the Γ channel and for the *X* channel $(X_{3-}+X_{4-}X_{5-})\times\Gamma_{4-}$. Again the transitions are allowed, as confirmed by Segura et al. [6].

5.3 Σ line Inspecting Fig. 2 [6], we note that the transition from Σ-VB to Σ-CB needs a very high energy laser beam. Therefore, we will not consider this transition. Nevertheless, the indirect transition Σ–Γ is of interest and we will discuss them here.

5.4 Spin inclusion and excitons in *R*-ZnO The EBS have been studied by several authors [5, 6]. They have not taken spin of electrons and holes into consideration. The hexagonal *W*-ZnO, from which the *R*-ZnO has been made, experiences strong magnetic properties evidenced by pronounced spin–orbit (S–O) interaction values. The strong magnetic properties and crystalline field split the VB into three sub-bands which contribute to the three A, B, and C excitons, and are seen by reflectance, photoluminescence and absorption techniques.

We believe that *R*-ZnO will also exhibit some magnetic properties that require an inclusion of spin. To our best knowledge, there are no magnetic experimental data on *R*-ZnO available. Nevertheless, we include the spin to our considerations in OPSRs in an attempt to predict some new features. When spin is included, the states of particles or quasi-particles are classified according to DVirrps. We have calculated the double-valued representation $D_{(1/2)}$ [11], reduced to the symmetry operations of O_h^5 group for points Γ, *L*, and *X* using Eq. (9.65) and Table 3.1 in Ref. [7]. With the help of the $D_{(1/2)}$ representation, we were able to determine the spinor representations for the *R*-ZnO at high symmetry points. The inclusion of electron spin in CBs results in the classification of states in terms of the spinor representations: $\Gamma_{6+}=\Gamma_{1+}\times D_{(1/2)}$, $L_{6+}=L_{1+}\times D_{(1/2)}$ and $X_{6+}=X_{1+}\times D_{(1/2)}$. All the representations are now doubly degenerate.

The holes in the VBs after an inclusion of spin are classified according to the following DVirrps: Γ_{8-} and Γ_{6-} contained in $\Gamma_{4-}\times D_{(1/2)}$; L_{4-}, L_{5-}, and L_{6-} contained in the KP: $L_{3-}\times D_{(1/2)}$ and X_{6+} in $X_{1+}\times D_{(1/2)}=X_{6+}$. It means that the state L_{3-} of the holes at the highest VB maximum at *L* point splits into three VBs (when spin is included) of L_{4-}, L_{5-}, and L_{6-} symmetries each of them two-fold degenerated. Similarly, holes at the Γ split onto fourfold degenerate (Γ_{8-}) heavy and two-fold degenerate (Γ_{6-}) light holes like states of holes in Si and Ge and GaAs.

Consequently, several direct and indirect excitons are expected to be observed experimentally. For direct *L* excitons we have three types of them as: $L_{6+}\times L_{4-}$ (let's call them L_1 excitons), $L_{6+}\times L_{5-}$ (L_2 excitons) and $L_{6+}\times L_{6+}$ (L_3 excitons). This is in analogy to *W*-ZnO's A, B, and C, Γ excitons [11]. We believe that the magneto-photoluminescence, reflectance and absorption will confirm our predictions. The *R*-ZnO structure (R-O_h^5, $Fm3n$ space group) has recently attracted much attention due to an unconventional EBS that can be used in mechanical and optoelectronic applications

6 Indirect electronic transitions and inter and intra-valley scattering processes in *R*-ZnO

6.1 Electronic indirect transitions in *R*-ZnO The vertical direct radiative transitions preserve the $\boldsymbol{k}$ vector and

InDrTrs involve participation of phonons. We must distinguish between the two kinds of InDrTrs; those with inclusion of electron and hole spin dependent on the magnitude of S–O interactions and those without. When S–O, spin–spin (S–S), or spin–lattice (S–L) interactions are neglible, we deal with SVirrps which are the classification of electron and hole states. In such cases of the InDrTrs in *R*-ZnO, an electron in the CB can drop radiatively from L_{1+} to L_{3-} and then be scattered in the VB by a phonon from L_{3-} to the Γ_{4-} VB. In the process, the radiative transition from L_{1+} to L_{3-} is allowed as discussed in Section 5. The scattering processes in the VB requires KP: $L_{4-} \times \Gamma_{4-} = L_{1+} + L_{2+} + 2L_{3+}$. The decomposition of the KP clearly indicates the symmetry allowed phonons: L_{1+} (no phonon), L_{2+} (longitudinal acoustic LA phonon), and L_{3+} (transverse acoustic TA phonon). In the second scattering process, an electron can be scattered from the L_{1+} to the Γ_{1+} CB, described by KP $L_{1+} \times \Gamma_{1+} = L_{1+}$ (longitudinal optical LO phonon) and then drop radiatively from Γ_{1+} to Γ_{4-}, which is allowed.

6.2 Inter- and intra-valley scattering processes in R-ZnO Regarding the theory of inter-valley scattering (InterVSc) and intra-valley scattering (IntraVSc) processes, we refer to the work by Lax–Hopfield (LH), and Birman–Lax–Loudon (BLL) [12, 13]. More about the IntraVSc by acoustic and optical phonons and InterVSc in GaAs, Si, and Ge [14]. Recently, Kunert et al. [15] considered the scattering processes in hexagonal *W*-ZnO.

In this section, we determine the allowed symmetries of vibrational modes of an electron scattered from one valley to another. There are three different scattering processes involved. In *R*-ZnO [5, 6], the electronic bands resolve valleys at Γ, (Γ_{1+}), $K(K_1)$, $V(V_1)$, and possibly $L(L_{1+})$ points. Point X consists of three non-equivalent valleys with electrons at $\boldsymbol{k}X$, $5\boldsymbol{k}X$, and $9\boldsymbol{k}X$ states, while at point L we deal with four non-equivalent valleys with electrons of $\boldsymbol{k}L$, $2\boldsymbol{k}L$, $3\boldsymbol{k}L$, and $4\boldsymbol{k}L$ momentum. The IntraVSc means scattering of electrons within three valleys at X point or within four valleys at the L point, while InterVSc refers to scattering processes between three X valleys and four L valleys. Theses scattering processes involve KPs between SVirrps (no-spin). Here we consider the following KPs for InterVSc: $\Gamma \times X$, $\Gamma \times L$, $\Gamma \times V$ and for IntraVSc: $\Gamma \times X$, $X \times X$, and $L \times L$.

For InterVSc we have: $\Gamma_{1+} \times X_{1+} = X_{1+}$ (LO and LA phonons dependent on masses of ions), $\Gamma_{1+} \times L_{1+} = L_{1+}$ (LO and LA phonons), and $\Gamma_{1+} \times V_1 = V_1$ (unknown). Our predictions of phonon symmetries participating in scattering processes is based on group theoretical connectivity relations. To the best of our knowledge, there are no experimental data on phonon dispersion curves and phonon density of states in *R*-ZnO.

In an IntraVSc process, which means scattering within or between valleys belonging to the same star, two kinds of phonons are involved, phonons with large momentum like $h\boldsymbol{k}L$, $h\boldsymbol{k}W$, or $h\boldsymbol{k}X$ and with very low momentum $h\boldsymbol{k} = 0$. The IntraVSc requires a special symmetric KP [11], and for *R*-ZnO, take the form $[\Gamma_{1+} \times \Gamma_{1+}]_2 = \Gamma_{1+}$, $[X_{1+} \times X_{1+}]_2 = \Gamma_{1+} + \Gamma_{3+}$, and $[L_{1+} \times L_{1+}]_2 = \Gamma_{1+} + \Gamma_{5+}$ for low momentum of Γ phonons and $[X_{1+} \times X_{1+}]_2 = X_{1+}$ and $[L_{1+} \times L_{1+}]_2 = X_{1+} + X_{4+}$ for large phonon momentum. Consequently, phonons involved in IntraVSc in *R*-ZnO are of symmetries: Γ_{1+} (TA and LA), Γ_{3+}, Γ_{5+} (TO and LO), and X_{4+} (TO).

7 Discussion We have derived optical selection rules based on the assignments of electronic bands listed in Table 1. We believe that electron states in CBs with no spin (Γ_{1+}, L_{1+}, and X_{1+}) and with spin (Γ_{6+}, L_{6+}, and X_{6+}) are properly assigned. Experimentally, it has been shown that the VB maxima in *R*-ZnO are at L point and Σ line, but not at the center of the BZ (Γ point). In many compounds, the highest VB maximum is at the Γ point and holes states (p_x, p_y, p_z) which transform as the VR. Since the center of the BZ is of the highest symmetry, we assigned it as Γ_{4-} = VR (no spin). The highest VB maximum has been assigned by L_{3-} two-dimensional representations according to which holes (p_x, p_y) supposed to transform. Our OPSRs are based mainly on theoretical derivations and are in agreement with absorption data. There is a lack of experimental data on *R*-ZnO, such as Raman, photoluminescence, and reflectance spectra. There is also no phonon dispersion relation and density of phonon states measured by X-ray and neutron scattering techniques. The forthcoming experimental work will verify our selection rules.

8 Conclusions An attempt has been made on assignments of the EBS of *R*-ZnO. Some optical selection rules related to direct and indirect transitions were discussed. Splitting of the maximum VB at point L due to possible S–O interaction onto three sub-bands of L_{4-}, L_{5-}, and L_{6-} symmetries, may result in the three observed exciton bands. We hope that magneto-photoluminescence and reflectivity will prove our predictions. It is well known that in the *W*-ZnO at point Γ, three excitons A, B, and C contribute to the optoelectronic devices application. It would mean that by pressure, one can "shift" the A, B, and C parabolic excitons in *W*-ZnO to the $L_1(L_{4-})$, $L_2(L_{5-})$, $L_3(L_{6-})$, and non-parabolic ones in *R*-ZnO.

References

[1] C. W. Litton, D. C. Reynolds, and T. C. Collins, Zinc Oxide Materials for Electronic and Optoelectronic Device Applications, Technology and Engineering (John Wiley & Sons, New York, 2011).
[2] K. Li, C. Kang, and D. Xue, Mater. Res. Bull. **47**, 2902–2905 (2012).
[3] H. Y. Wu, X. L. Cheng, C. H. Hu, and P. Zhou, Physica B **405**, 606–612 (2010).
[4] M. J. S. Spencer, Progr. Mater. Sci. **57**, 437–486 (2012).
[5] J. E. Jaffe, R. Pandey, and A. B. Kunz, Phys. Rev. **43**, 14030 (1991).
[6] A. Segura, J. A. Sans, F. J. Manjon, A. Munoz, and H. Cabrera, Appl. Phys. Lett. **83**, 278 (2003).

Original Paper

[7] A. P. Cracknell, B. L. Davies, S. C. Miller, and W. F. Love, Kronecker Product Tables, Vols. 1–4 (IFI/Plenum, New York, Washington, London, 1979).
[8] L. P. Bouckaert, R. Smoluchowski, and E. Wigner, Phys. Rev. **50**, 266–280 (1936).
[9] M. Hamermesh, Group Theory and Its Application to Physical Problems (Addison-Wesley Publ. Co., Inc., Reading, Massachusetts, London, 1962).
[10] H. W. Kunert, J. Popenda, and M. Suffczynski, J. Physique **39**, 526 (1978).
[11] H. W. Kunert, Cryst. Eng. **4**, 233–240 (2001).
[12] M. Lax and J. J. Hopfield, Phys. Rev. **124**, 115 (1961).
[13] J. L. Birman, M. Lax, and R. Loudon, Phys. Rev. **145**, 620 (1966).
[14] Y. Yu and M. Cardona, Fundamentals of Semiconductors, Physical and Material Properties (Springer-Verlag, Berlin, Heidelberg, New York, 1966).
[15] H. W. Kunert, M. R. Wagner, A. G. J. Machatine, P. Niyongabo, J. B. Malherbe, A. Hoffmann, J. Barnas, and W. Florek, Phys. Status Solidi B **247**(7), 1802–1806 (2010).